Design and Simulation of Battery-Less Effective Water Pumping System using New MPPT Algorithm

A Thesis Submitted

In Partial Fulfillment of the Requirement for the Degree

Of

MASTER OF SCIENCE IN

ELECTRICAL AND ELECTRONIC ENGINEERING

by

Anjan Debnath

Department of Electrical and Electronic Engineering

BANGLADESH UNIVERSITY OF ENGINEERING AND TECHNOLOGY

Dhaka, Bangladesh

May, 2018

APPROVAL

The thesis titled "Design and simulation of battery-less effective water pumping system using new MPPT algorithm" submitted by **Anjan Debnath**, Roll No. **0409062202 P**, Session: **April 2009** has been accepted as satisfactory in partial fulfillment of the requirement for the degree of Master of Science in Electrical and Electronic Engineering on 30 May, 2018.

BOARD OF EXAMINERS

1. Dr. Md. Ziaur Rahman Khan
Professor
Department of Electrical and Electronic Engineering
Bangladesh University of Engineering and Technology,
Dhaka-1205, Bangladesh
— Chairman (Supervisor)

2. Dr. Quazi Deen Mohd Khosru
Professor and Head of the Department
Department of Electrical and Electronic Engineering
Bangladesh University of Engineering and Technology,
Dhaka-1205, Bangladesh
— Member (Ex-officio)

3. Dr. Mohammad Jahangir Alam
Professor
Department of Electrical and Electronic Engineering
Bangladesh University of Engineering and Technology,
Dhaka-1205, Bangladesh
— Member

4. Dr. Md. Anwarul Abedin
Professor,
Department of Electrical and Electronic Engineering
Dhaka University of Engineering and Technology,
Gazipur, Dhaka, Bangladesh
— Member (External)

DECLARATION

It is hereby declared that this thesis or any part of it has not been submitted elsewhere for the award of any degree or diploma. Any material reproduced in this project has been properly acknowledged.

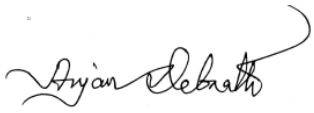

ANJAN DEBNATH

Roll No: 0409062202 P

ACKNOWLEDGMENT

First of all, I would like to express my gratitude to my supervisor, Dr. Md. Ziaur Rahman Khan for giving me the opportunity of working under his supervision. It would have not been possible to complete this work without his invaluable guidance, advice and support. I have learnt a lot from him during the realization of this thesis.

I would like to thank my friends, Sukanta Roy and Md. Nazmul Huda who provided valuable information for my work during various stages of my thesis. A number of good ideas generated from our numerous discussions and their feedback are incorporated in this thesis.

And last but not least, to my family, who have encouraged, motivated and supported me during these long two and half years of thesis work.

Anjan Debnath

6th of May, 2018

ABSTRACT

This thesis conducts the design and simulation of a simple but efficient photovoltaic water pumping system and this work also analyzes a mathematical linear programming based graphical model to provide the best economical solution for water pumping system by comparing hybrid, solar-only and wind-only system. It provides theoretical studies of photovoltaic and modeling techniques using equivalent electric circuits. The system employs a new maximum power point tracker (MPPT) which is suitable for rapid changing weather conditions. The investigation includes discussion of various MPPT algorithms and their comparisons and drawbacks and it has been shown that the proposed model has been successfully resolved the drawbacks from existing models. A mathematical model of DC motor has also been developed using actual output characteristic data and verified using MATLAB simulations. MATLAB simulations are also performed for comparing the number of iterations before reaching to MPP point of the proposed method and the most popular existingMPPT algorithms using actual irradiance and temperature data and has shown that the proposed model has taken much less number of iterations comparing to existing models and hence makes it suitable for rapid changing weather conditions. It also conducts a performance analysis by comparing the duty cycles and maximum power points with the exact duty cycles and maximum power points and justifies the validity of the proposed model. The thesis work chooses output sensing direct control method which requires two sensors only with a view to making the whole system cost effective. Simulations also make comparisons with the system without MPPT in terms of total energy produced. The results validate that the proposed MPPT algorithm can significantly increase the efficiency and the performance of PV water pumping system compared with the system without MPPT. Finally, the research develops a mathematical graphical sizing technique using linear programming to find an economical solution for water pumping system in two different regions of Bangladesh and found out that for both regions, Khulna and Kutubdia, hybrid system is the most cost effective solution based on the corresponding weather data.

CONTENTS

LIST OF TABLES

LIST OF FIGURES

Chapter 1: Introduction

1.1 Introduction

Water pumping worldwide is generally dependent on conventional electricity or diesel generated electricity. Solar water pumping minimizes the dependence on diesel, gas or coal based electricity[1, 2]. The use of diesel or propane based water pumping systems require not only expensive fuels, but also create noise and air pollution. The overall upfront cost, operation and maintenance cost, and replacement of a diesel pump are 2–4 times higher than a solar photovoltaic (PV) pump. Solar pumping systems are environment friendly and require low maintenance with no fuel cost[3][4]. Keeping in view the shortage of grid electricity in rural and remote areas in most parts of world, PV pumping is one of the most promising applications of solar energy. The technology is similar to any other conventional water pumping system except that the power source is solar energy. PV water pumping is gaining importance in recent years due to non-availability of electricity and increase in diesel prices. The flow rate of pumped water is dependent on incident solar radiation and size of PV array. A properly designed PV system results in significant long-term cost savings as compared to conventional pumping systems[5]. In addition, tanks can be used for water storage in place of requirement of batteries for electricity storage.

Agricultural production in developing countries is largely dependent on rains and is adversely affected by the non-availability of water in summers. However, maximum solar radiation is available in summers as such more water can be pumped to meet increased water requirements. Urban water supply systems are also dependent on electricity to pump water in towns. There is a wide scope to utilize PV pumping systems for water supplies in rural, urban, community, industry and educational institutions.

Direct coupled DC solar pumping was first introduced in the field in the late 1970s. Earlier PV water pumping systems have limitations of overall performance of the system due to lack of proper design. Since then, manufacturers have refined their products to improve the performance and reliability. The steady fall in prices of solar photovoltaic (PV) panels have resulted in making solar pumping economically viable for an increasingly wide range of applications. Direct coupled DC solar pumps are simple and

reliable [6] but cannot operate at maximum power point of PV generator as the solar radiation varies during the day from morning till evening. However, adding a maximum power point tracker (MPPT) and controls/protections improve the performance of a PV pump. PV water pumping systems have shown significant advancements in the last decade. The first generation PV pumping systems used centrifugal pumps usually driven by DC motors and variable frequency alternating current (AC) motors, with proven long-term reliability and hydraulic efficiency varying from 25% to 35%. The second generation PV pumping systems use positive displacement pumps, progressing cavity pumps or diaphragm pumps, generally characterized by low PV input power requirements, low capital cost and high hydraulic efficiencies of even 70% [7]. Advancement has taken place in the tracking mechanism of PV arrays from manual tracking to dual axis automatic tracking systems by microcontroller programming. Tracking the sun reduces the physical size of PV panel area required for a given output, improves power yield, overall efficiency of the system and return on investment. Tracking of a solar pumping system extends the time for peak water yield. The solar pumps available in the market can lift water from 5 m to more than 200 m with outputs of up to 250 m^3/day. For the past 15 years significant improvement has been done in helical motor pumps (positive displacement pumps) which are submersible and last for many years and are powered by similar motors as used for centrifugal pumps. Advancement has been in the field of controllers for large size PV arrays in the order of 25 kW with 100 kW controllers expected to be developed in near future [8]. With penetration of lot of renewable energy to grid along with non-linear loads will cause Power Quality disturbances. The fluctuating power sources like wind mill and solar panel is causing uneven power production due to voltage dips and sags. In [9-11], a solution has been provided which will help in designing electronics to compensate the harmful effects of the disturbances. The noble method is able to extract the PQ disturbances present in the system [12].

PV module costs have significantly declined and are available at a rate of US$ 0.59/Wp in 2014 as compared to around US$ 1/Wp in 2012 in India. This significantly affects the overall cost of the pumping system since PV modules represent 60–80% of the total cost of a PV system. The steady increase in cost of diesel and gasoline prices

over the years and decrease in PV system costs make PV pumping attractive from financial perspective also. Furthermore, crystalline PV modules with high efficiencies of 16.84–21.5% are available in the International market in 2014 [4].

The main objective of this research is to first model and simulate a new algorithm based efficient photovoltaic water pumping system. The thesis also provides theoretical studies of photovoltaic (PV) and its modeling techniques. It also investigates in detail the maximum power point tracker (MPPT), a power electronic device that significantly increases the system efficiency. It presents MATLAB simulations of the system and makes comparisons with a system without MPPT. The MATLAB simulation of the thesis also will show the comparison with the most common method known as Perturb and Observe method. At last, the research will develop a mathematical technique for optimizing cost for water pumping system in two different regions of Bangladesh.

1.2 Motivation

The finite global supply of recoverable fossil fuels implies that at some point in the future, alternative sources of energy will become the primary source of energy to meet global demand. Photovoltaic power represents promising alternatives that will likely initially supplement fossil fuel based energy supply, and eventually replace the fossil fuel energy sources as the availability of the latter declines. There is therefore a need to systematically analyze and understand how solar systemoperates as an optimal system.

When compared to fossil fuels, solar cells are relatively untapped sources of energy, thus there still remains a lot of work to be done to make solar cells as efficient and reliable as possible. One approach to understanding and improving solar cell efficiency is digital modeling and simulation. After successfully modeling and simulating solar system, it is possible to develop methods to optimizing the system operation with programmable controller. There are very few sources to study MPPT that provides comprehensive and detailed explanations about it. Therefore, this thesis investigates it in detail and provides better explanations for students who are interested in this research area. In order to understand and design MPPT, it is necessary to have a

good understanding of the behaviors of PV. The thesis facilitates it using MATLAB models of PV cell and module. Each subsystem in the PV water pumping system is modeled for MATLAB simulations and the functionality of MPPT for water pumping systems is verified and validated. Finally, it will carry a case study where a linear programming tool will be utilized as a mathematical technique in order to work out the best cost effective strategy for water pumping system in Kutubdia and Khulna region of Bangladesh.

This thesis is limited to providing theoretical studies and simulations of PV water pumping system with MPPT. The system will not be built in this thesis; that is left as future work. Thus, it will not cover a discussion about actual implementation of microcontrollers, nor other hardware implementation, beyond a discussion on component selection for the DC-DC converter. A major assumption made in simulations is the use of an ideal DC-DC converter, as opposed to a more realistic model that includes losses. The model, however, should provide sufficient results for verification of MPPT functionality.

1.3 Thesis Organization

The second chapter provides the basic structure and operating principle of Solar cell and mathematical modeling of a solar module. This chapter also includes photovoltaic water pumping system along with the block diagram of the developed system, MPPT charge controller and overview of the pump. The chapter also discusses the necessity of a MPPT tracker to a water pumping system in contrast to a direct coupled system and shows the outcomes graphically. It also provides the topology of a CUK converter and load matching mechanism in order to utilize the maximum output. The last part of the chapter furnishes a comparison study of the existing algorithms along with their drawbacks. The third chapter includes the flowchart and mathematical model of the developed system with the controller part. Chapter four discusses the results where MATLAB simulations graphs and calculations are provided.Chapter five analyzes what could be most economical scheme by comparing Hybrid, Solar-Only and Wind-Only system and chapter six discusses the conclusion and future scope of the work.

Chapter 2: Photovoltaic Modules and Water Pumping System

2.1 Structure of Solar Cell

Solar cells are the basic components of photovoltaic panels. Most are made from silicon even though other materials are also used. Solar cells take advantage of the photoelectric effect: the ability of some semiconductors to convert electromagnetic radiation directly into electrical current. The charged particles generated by the incident radiation are separated conveniently to create an electrical current by an appropriate design of the structure of the solar cell, as will be explained in brief below. For further details, the reader can consult references [13] and [14].

A solar cell is basically a p-n junction which is made from two different layers of silicon doped with a small quantity of impurity atoms: in the case of the n-layer, atoms with one more valence electron, called donors, and in the case of the p-layer, with one less valence electron, known as acceptors. When the two layers are joined together, near the interface the free electrons of the n-layer are diffused in the p-side, leaving behind an area positively charged by the donors. Similarly, the free holes in the p-layer are diffused in the n-side, leaving behind a region negatively charged by the acceptors. This creates an electrical field between the two sides that is a potential barrier to further flow. The equilibrium is reached in the junction when the electrons and holes cannot surpass that potential barrier and consequently they cannot move. This electric field pulls the electrons and holes in opposite directions so the current can flow in one way only: electrons can move from the p-side to the n-side and the holes in the opposite direction.

Metallic contacts are added at both sides to collect the electrons and holes so the current can flow. In the case of the n-layer, which is facing the solar irradiance, the contacts are several metallic strips, as they must allow the light to pass to the solar cell, called fingers.

2.2 Operating Principle

The photons of the solar radiation shine on the cell. Three different cases can happen: some of the photons are reflected from the top surface of the cell and metal fingers. Those that are not reflected penetrate in the substrate. Some of them, usually the ones with less energy, pass through the cell without causing any effect. Only those with energy level above the band gap of the silicon can create an electron-hole pair. These pairs are generated at both sides of the p-n junction. The minority charges (electrons in the p-side, holes in the n-side) are diffused to the junction and swept away in opposite directions (electrons towards the n-side, holes towards the p-side) by the electric field, generating a current in the cell, which is collected by the metal contacts at both sides.. This is the light-generated current which depends directly on the irradiation: if it is higher, then it contains more photons with enough energy to create more electron-hole pairs and consequently more current is generated by the solar cell.

2.3 Electrical Equivalent Circuit of Solar Cell

The solar cell can be represented by the electrical model shown in Figure 2-1. Its current-voltage characteristic is expressed by the following equation **(2-1)**:

$$I = I_L - I_o\left(e^{\frac{q(V-IR_S)}{AkT}-1}\right) - \frac{V-IRs}{R_P} \qquad (2\text{-}1)$$

where I and V are the solar cell output current and voltage respectively, Io is the dark saturation current, q is the charge of an electron, A is the diode quality (ideality) factor, k is the Boltzmann constant, T is the absolute temperature and Rs and Rp are the series and shunt resistances of the solar cell. Rs is the resistance offered by the contacts and the bulk semiconductor material of the solar cell. The origin of the shunt resistance Rp is more difficult to explain. It is related to the non ideal nature of the p–n junction and the presence of impurities near the edges of the cell that provide a short-circuit path around the junction [13]. In an ideal case Rs would be zero and Rp infinite. However, this ideal scenario is not possible and manufacturers try to minimize the effect of both resistances to improve their products.

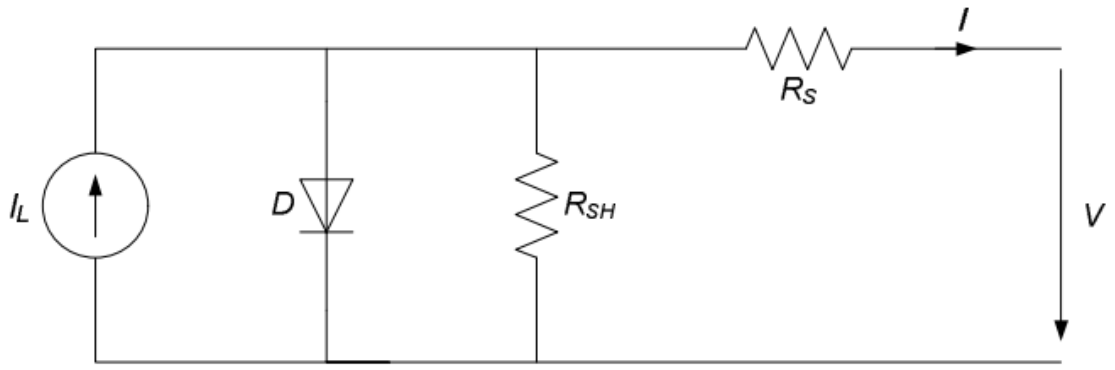

Figure 2-1: Equivalent Circuit of a Solar Cell

Sometimes, to simplify the model, as in [15], the effect of the shunt resistance is not considered, i.e. Rp is infinite, so the last term in equation (**2-1**) is neglected.

A PV panel is composed of many solar cells, which are connected in series and parallel so the output current and voltage of the PV panel are high enough to the requirements of the grid or equipment. Taking into account the simplification mentioned above, the output current-voltage characteristic of a PV panel is expressed by equation (**2-2**), where np and ns are the number of solar cells in parallel and series respectively [15].

$$I \approx n_P I_L - n_P I_o \left(e^{\frac{q(V - IR_S)}{AkTn_S}} - 1 \right) \tag{2-2}$$

2.4 Open Circuit Voltage, Short Circuit Current and MPP

Two important points of the current-voltage characteristic must be pointed out: the open circuit voltage V_{OC} and the short circuit current I_{SC}. At both points the power generated is zero. V_{OC} can be approximated from equation (**2-1**) when the output current of the cell is zero, i.e. I=0 and the shunt resistance R_{SH} is neglected. It is represented by equation (**2-3**). The short circuit current I_{SC} is the current at V = 0 and is approximately equal to the light generated current I_L as shown in equation (**2-4**).

$$V_{OC} \approx \frac{AkT}{q} \ln\left(\frac{I_L}{I_O} + 1\right) \tag{2-3}$$

$$I_{SC} \approx I_L \tag{2-4}$$

The maximum power is generated by the solar cell at a point of the current-voltage characteristic where the product V*I is maximum. This point is known as the MPP and is unique, as can be seen in Figure 2-2, where the previous points are represented.

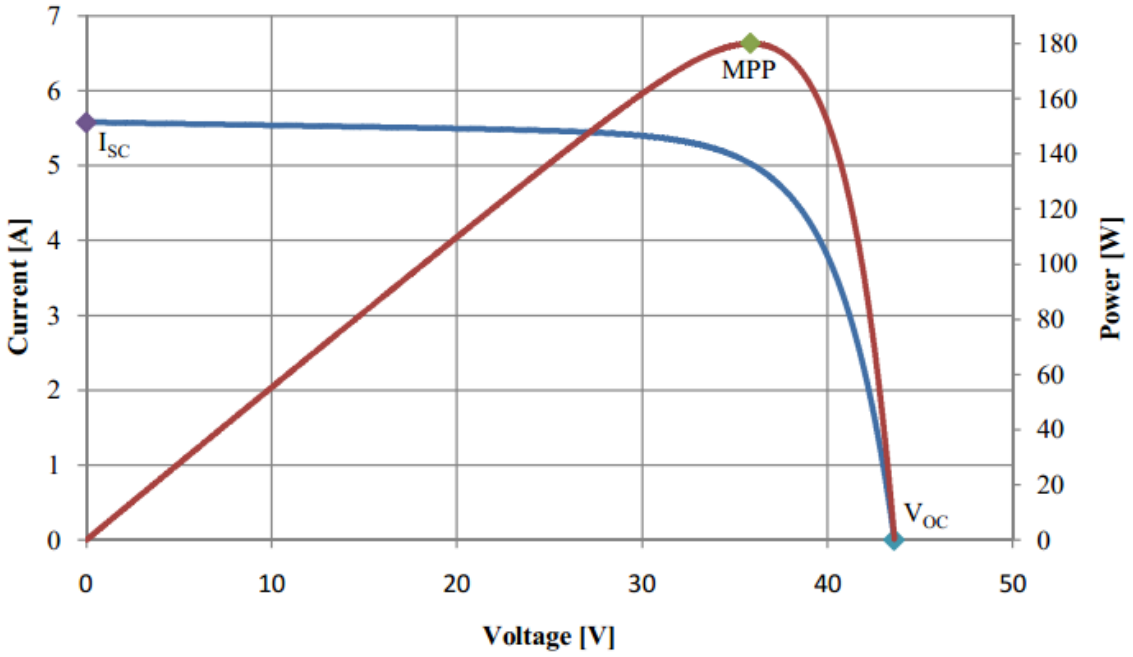

Figure 2-2: Short Circuit Current, Open Circuit Voltage and MPP points**[13]**

2.5 Fill Factor

Using the MPP current and voltage, I_{MPP} and V_{MPP}, the open circuit voltage (V_{OC}) and the short circuit current (I_{SC}), the fill factor (FF) can be defined as:

$$FF = \frac{I_{MPP}V_{MPP}}{I_{SC}V_{OC}} \qquad (2\text{-}5)$$

It is a widely used measure of the solar cell overall quality [13]. It is the ratio of the actual maximum power (I_{MPP}, V_{MPP}) to the theoretical one (I_{SC}, V_{OC}), which is actually not obtainable. The reason for that is that the MPP voltage and current are always below the open circuit voltage and the short circuit current respectively, because of the series and shunt resistances and the diode depicted in Figure 2-1. The typical fill factor for commercial solar cells is usually over 0.70.

2.6 MATLAB Modeling of PV Module

BP Solar BP SX 150S PV module is chosen for a MATLAB simulation model. The module is made of 72 multi-crystalline silicon solar cells in series and provides 150W of nominal maximum power [16]. Table 2-1 shows its electrical specification.

Table 2-1: PV Module Specifications

Electrical Characteristics	
Maximum Power (P_{MAX})	150 W
Voltage at P_{MAX} (V_{MP})	34.5 V
Current at P_{MAX} (I_{MP})	4.35 A
Open Circuit Voltage (V_{OC})	43.5 V
Short Circuit Current (I_{SC})	4.75 A

The strategy of modeling a PV module is no different from modeling a PV cell. It uses the same PV cell model. The parameters are the all same, but only a voltage parameter (such as the open-circuit voltage) is different and must be divided by the number of cells.

The study done by Walker [17] of University of Queensland, Australia, uses the electric model with moderate complexity, shown in Figure 2-3, and provides fairly accurate results. The model consists of a current source (Isc), a diode (D), and a series resistance (Rs). The effect of parallel resistance (Rp) is very small in a single module, thus the model does not include it and considered Rp = ∞ in the equation(**2-1**) and the entire equation has been reduced to the following:

$$I = I_{SC} - I_o\left(e^{\frac{q(V-IR_S)}{nkT}} - 1\right) \qquad (2\text{-}6)$$

To make a better model, it also includes temperature effects on the short-circuit current (Isc) and the reverse saturation current of diode (Io). It uses a single diode with the diode ideality factor (n) set to achieve the best I-V curve match.

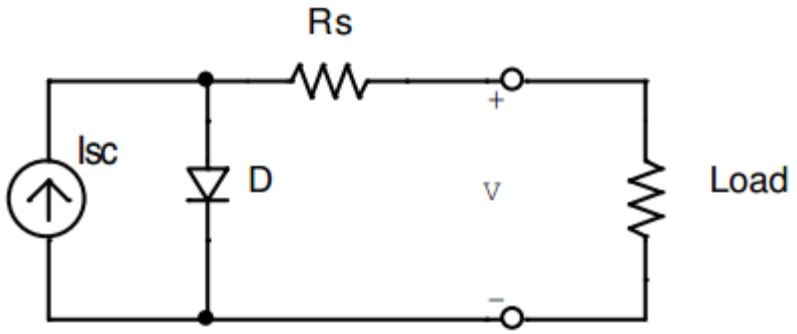

Figure 2-3: Electrical Modeling Circuit for MATLAB

First, calculate the short-circuit current (Isc) at a given cell temperature (T):

$$I_{SC}|_T = I_{SC}|_{T_{ref}} * (1 + a(T - T_{ref})) \quad (2\text{-}7)$$

where: Iscat Tref is given in the datasheet (measured under irradiance of 1000W/m2), Trefis the reference temperature of PV cell in Kelvin (K), usually 298K (25oC), a is the temperature coefficient of Isc in percent change perdegree temperature also given in the datasheet.

The short-circuit current (Isc) is proportional to the intensity of irradiance, thus Isc at a given irradiance (G) is:

$$\mathrm{I_{SC}}|_G = (\frac{G}{G_O})I_{SC}G_O \quad (2\text{-}8)$$

where: Go is the nominal value of irradiance, which is normally 1KW/m^2

The series resistance (Rs) of the PV module has a large impact on the slope of the I-V curve near the open-circuit voltage (Voc), as shown in

Figure 2-4, hence the value of Rs is calculated by evaluating the slope dV/dI of the I-V curve at the Voc [17].

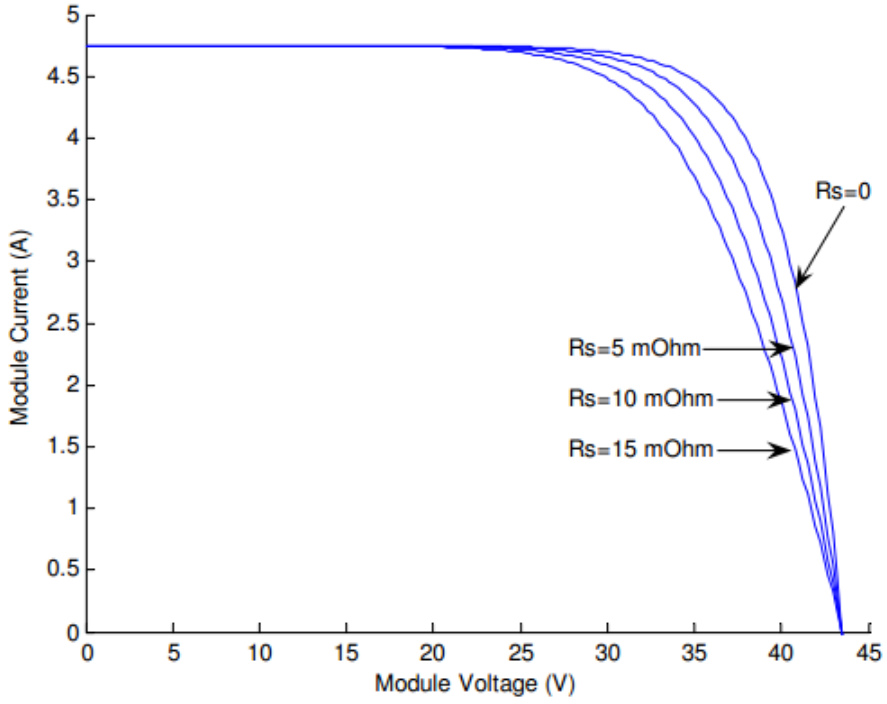

Figure 2-4: Effect of series resistance (1 KW/m^2, 25^{o}C)

The equation for Rs can be deduced in the following ways:

$$I = I_{sc} - I_o\left(e^{\frac{q(V+IR_S)}{nkT}} - 1\right) \tag{2-9}$$

$$dI = 0 - I_O * \mathrm{q}(\frac{\mathrm{dV} + \mathrm{R_S dI}}{\mathrm{nkT}}) * e^{\frac{q(V+IR_S)}{nkT}} \tag{2-10}$$

$$R_S = -\frac{dI}{dV} - \frac{nkT/q}{I_O * e^{\frac{q(V+IR_S)}{nkT}}} \tag{2-11}$$

Then, evaluate the equation (**2-11**) at the open circuit voltage that is V=Voc (also let I=0).

$$\mathrm{R_S} = -\frac{\mathrm{dV}}{\mathrm{dI}}|_{\mathrm{V_{OC}}} - \frac{nkT/q}{I_O * e^{\frac{q(V_{OC})}{nkT}}} \tag{2-12}$$

Where: $\frac{\mathrm{dV}}{\mathrm{dI}}|_{\mathrm{V_{OC}}}$ is the slope of the I-V curve at $\mathrm{V_{OC}}$

The calculation using the slope measurement of the I-V curve published on the BPSX 150 datasheet gives a value of the series resistance per cell, Rs = 5.1mΩ

Now, it is possible to solve equation (**2-9**) using Newton's Method for rapid convergence [17]. The Newton's method is described as:

$$x_{n+1} = x_n - \frac{f(x_n)}{f'(x_n)} \tag{2-13}$$

Rewriting the equation (**2-9**) gives the following function:

$$f(I) = I_{SC} - I - I_o\left(e^{\frac{q(V+IR_S)}{nkT}} - 1\right) = 0 \tag{2-14}$$

Plugging this into the equation (**2-13**) gives a following recursive equation, and the output current (I) is computed iteratively.

$$I_{n+1} = I_n - \frac{I_{SC} - I - I_o\left(e^{\frac{q(V+IR_S)}{nkT}} - 1\right)}{-1 - I_O(\frac{qR_S}{nkT})e^{\frac{q(V+I_nR_S)}{nkT}}} \tag{2-15}$$

As mentioned earlier, the I-V characteristics of a photovoltaic cell strongly depend on insolation and temperature (equations (**2-7**) and (**2-8**)). This becomes very apparent when evaluating equation (**2-6**) for selected values of temperature and irradiance and plotting the results as an I-V graph (Figure 2-5 and Figure 2-6). Figure 2-5 shows that the output current I of an array is greatly influenced by the change in insolation S, whereas the output voltage V stays approximately constant. In contrast, for a changing temperature one can see that the voltage varies widely while the current remains unchanged (Figure 2-6)

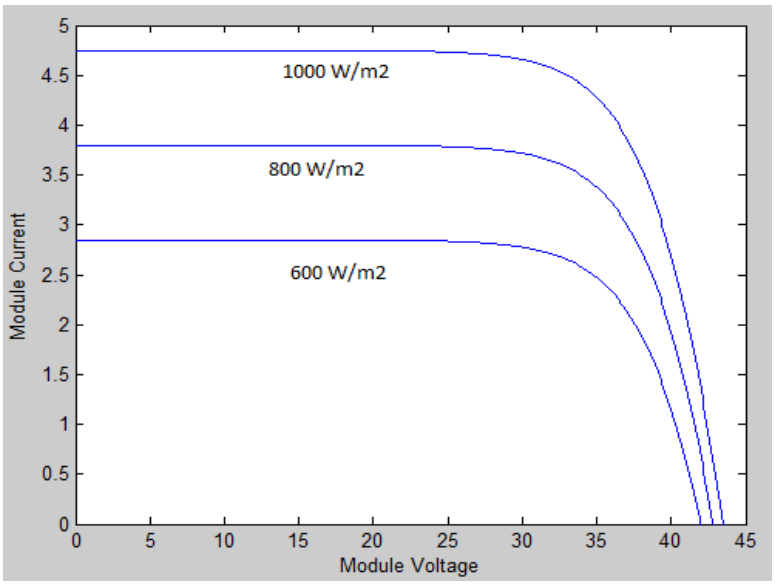

Figure 2-5: I-V characteristics of BPSX 150 PV module using MATLAB at 25ºC

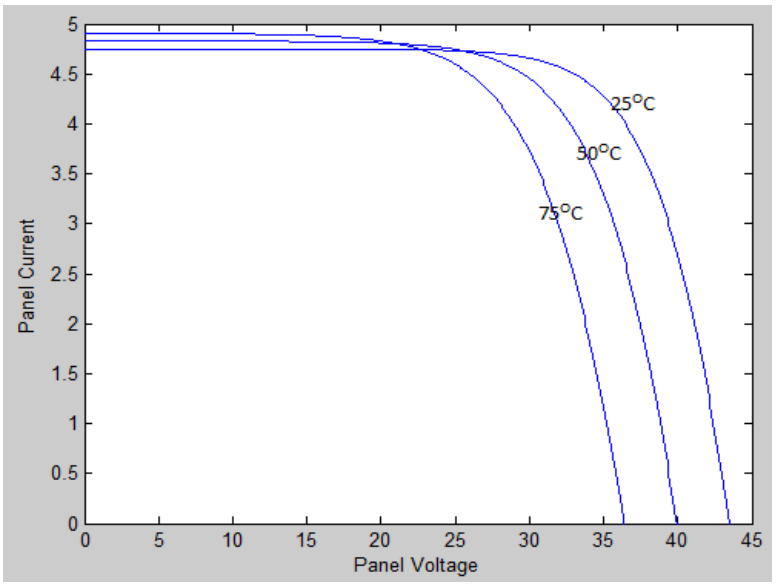

Figure 2-6: I-V characteristics of BPSX 150 PV module using MATLAB at an Irradiance of 1 KW/m^2

The P-V characteristics for a photovoltaic cell array can be obtained from the I-V characteristics and the relation for the output power P=VI as shown in Figure 2-7 and Figure 2-8. These figures clearly show how the dependency of output current I and output voltage V on temperature and insolation translate into a dependency of the output power on the same two parameters.

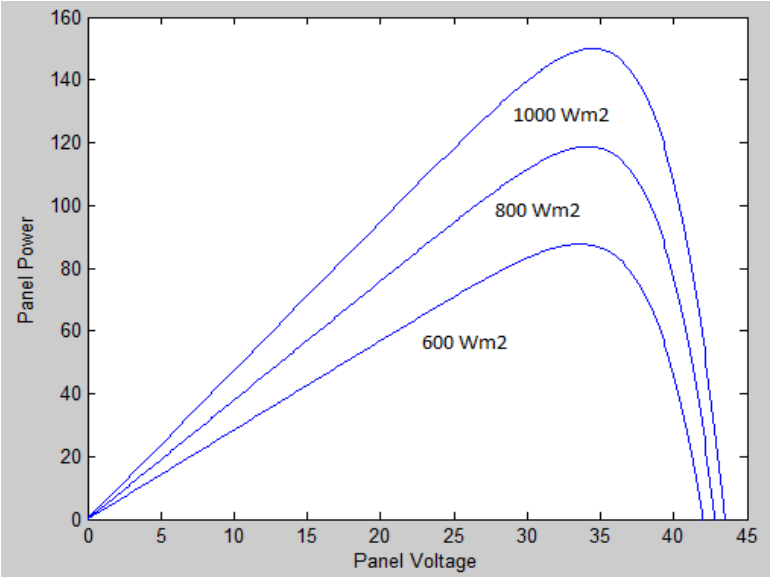

Figure 2-7: P-V characteristics of BPSX 150 PV module using MATLAB at 25ºC

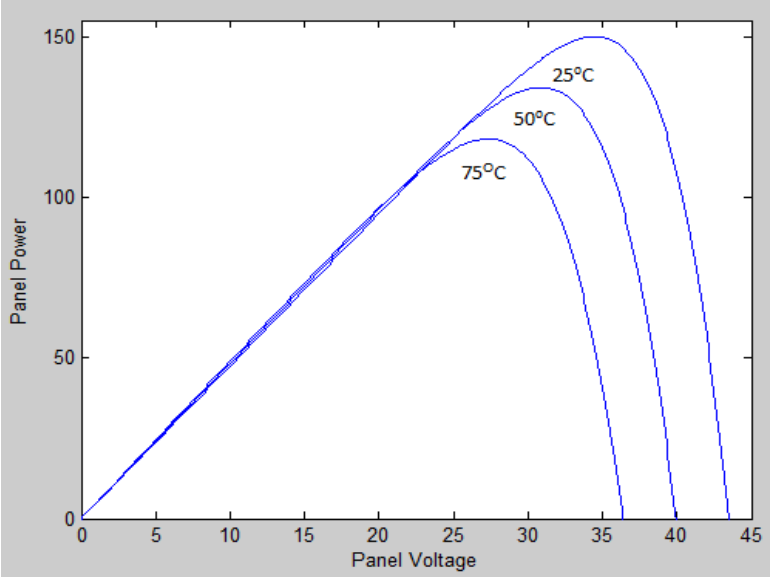

Figure 2-8: P-V characteristics of BPSX 150 PV module using MATLAB at an Irradiance of 1 KW/m^2

Figure 2-7 confirms the expected behavior of a device that converts solar energy into electrical energy: the power output of a solar panel is greatly reduced for a decreasing insolation.

2.7 The I-V Curve and Maximum Power Point

Figure 2-9 shows the I-V curve of the BP SX 150S PV module simulated with the MATLAB model. A PV module can produce the power at a point, called an operating point, anywhere on the I-V curve. The coordinates of the operating point are the operating voltage and current. There is a unique point near the knee of the I-V curve, called a maximum power point (MPP), at which the module operates with the maximum efficiency and produces the maximum output power.

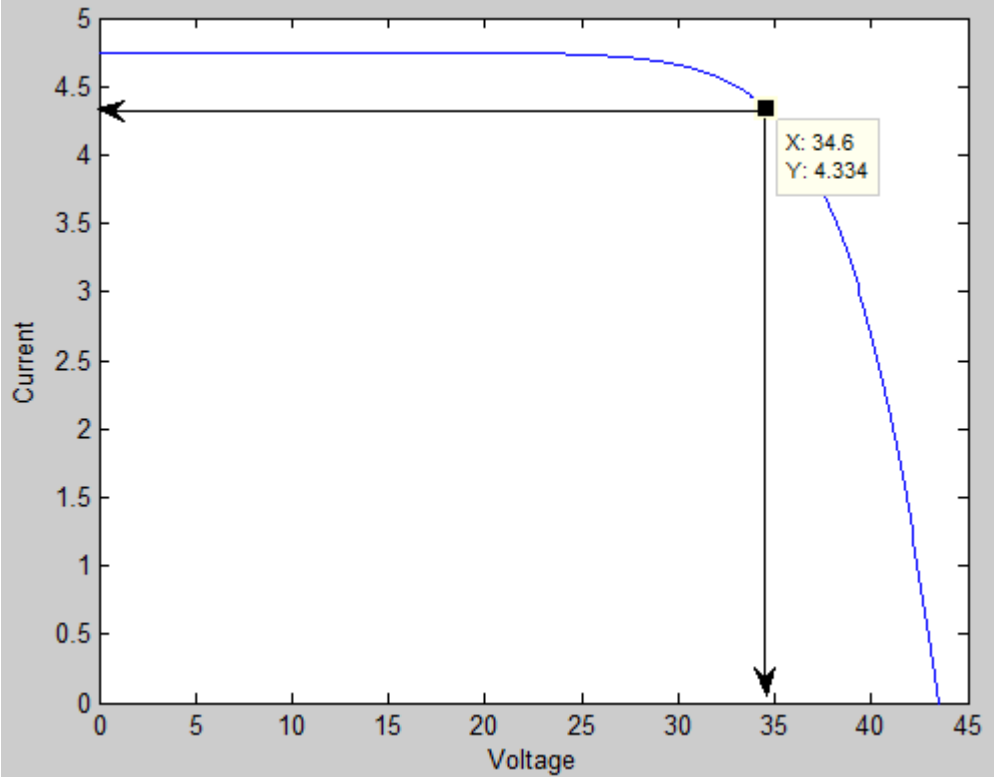

Figure 2-9: Simulated I-V curve of BP SX 150S PV module (1KW/m^2, 25^{o}C)

The power vs. voltage plot is overlaid on the I-V plot of the PV module, as shown in Figure 2-10. It reveals that the amount of power produced by the PV module varies greatly depending on its operating condition. It is important to operate the system at the MPP of PV module in order to exploit the maximum power from the module.

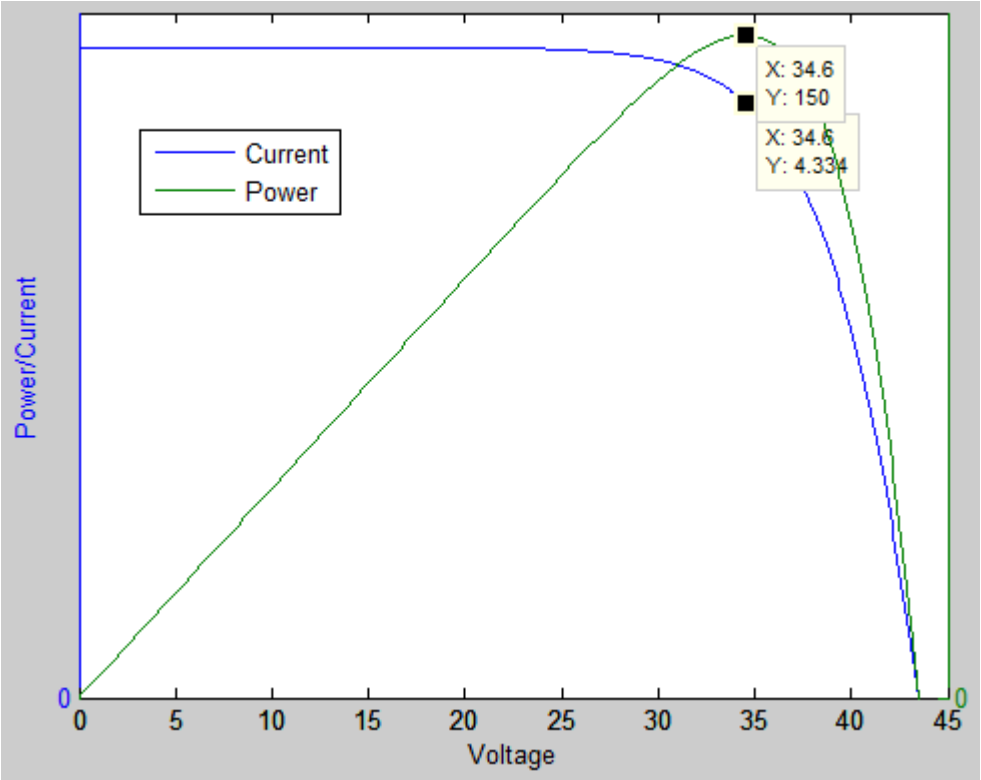

Figure 2-10: Simulated I-V and P-V curves of BP SX 150S PV module (1KW/m^2, 25^{o}C)

2.8 Solar Powered Water Pumping System

A water pumping system needs a source of power to operate. In general, AC powered system is economic and takes minimum maintenance when AC power is available from the nearby power grid. However, in many rural areas, water sources are spread over many miles of land and power lines are scarce. Installation of a new transmission line and a transformer to the location is often prohibitively expensive. Windmills have been installed traditionally in such areas; many of them are, however,

inoperative now due to lack of proper maintenance and age. Today, many stand-alone type water pumping systems use internal combustion engines. These systems are portable and easy to install. However, they have some major disadvantages, such as: they require frequent site visits for refueling and maintenance, and furthermore diesel fuel is often expensive and not readily available in rural areas of many developing countries. The consumption of fossil fuels also has an environmental impact, in particular the release of carbon dioxide (CO2) into the atmosphere. CO2 emissions can be greatly reduced through the application of renewable energy technologies, which are already cost competitive with fossil fuels in many situations. Good examples include large-scale grid-connected wind turbines, solar water heating, and off-grid stand-alone PV systems [18]. The use of renewable energy for water pumping systems is, therefore, a very attractive proposition.

Windmills are a long-established method of using renewable energy; however they are quickly phasing out from the scene despite success of large-scale grid-tied wind turbines.

PV systems are highly reliable and are often chosen because they offer the lowest life-cycle cost, especially for applications requiring less than 10KW, where grid electricity is not available and where internal-combustion engines are expensive to operate [18]. If the water source is 1/3 mile (app. 0.53Km) or more from the power line, PV is a favorable economic choice [19]. Table 2-2 shows the comparisons of different stand-alone type water pumping systems.

Table 2-2: Comparison among PV, Diesel and Windmill System [19]

System Type	Advantages	Disadvantages
PV Powered System	• Low Maintenance • Unattended Operation • Reliable long life • No fuel and no fumes • Easy to install • Low recurrent costs	• Relatively high initial cost • Low output in cloudy weather
Diesel or Gas Powered System	• Moderate Capital cost • Easy to install • Can be portable • Extensive experience available	• Needs maintenance and replacement • Site visit necessary • Noise, fumes , dirt problems • Fuel often expensive and supply intermittent
Windmill	• No fuel and no fumes • Potentially long lasting • Works well in windy sites	• High maintenance • Seasonal disadvantages • Costly repair • Laborious Installation

2.9 Energy Storage Devices

Needless to say, photovoltaic are able to produce electricity only when the sunlight is available, therefore stand-alone systems obviously need some sort of backup energy storage which makes them available through the night or bad weather conditions. Among many possible storage technologies, the lead-acid battery continues to be the workhorse of many PV systems because it is relatively inexpensive and widely available. In addition to energy storage, the battery also has ability to provide surges of current that are much higher than the instantaneous current available from the array, as well as the inherent and automatic property controlling the output voltage of the array so that loads receive voltages within their own range of acceptability [20]. While batteries may seem like a good idea, they have a number of disadvantages. The type of lead-acid battery suitable for PV systems is a deep-cycle battery [21], which is different from one used for

automobiles, and it is more expensive and not widely available. Battery lifetime in PV systems is typically three to eight years, but this reduces to typically two to six years in hot climate since high ambient temperature dramatically increases the rate of internal corrosion [18]. Batteries also require regular maintenance and will degrade very rapidly if the electrolyte is not topped up and the charge is not maintained. They reduce the efficiency of the overall system due to power loss during charge and discharge. Typical battery efficiency is around 85% but could go below 75% in hot climate [18]. From all those reasons, experienced PV system designers avoid batteries whenever possible.

For water pumping systems, appropriately sized water reservoirs can meet the requirement of energy storage during the downtime of PV generation. The additional cost of reservoir is considerably lower than that incurred by the battery equipped system. As a matter of fact, only about five percent of solar pumping systems employ a battery bank [19].

2.10 Developed System

The simulated water pumping system developed in this thesis is a stand-alone type without backup batteries. As shown in Figure 2-11[16, 19], the system is very simple and consists of a single PV module, a maximum power point tracker (MPPT), and a DC water pump. The size of the system is intended to be small; therefore it could be built in the lab in the future. The system including the subsystems will be simulated to verify the functionalities.

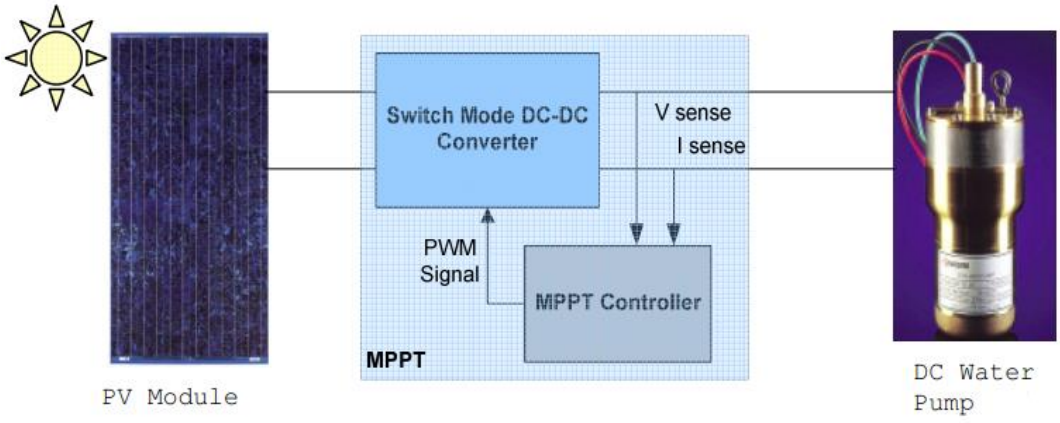

Figure 2-11: Block Diagram of the Developed System[22]

2.10.1 Photovoltaic System

A photovoltaic (PV) system consists of solar panels that generate electricity by the direct conversion of the sun's energy into electricity. The solar panels consist mainly of semiconductor material, with Silicon being the most commonly used. The components of a PV system are the solar cells connected in a suitable form and the electronic devices that interface the storage elements and the AC or DC loads.

One of the major tasks in controlling photovoltaic cells for power generation is improving cell efficiency and maximizing energy extraction. This requires I-V (current to-voltage) measurements to characterize performance and determine the load impedance that best matches the cell's source impedance. The best match can then be determined on a point on the I-V curve of the solar cell.

2.10.2 MPPT Charge Controller

The MPPT charge controller unit is a global block that includes the Maximum Power Point Tracking with a DC/DC converter. Figure 2-12 gives a general description of the charging unit block.

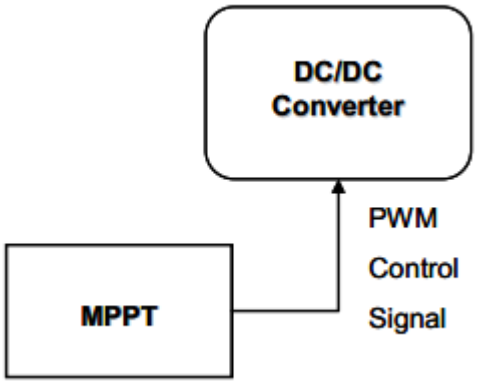

Figure 2-12: Block Diagram of the MPPT controller

MPPT is a power electronic device interconnecting a PV power source and a load, maximizes the power output from a PV module or array with varying operating conditions, and therefore maximizes the system efficiency. The MPPT constantly tracks the varying maximum operating point and adjusts the solar panel operating voltage in order to constantly extract the most available power. The MPPT charge controller

maximizes solar cell efficiency while also controlling the charging state of the battery. The MPPT charge controller is basically a DC-DC converter that accepts a DC input voltage and outputs a DC voltage higher, lower or the same as the input voltage. This capability of the converter makes it ideal for converting the solar panel maximum power point voltage to the load operating voltage. Most MPPT charge controllers are based on either the buck converter (step-down), boost convert (step-up) or buck-boost converter setup (CUK converter) [23].

2.10.3 Water Pump

Two types of pumps are commonly used for PV water pumping applications: positive displacement and centrifugal [24]. Positive displacement types are used in low-volume pumps [19] and cost-effective. Centrifugal pumps have relatively high efficiency [24] and are capable of pumping a high volume of water. A typical size of system with this type pump is at least 500W or larger. There is a growing trend among the pump manufacturers to use them with brushless DC motors (BDCM) for higher efficiency and low maintenance [24]. However, the cost and complexity of these systems will be significantly higher. Water pumps are driven by various types of motors. AC induction motors are cheaper and widely available worldwide. The system, however, needs an inverter to convert DC output power from PV to AC power, which is usually expensive, and it is also less efficient than DC motor-pump systems [24]. In general, DC motors are preferred because they are highly efficient and can be directly coupled with a PV module or array. Brushed types are less expensive and more common although brushes need to be replaced periodically (typically every two years) [24]. There is also an aforementioned brushless type.

The water pump chosen here for its size and cost is the Kyocera SD 12-30 submersible solar pump, pictured in Figure 2-13. It is a diaphragm-type positive displacement pump equipped with a brushed permanent magnet DC motor and designed for use in stand-alone water delivery systems, specifically for water delivery in remote locations. The rated maximum power consumption is 150W. It operates with a low

voltage (12~30V DC), and its power requirement is as little as 35W [25]. A mathematical model of this water pump is developed for simulations in Chapter 3.

Figure 2-13: SD Series Solar Pump[26]

2.11 I-V Curve of Different Loads

The I –V curve of a photovoltaic cell, module, or array does not by itself tell us anything about just where on that curve the system will actually be operating. This determination is a function of the load into which the PV delivers its power. Loads do have their own I-V curves: When a PV module is directly coupled to a load, the same voltage is across both the PV and load, and the same current runs through the PV and load. The intersection point of the two curves is the operating point as shown in Figure 2-14.

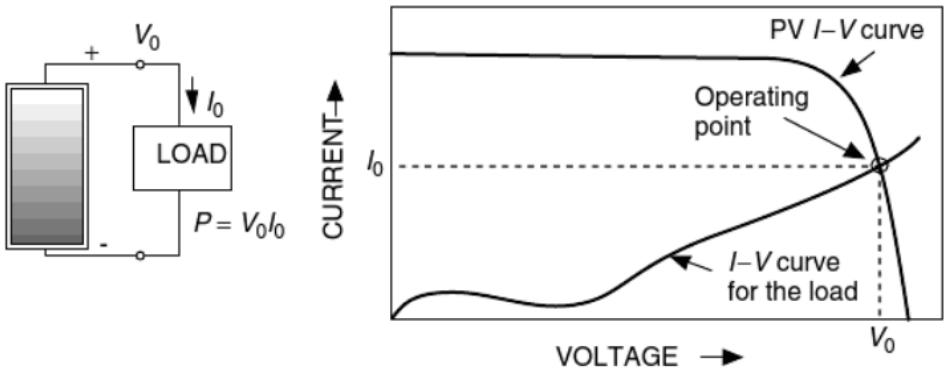

Figure 2-14: Direct Coupled Load and corresponding I-V curve[27]

2.11.1 I-V Curve of Resistive Load

A resistive load has a straight line with a slope of $1/R_{load}$ as shown in Figure 2-15. In other words, the impedance of load dictates the operating condition of the PV module. In general, this operating point is seldom at the PV module's MPP, thus it is not producing the maximum power. A study shows that a direct-coupled system utilizes a mere 31% of the PV capacity [28]. With a fixed resistance the operating point slips off the MPP as the solar irradiance changes as shown in Figure 2-16. A PV array is usually oversized to compensate for a low power yield during winter months. This mismatching between a PV module and a load requires further over-sizing of the PV array and thus increases the overall system cost

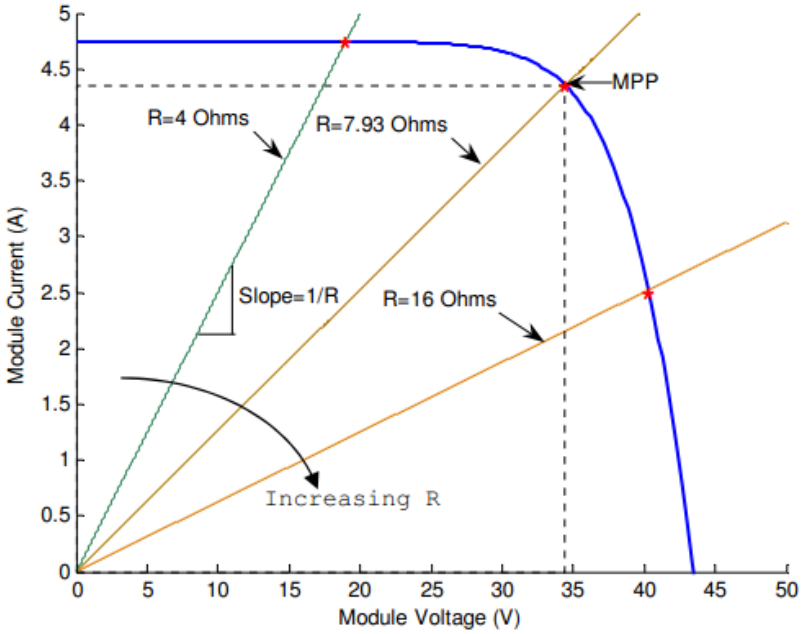

Figure 2-15: I-V characteristics of BPSX 150 PV Module using MATLAB at 25ºC[27]

To mitigate this problem, a maximum power point tracker (MPPT) can be used to maintain the PV module's operating point at the MPP. MPPTs can extract more than 97% of the PV power when properly optimized [29].

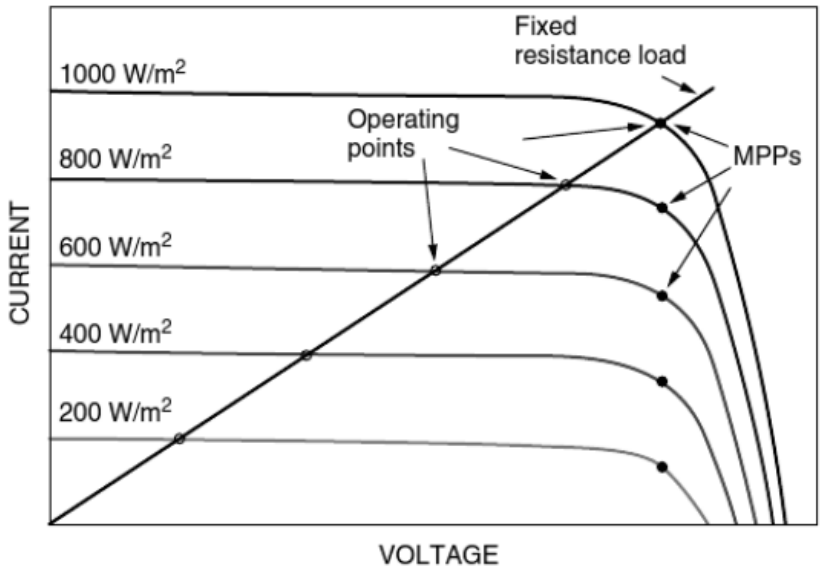

Figure 2-16: Shifting of Operating Point for a fixed Resistance[27]

2.11.2 I-V Curve of DC Motor

DC motors (such as those used in PV-water-pumping systems) exhibit a current–voltage relationship that is similar to that of a resistor.The motor has a unique curve for each operating speed. Several of these are displayed in the following Figure 2-17:

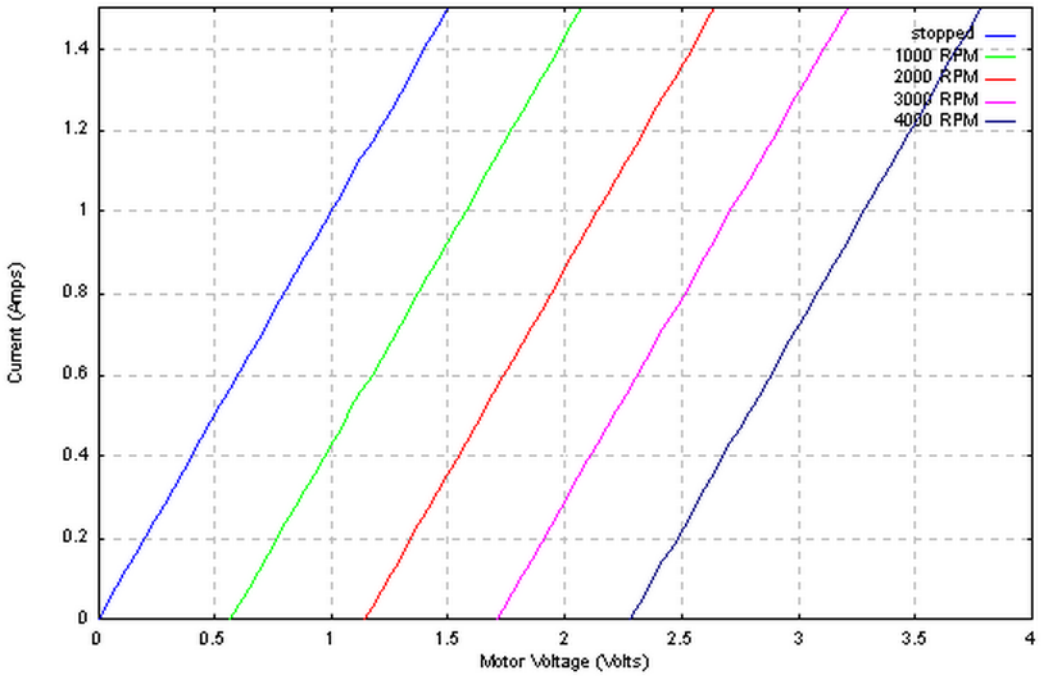

Figure 2-17: I-V Curve of DC Motor at various speeds

As the motor spins, it develops a voltage (back emf) that is proportional to the motor speed (ω). The voltage – current relationship for a dc motor is given by:

$V = IR_a + e,$

Where: e = kω, Ra is the motor armature resistance and k is the constant. Figure 2-18 shows the detail below:

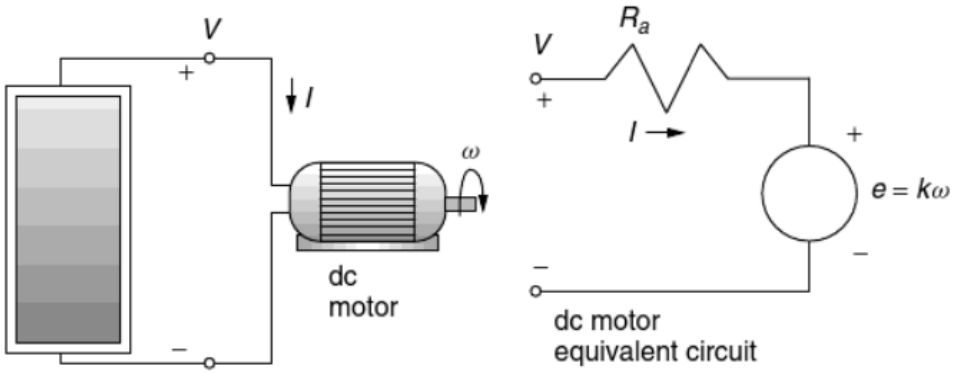

Figure 2-18: Direct Coupled Motor Load and its electrical equivalent circuit[30]

At start-up, while ω = 0, the current rises rapidly with increasing voltage until it is sufficient to create enough torque to break the motor loose from static friction. Once the motor starts to spin, the back emf drops the current, and thereafter I rises more slowly with increasing voltage (Figure 2-19).

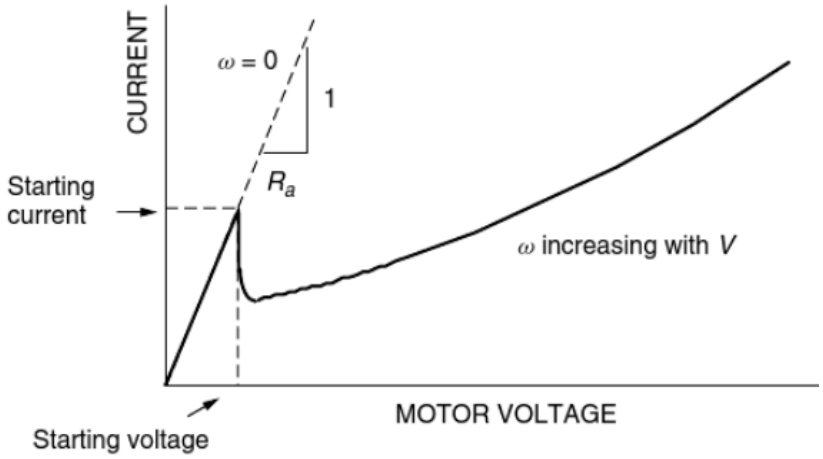

Figure 2-19: Starting of a DC Motor as voltage increases[30]

The mismatch of operating points with the ideal MPP is apparent in the Figure 2-20 below. It is noticeable that the motor doesn't have enough current to overcome static friction until insolation reaches at least 400 W/m^2. Once it starts spinning, however, it only needs about 200 W/m^2 to keep running. This means that the system cannot utilize a fair amount of morning insolation just because there is insufficient starting torque. Also, when the motor is operated under the locked condition for a long time, it may result in

shortening of the life of the motor due to input electrical energy converted to heat rather than to mechanical output[30].

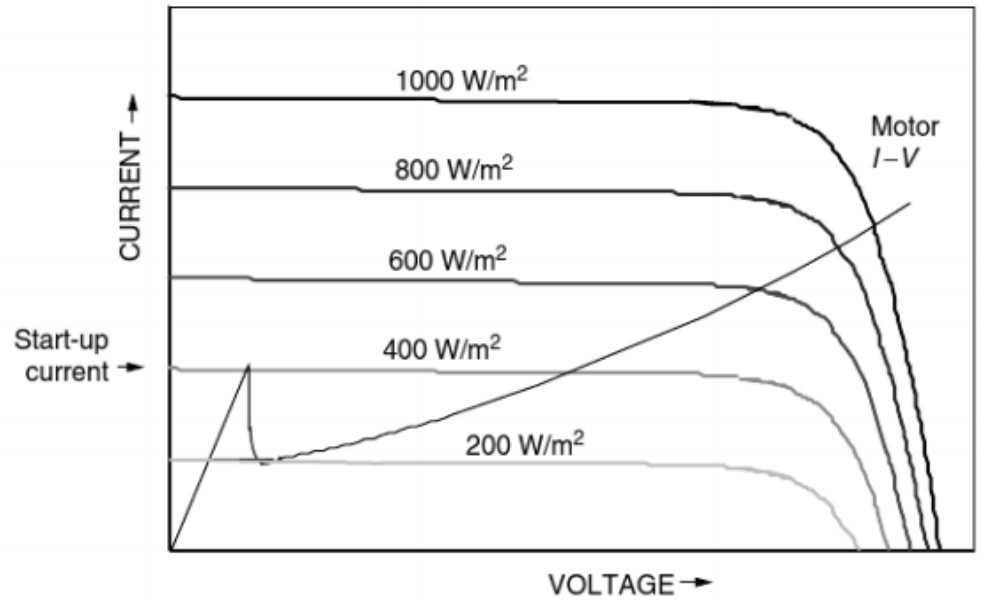

Figure 2-20: PV I-V curves with varying irradiance and a DC motor I-V curve[30]

2.12 DC-DC Converter

The heart of MPPT hardware is a switch-mode DC-DC converter. It is widely used in DC power supplies and DC motor drives for the purpose of converting unregulated DC input into a controlled DC output at a desired voltage level [31]. MPPT uses the same converter for a different purpose: regulating the input voltage at the PV MPP and providing load-matching for the maximum power transfer.

2.12.1 CUK Converter

In a motor-pump system, step down of voltage is required to generate high starting current to provide the necessary starting torque for motor. Buck converter would have been the simplest; however it has several disadvantages[32] such as discontinuous input current, so it requires good filter design. CUK converter could be the good candidate for that purpose as it can take continuous and ripple free current from PV array which is

important for MPPT efficiency. Another advantage is it provides capacitive isolation which protects against switch failure (unlike buck converter) [32].

The CUK converter switching topology is shown in Figure 2-21.The inductor on the input acts as a filter for the dc supply to prevent large harmonic current. Unlike BUCK converter topology, where the energy transfer is associated with the inductor, energy transfer for the CUK converter depends on the capacitor C_1[32].

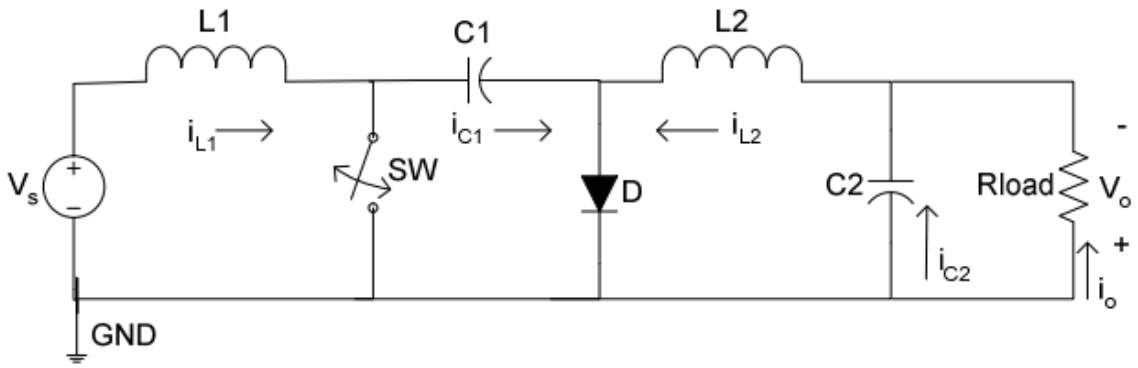

Figure 2-21: CUK Converter circuit diagram[33]

The analysis begins with the following assumptions:

i) Both inductors are very large and the currents in them are constant.

ii) Both capacitors are very large and the voltages across them are constant.

iii) The circuit is operating in the steady state, meaning that voltage and current waveforms are periodic.

iv) For a Duty ratio of D, the switch is closed for time DT and open for (1-D).T.

v) The switch and diode are ideal.

The average voltage across C_1 is computed from Kirchhoff's voltage law around the outermost loop. The average voltage across inductor is zero steady state operation, resulting in:

$$V_{C1} = V_s + V_o \tag{2-16}$$

The initial condition is when the input voltage is turned on and switch (SW) is off. The diode (D) is forward biased, and the capacitor (C1) is being charged. The operation of circuit can be divided into two modes.

Mode 1: When SW turns ON, the circuit becomes one shown in Figure 2-22

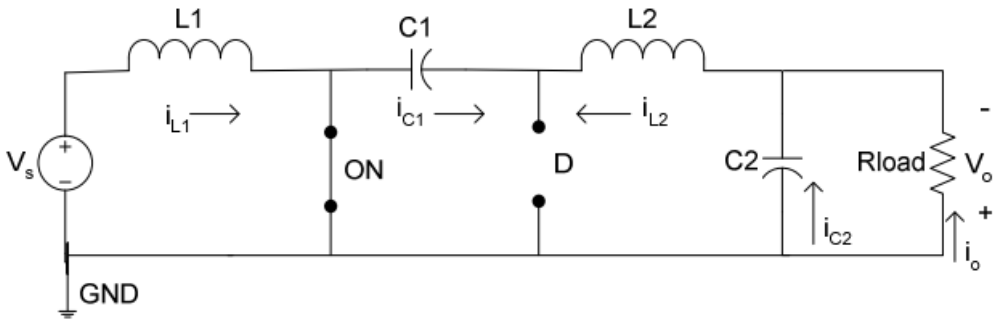

Figure 2-22: CUK converter when switch is ON[33]

The voltage of the capacitor (C_1) makes the diode (D) reverse-biased and turned off. The capacitor (C_1) discharge its energy to the load through the loop formed with SW, C_2, R_{load}, and L_2. The inductors are large enough, so assume that their currents are ripple free. Thus, the following relationship is established [32].

$$-I_{C1} = I_{L2} \tag{2-17}$$

Mode 2: When SW turns OFF, the circuit becomes one shown in Figure 2-23

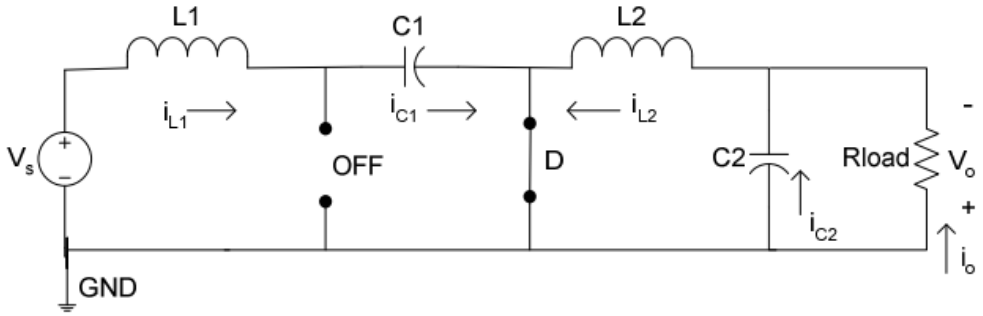

Figure 2-23: CUK converter when switch is OFF[33]

The capacitor (C_1) is getting charged by the input (Vs) through the inductor (L_1). The energy stored in the inductor (L_2) is transfer to the load through the loop formed by D, C_2, and R_{load}. Thus, the following relationship is established [32].

$$I_{C1} = I_{L1} \tag{2-18}$$

For periodic operation, the average capacitor current is zero. Thus, using equation (**2-17**) and equation (**2-18**):

$$[I_{C1|SW|ON} * DT + [I_{C1|SW|OFF}] * (1 - DT) = 0 \tag{2-19}$$

$$-I_{L2}.DT + I_{L1}.(1 - D)T = 0 \tag{2-20}$$

$$\frac{I_{L1}}{I_{L2}} = \frac{D}{1 - D} \tag{2-21}$$

Where: D is the duty cycle (0 < D < 1), and T is the switching period.

For ideal converter,

$$P_{in} = P_{out} \tag{2-22}$$

$$V_S * I_{L1} = V_o * I_{L2} \tag{2-23}$$

$$\frac{V_o}{V_S} = \frac{D}{1 - D} \tag{2-24}$$

Its relationship to the Duty Cycle (D) is:

- If 0 < D < 0.5, the Output is smaller than the Input
- If D = 0.5, the Output is same as the Input
- If 0.5 < D < 1, the Output is larger than the Input

2.12.2 Load Matching Mechanism

When PV is directly coupled with a load, the operating point of PV is dictated by the load or impedance. The impedance of load is described as below:

$$\mathrm{R_{load}} = \frac{\mathrm{V_O}}{\mathrm{I_O}} \tag{2-25}$$

Where: Vo is the output voltage and Io is the output current.

The optimal load for PV is described as:

$$R_{opt} = \frac{V_{MPP}}{I_{IMPP}} \tag{2-26}$$

Where: V_{MPP} and I_{MPP} are the voltage and current at the MPP respectively.

When the value of R_{load} matches with that of R_{opt}, the maximum power transfer from PV to the load will occur. These two are, however, independent and rarely matches in practice. The goal of the MPPT is to match the impedance of load to the optimal impedance of PV.

For an ideal CUK converter using equation (**2-24**),

$$V_S = \frac{1-D}{D} V_O \tag{2-27}$$

Using equation (**2-21**):

$$\frac{I_S}{I_O} = \frac{I_{L1}}{I_{L2}} = \frac{V_O}{V_S} \tag{2-28}$$

From equation (**2-27**) and equation (**2-28**),

$$I_S = \frac{D}{1-D} I_O \tag{2-29}$$

The input impedance of the converter is:

$$R_{in} = \frac{V_S}{I_S} = \frac{(1-D)^2}{D^2} * \frac{V_O}{I_O} = \frac{(1-D)^2}{D^2} * R_{load} \tag{2-30}$$

As shown in Figure 2-24, the impedance seen by PV is the input impedance of the converter (Rin). By changing the duty cycle (D), the value of Rin can be matched with that of Ropt. Therefore, the impedance of the load can be anything as long as the duty cycle is adjusted accordingly.

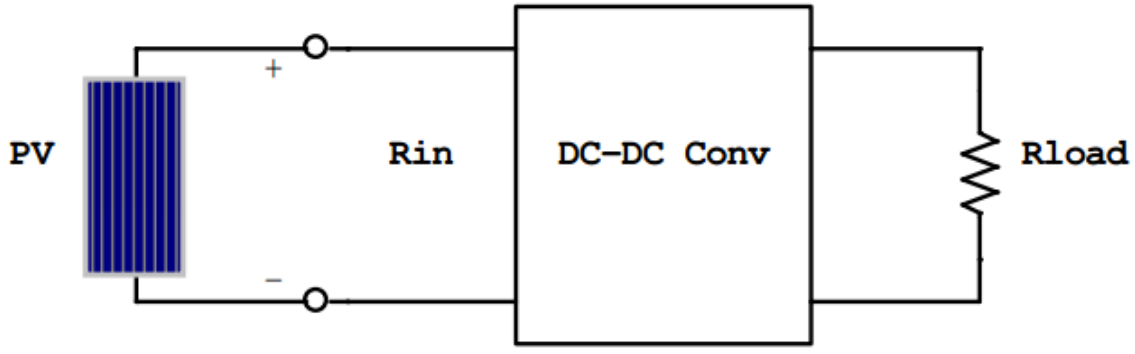

Figure 2-24: Input impedance of converter seen by PV[34]

2.13 Maximum Power Point Tracking Algorithms

Over the past decades many methods to find the MPP have been developed and published. These techniques differ in many aspects such as required sensors, complexity, cost, range of effectiveness, convergence speed, correct tracking when irradiation and/or temperature change, hardware needed for the implementation or popularity, among others. A complete review of 19 different MPPT algorithms can be found in [35].

Among these techniques, the P&O and the InCond algorithms are the most common. These techniques have the advantage of an easy implementation but they also have drawbacks, as will be shown later. Other techniques based on different principles are fuzzy logic control, neural network, fractional open circuit voltage or short circuit current, current sweep, etc. In the next section the most popular MPPT techniques are discussed.

2.13.1 Perturb and observe

The P&O algorithm is called "hill-climbing", but both names refer to the same algorithm depending on how it is implemented. Hill-climbing involves a perturbation on the duty cycle of the power converter and P&O a perturbation in the operating voltage of the DC link between the PV array and the power converter [35]. In the case of the Hill climbing, perturbing the duty cycle of the power converter implies modifying the voltage of the DC link between the PV array and the power converter, so both names refer to the same technique. In this method, the sign of the last perturbation and the sign of the last increment in the power are used to decide what the next perturbation should be. As can be seen in Figure 2-25, on the left of the MPP incrementing the voltage increases the power whereas on the right decrementing the voltage increases the power.

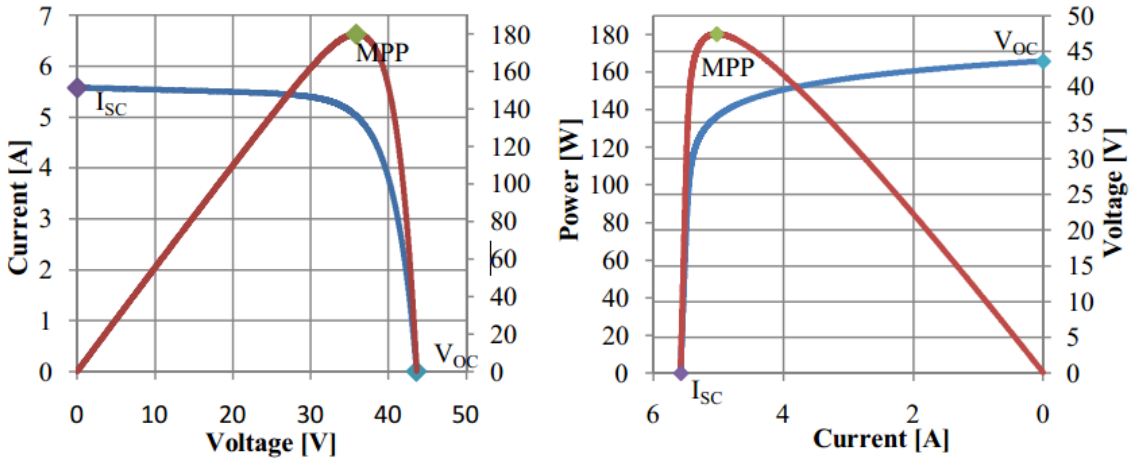

Figure 2-25: PV Panel Characteristics curves[34]

If there is an increment in the power, the perturbation should be kept in the same direction and if the power decreases, then the next perturbation should be in the opposite direction. Based on these facts, the algorithm is implemented [35]. The process is repeated until the MPP is reached. Then the operating point oscillates around the MPP. This problem is common also to the InCond method. A scheme of the algorithm is shown in Figure 2-26.

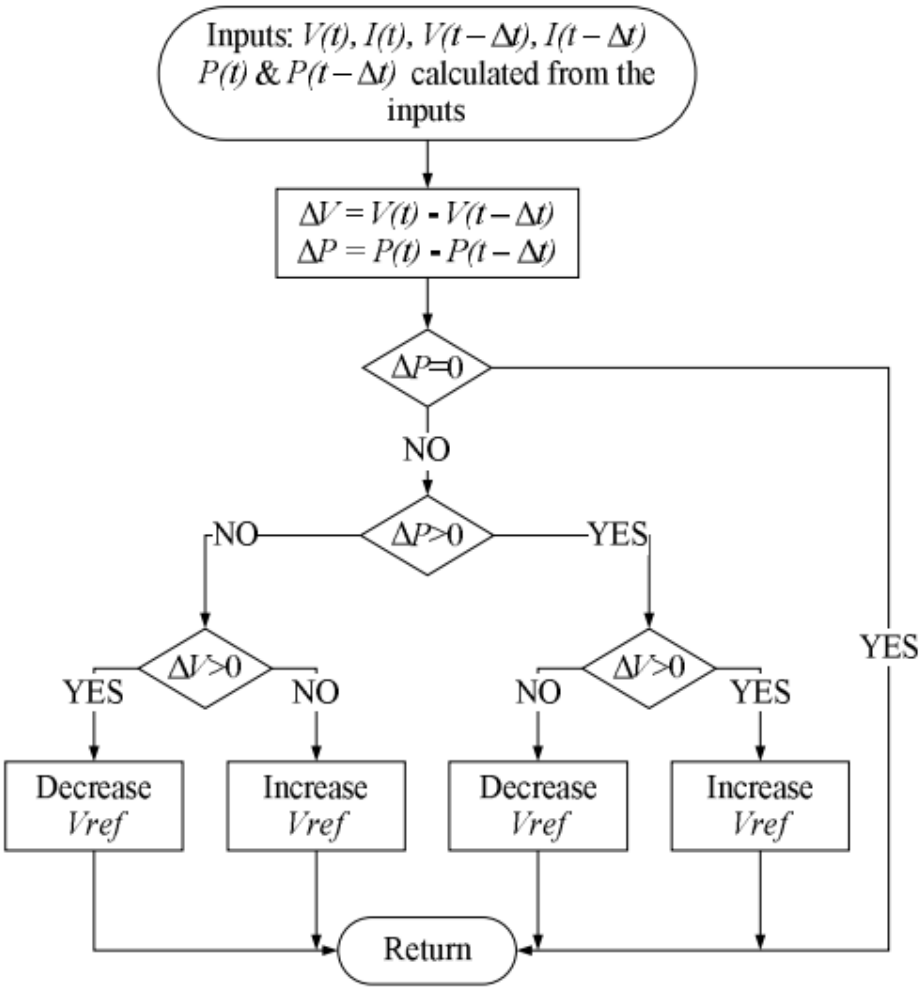

Figure 2-26: Flowchart of P&O algorithm[34]

2.13.2 Incremental conductance

The incremental conductance algorithm is based on the fact that the slope of the curve power vs. voltage (current) of the PV module is zero at the MPP, positive (negative) on the left of it and negative (positive) on the right, as can be seen in Figure 2-25:

- $\Delta V/\Delta P = 0$ ($\Delta I/ \Delta P = 0$) at the MPP
- $\Delta V/ \Delta P > 0$ ($\Delta I/ \Delta P < 0$) on the left
- $\Delta V/ \Delta P < 0$ ($\Delta I/ \Delta P > 0$) on the right

By comparing the increment of the power vs. the increment of the voltage (current) between two consecutives samples, the change in the MPP voltage can be determined. A scheme of the algorithm is shown in Figure 2-27.

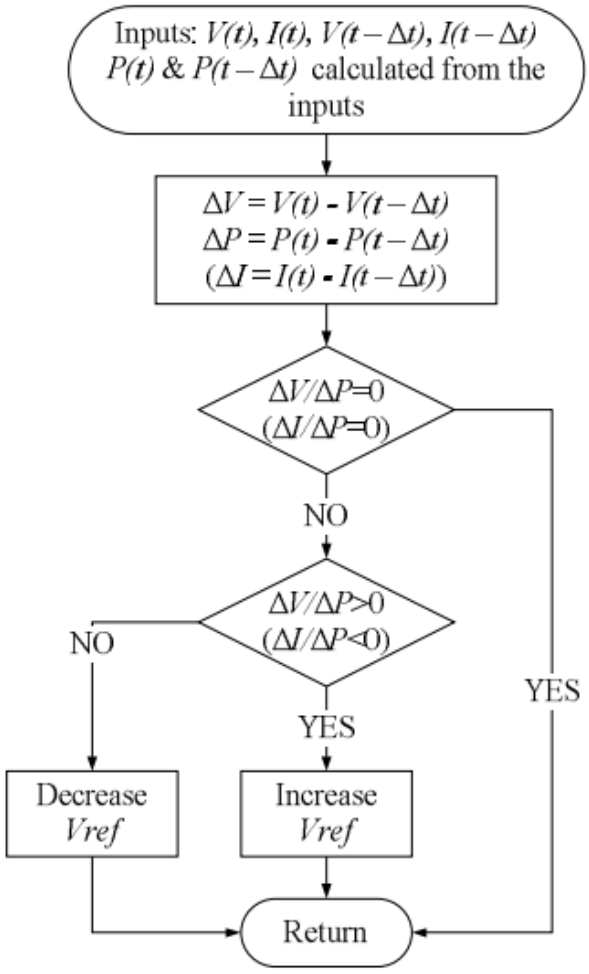

Figure 2-27: Flowchart of Incremental Conductance Algorithm[34]

In both P&O and InCond schemes, how fast the MPP is reached depends on the size of the increment of the reference voltage.

2.13.3 Drawbacks of P&O and Incremental Conductance and other algorithms

The drawbacks of these techniques are mainly two. The first and main one is that they can easily lose track of the MPP if the irradiation changes rapidly [36], [28, 37, 38]. In case of step changes they track the MPP very well, because the change is instantaneous, and the curve does not keep on changing. However, when the irradiation

changes following a slope, the curve in which the algorithms are based changes continuously with the irradiation, so the changes in the voltage and current are not only due to the perturbation of the voltage. As a consequence, it is not possible for the algorithms to determine whether the change in the power is due to its own voltage increment or due to the change in the irradiation.

The other handicap of both methods is the oscillations of the voltage and current around the MPP in the steady state [36], [38], [39] and [40]. This is due to the fact that the control is discrete, and the voltage and current are not constantly at the MPP but oscillating around it. The size of the oscillations depends on the size of the rate of change of the reference voltage. The greater it is, the higher is the amplitude of the oscillations. However, how fast the MPP is reached also depends on this rate of change and this dependence is inversely proportional to the size of the voltage increments. The traditional solution is a tradeoff: if the increment is small so that the oscillations decrease, then the MPP is reached slowly and vice versa, so a compromise solution has to be found.

To overcome these drawbacks some solutions have been published in recent years. Regarding the rapid change of the irradiation conditions, Sera et al. published in [37] an improved P&O method, called "dP-P&O", in which an additional measurement is performed without perturbation in the voltage and current. In this way, every three consecutive samples the effect of the perturbation in the voltage (current) and the effect of the change in the atmospheric conditions can be evaluated so that the increment in the power used in the algorithm only contains the effect caused purely by the MPPT algorithm. Then the correct decision about the direction of the next perturbation can be taken. The efficiency of the tracking is improved. Although the method was tested using irradiation slopes, they were not the ones developed in the new European Standard EN 50530 [41].

In relationship with the oscillations around the MPP in steady state, Zhang et al. developed in [39] a variable perturbation step for the P&O algorithm to reduce the oscillation around it. This modified P&O method determines also if the operating point is near to or far from the MPP and adjusts the size of the perturbation according to that: if the operating point is near to the MPP, the perturbation size is reduced and if the point

is far, then it is increased. This technique improves the convergence speed and reduces the oscillation around the MPP. A similar technique is found in [42]: a variation of the traditional P&O algorithm in which the amplitude of the voltage perturbation is adapted to the actual operating conditions: large perturbation amplitudes are chosen far from the maximum whereas small ones are used near the MPP. The developed algorithm requires initial panel identification and has to be tuned for each plant. With this technique the dynamic response and the steady state stability are improved. Unfortunately, the last two algorithms do not improve the tracking under changing irradiance conditions. Although the authors claim the performance is better, the algorithms have only been tested with irradiation step changes but not with irradiation ramps as developed in the European Standard mentioned above [41].

There is an another method entitled as "Fractional Open Circuit Voltage" which uses the approximately linear relationship between the MPP voltage (V_{MPP}) and the open circuit voltage (V_{OC}), which varies with the irradiance and temperature [35]:

$$V_{MPP} \approx k_1 V_{OC} \tag{2-31}$$

Where k_1 is a constant depending on the characteristics of the PV array and it has to be determined beforehand by determining the V_{MPP} and V_{OC} for different levels of irradiation and different temperatures. According to [35] the constant k_1 has been reported to be between 0.71 and 0.78. Once the constant of proportionality, k_1, is known, the MPP voltage V_{MPP} can be determined periodically by measuring V_{OC}. To measure V_{OC} the power converter has to be shut down momentarily so in each measurement a loss of power occurs. Another problem of this method is that it is incapable of tracking the MPP under irradiation slopes, because the determination of VMPP is not continuous. One more disadvantage is that the MPP reached is not the real one because the relationship is only an approximation.

To overcome these drawbacks, some solutions have beendeveloped, as is reported in [35]. For example, pilot cells can be used to obtain V_{OC}. They are solar cells that represent the PV array's cells and which are not used to produce electricity but to obtain characteristics parameters such as V_{OC} without interfering with the power converters. These pilot cells have to be carefully chosen and placed to represent the PV array

characteristics and the irradiation conditions. One drawback of using these pilot cells is that the cost of the system is increased. Depending on the application, this technique can be used because it is very easy to implement and it is cheap - it does not require DSP or microcontroller control and just one voltage sensor is used [35]. However, according to [35] this method is not valid under partial shading of the PV array because then the constant k1changes. To update then k_1 a voltage sweep is developed though this increases the complexity of the system, the cost increases and there are more power losses during the sweep. Just like in the fractional open circuit voltage method, there is another method called as "Fractional Short Circuit Current", where the following relationship has been assumed:

$$I_{MPP} \approx k_2 I_{SC} \tag{2-32}$$

The coefficient of proportionality k_2 has to be determined according to each PV array, as in the previous method happened with k_1. According to [35] the constant k_2 has been reported to be between 0.78 and 0.92. Measuring the short circuit current while the system is operating is a problem. It usually requires adding an additional switch to the power converter to periodically short the PV array and measure I_{SC}. In [43]I_{SC} is measured by shorting the PV array with an additional field-effect transistor added between the PV array and the DC link capacitor. One other option is shown in [44]: a boost converter is used and the switch of the converter is used to short the PV array. Short circuiting the PV array also leads to a loss of power. One last handicap is that the real MPP is not reached because the proportional relationship is an approximation.

The amount of literature presenting slight modifications of the existing methods or adapting them to different hardware configurations is so extensive that it is not possible to present it in this thesis. In any case, none of the solutions reviewed before solves the problems satisfactorily and none has been tested under the slopes developed in [41] to test the dynamic efficiency of the MPPT algorithms. These profiles simulate rapid environmental changes such as clouds. It is very important to track the MPP during these situations to obtain the maximum power from the PV module. As will be shown in the next chapter, this thesis proposes a new algorithm so that the tracking under irradiation profiles containing slopes is very good.

Chapter 3: Development and design of proposed MPPT Algorithm, Controller and mathematical modeling of motor-pump load

3.1 Introduction

In this chapter, the proposednew MPPT algorithm has been presented. The main two drawbacksof existing algorithms as discussed in the previous chapter are large oscillations around MPP point and movement towards wrong direction while searching MPP point due to rapid irradiance changes have been addressed andresolved using the newly designed algorithm. It is as simple as the normal P&O method, but also, far better than that in speed of convergence. Unlike the IncCond method's complex structure, the developed algorithm is efficiently simple by offering very accurate tracking under varying weather conditions.

Figure 3-1, the flowchart of the proposed algorithm, depicting the construction of the algorithm. In developing the algorithm, a straight line approximation technique is utilized which is based on the P-V curve shapes. There are no evidences of significantly different P-V curve shape rather inverted tilted 'V'. So, the developed algorithm can be employed universally for a controller coupled with any kind of PV panel without taking panel's preset values. The steps in the developed flowchart in Figure 3-1 hold the following description.

1. At first, it senses voltage V_1 and I_1 by voltage and current sensor, respectively, and measure the power, P_1. Then perturb the voltage by the small amount, b and take another voltage, V_2. Measure the power, P_2.
2. If $\Delta P = P_2 - P_1 > 0$, the operating point lies at the left side of MPP point, else the operating point will be at the right side of MPP point.
3. It perturbs the voltage by a large amount, c and sensed the new voltage, V_3. By small perturbation b, measure voltage V_4 and calculate $\Delta P = (P_4 - P_3)$.

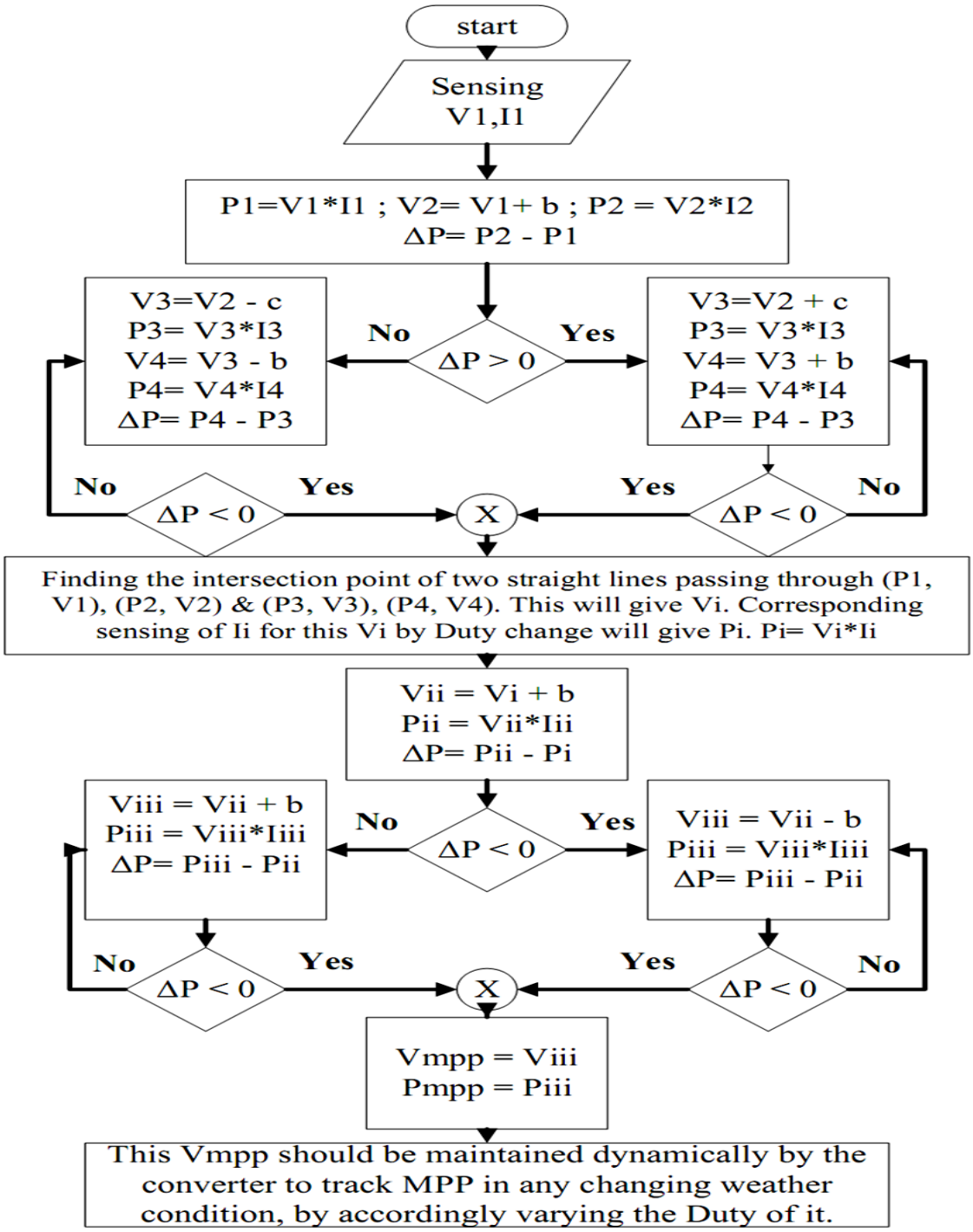

Figure 3-1: Flowchart of Developed algorithm

4. If $\Delta P<0$, we found our desired four points (V_1, P_1), (V_2, P_2) and (V_3, P_3), (V_4, P_4) to draw the two straight lines. We will find then the intersecting point V_i. If $\Delta P>0$, we need to repeat Step 3 until we get $\Delta P>0$.
5. The point V_i is not the desired MPP point, rather it is very close to MPP. To track this, we need to perturb the voltage by small amount b and get ΔP again.
6. If $\Delta P<0$, we are at the right side of MPP, else we are at the left side of MPP point.
7. If we are at the left side of MPP ($\Delta P>0$), the algorithm will keep on perturbing the voltage by small amount 'b' to the right side. Once $\Delta P<0$, the algorithm stops and P_{iii} is our desired MPP point. However, if it starts from the right side of MPP ($\Delta P<0$), the algorithm will then keep on perturbing the voltage by small amount 'b' to the left side. Once $\Delta P<0$ is satisfied, the algorithm stops and P_{iii} is the desired MPP point.

3.2 Mathematical Model of the Proposed Algorithm

In the developedmethod, MPP can be tracked very quickly and this operation is graphically illustrated in Figure 3-2. To understand the proposed algorithm, let's take the operating point P_1 which is left side of MPP point. By small perturbation of voltage, another point P_2 can be found as:

$$\Delta P = P_2 - P_1 > 0 \tag{3-1}$$

Now, by straight line approximation, we can write an equation:

$$P = m_1 V + C_1 \tag{3-2}$$

Where: $m_1 = \frac{P_2 - P_1}{V_2 - V_1}$ and $c_1 = \frac{V_1 P_2 - V_2 P_1}{V_2 - V_1}$

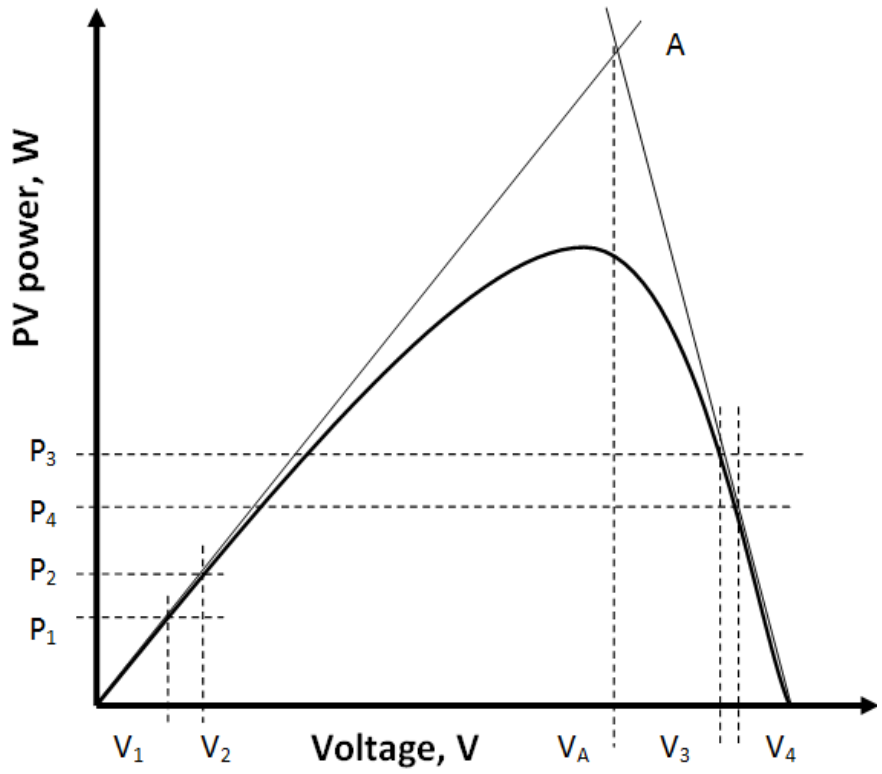

Figure 3-2: Straight Line approach to find the MPP point

Now by taking another two points in the right side of MPP where the following condition does match, another equation can be written also.

$$\Delta P = P_4 - P_3 < 0 \tag{3-3}$$

$$P = m_2 V + C_2 \tag{3-4}$$

Where: $m_2 = \frac{P_4 - P_3}{V_4 - V_3}$ and $c_1 = \frac{V_3 P_4 - V_4 P_3}{V_3 - V_4}$

By solving equations (**3-2**) and (**3-4**), the intersecting point V_A can be found as follows:

$$m_1 V + C_1 = m_2 V + C_2 \tag{3-5}$$

$$V_A = \frac{C_2 - C_1}{m_1 - m_2} \tag{3-6}$$

After getting V_A which should be near to MPP point, the algorithm would reach to MPP point very fast according to Figure 3-1.

3.2.1 Response of the proposed algorithm when Irradiance increases rapidly

Here, the reaction towards rapid changing weather condition has been analyzed. In Figure 3-3, it is visualized, how the normal P&O method fails for a large variation in irradiance. Starting from an operating point located at P_1 (right side of MPP) we see, after a little perturbation, the new value is P_2. If the irradiance does not change during the perturbation, then P_2 will be lying on the same curve with G_1, I_1. So:

$$\Delta P = P_2 - P_1 < 0 \tag{3-7}$$

$$\Delta V = V_k - V_{k-1} > 0 \tag{3-8}$$

Consequently, P&O algorithm will drive the operating point to leftward according to Figure 2-26, which is the correct direction. However, if the irradiance changes rapidly during the perturbation, then P_2 point should lie on the I_2 curve at corresponding V_K. Let's call it P_2'.

$$\Delta P = P_2' - P_1 > 0 \tag{3-9}$$

$$\Delta V = V_k - V_{k-1} > 0 \tag{3-10}$$

Then, the operating point would be driven into the right side by P&O algorithm according to Figure 2-26, even though it should have driven it to the left and eventually driving the point in the wrong direction.

Whereas the developed method would draw the straight line passing through these two points P_1, P_2' and will take another two points P_3', P_4' on I_2 curve and draw the straight line. Getting the intersection point, V_A of these two straight lines on the I_2 curve, the algorithm drives the operating point to move to leftward to reach the MPP point on I_2 curve according to Figure 3-1.

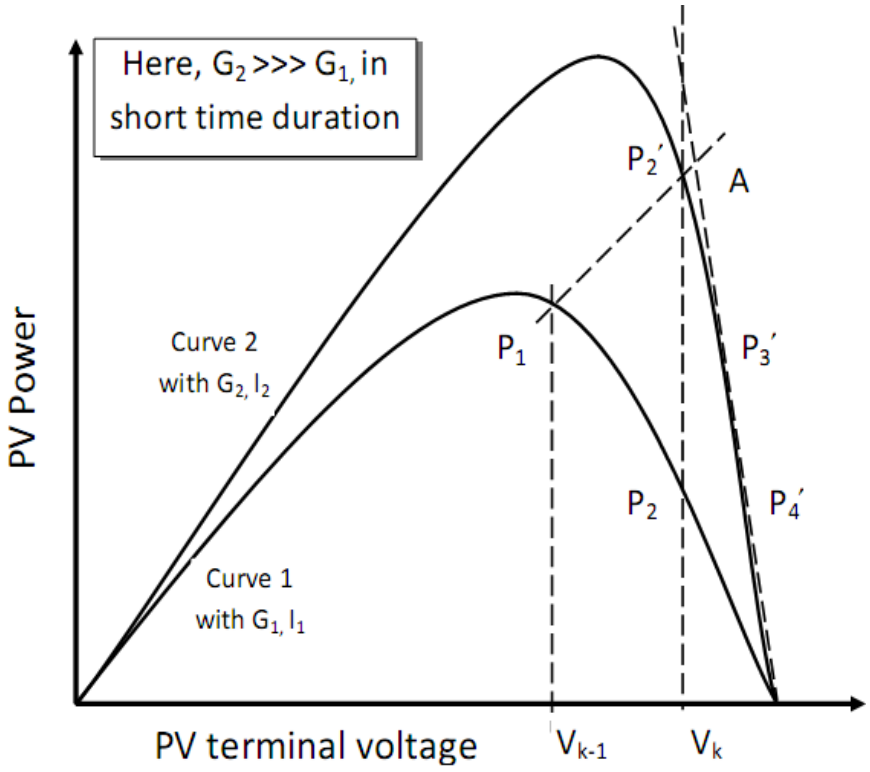

Figure 3-3: Responseof proposed method for rapidly increasing irradiance

3.2.2 Response of the proposed algorithm when Irradiance decreases rapidly

In this section, the response of the proposed algorithm when irradiance decreases rapidly, has been analyzed. As we see in the Figure 3-4, irradiance drops from G_1 to G_2. If the operating point of PV panel initially lies at G_1 at $P_1$and perturbation drags the operating point at P_2, assuming irradiance does not change during that perturbation, then

$$\Delta P = P_2 - P_1 > 0 \tag{3-11}$$

$$\Delta V = V_2 - V_1 < 0 \tag{3-12}$$

Since $\Delta P > 0$, $\Delta V < 0$ P&O algorithm would go towards leftward to reach at the MPP points which is the correct direction. However, during the perturbation if irradiance changes sharply as it happens here, from G_1 to G_2 then

$$\Delta P = P_2' - P_1 < 0 \tag{3-13}$$

$$\Delta V = V_2' - V_1 < 0 \tag{3-14}$$

Since $\Delta P < 0, \Delta V < 0$, P&O algorithm would go rightward, subsequently, goes away from MPP point. In contrast, the proposed algorithm would solve line: P_1P_2' and line: $P_3'P_4'$to get the intersecting point denoted by A in the Figure 3-4 which is very close to MPP point and then eventually it will reach to MPP point according to the proposed algorithm illustrated in Figure 3-1.

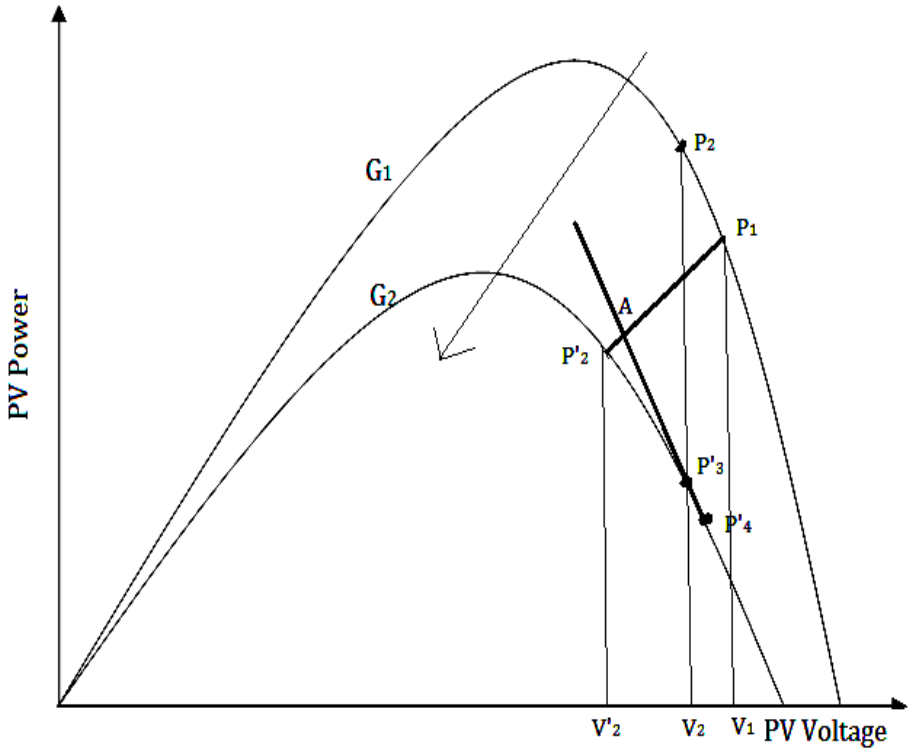

Figure 3-4: Response of proposed method for rapidly decreasing irradiance

3.3 The Controller Design

The developed system works in two modes, namely, MPP mode and Protection mode, which is depicted inFigure 3-5. The protection scheme is required in order to

protect the motor-pump load from over voltage or over current. Here, the only output voltage and current will be extracted using voltage and current sensors while duty cycle would be varying. The system utilizes SD series pump having a rated power of 120 W and at a rated voltage of 30 V [45].. In running the system, the protection voltage has been set to 30 V and protection current at 4 A, for making a safer zone of operation.

Whenever Irradiance and temperature changes, accordingly MPP points on P-V curves also changes. For high irradiance, MPP point can easily exceed the rated power of the motor-pump load; however, the integration of the controller does not allow the system to go beyond the rated power, making sure the protection of the whole system.

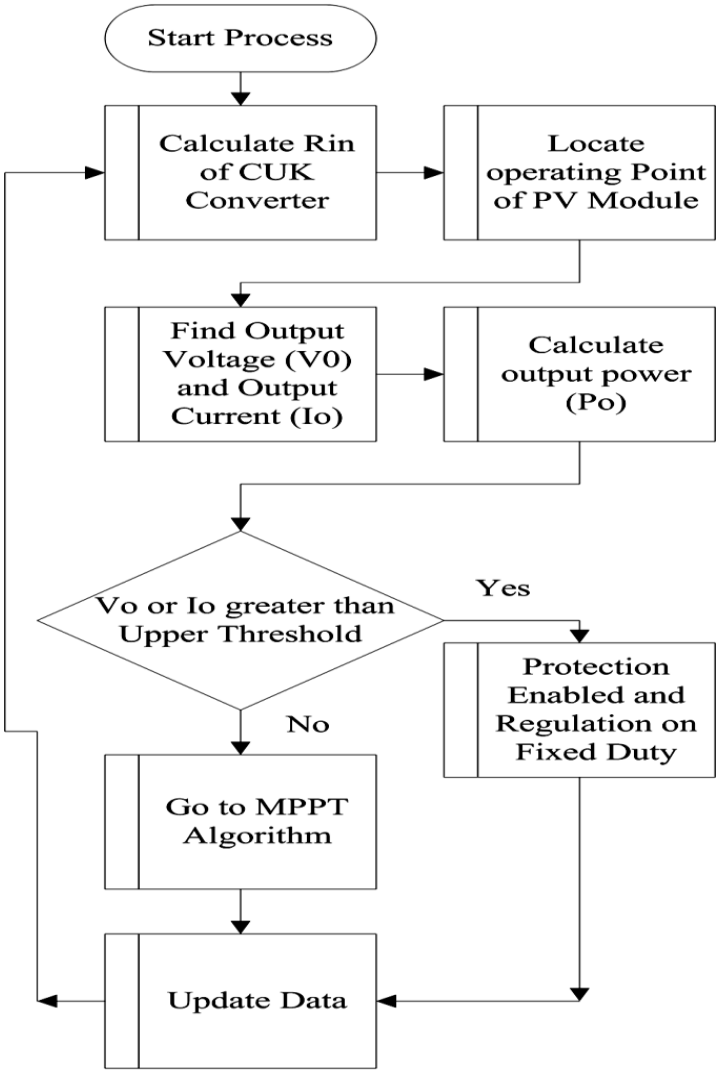

Figure 3-5: Operational Flowchart of the controller

3.4 DC Motor-Pump Load and its mathematical modeling

The flow rate of water in positive displacement pumps is directly proportional to the speed of the pump motor, which is governed by the available driving voltage[26]. They have constant load torque to the pump motors, and it is expressed by the total dynamic head in terms of its equivalent vertical column of water; for example, vertical lift and friction converted to vertical lift [45]. Figure 3-6shows the relationship between flow rate of water and total dynamic head for the Kyocera SD 12-30 solar pump[26]. It has the normal operating voltage of 12 to 30V and the maximum power of 120W.

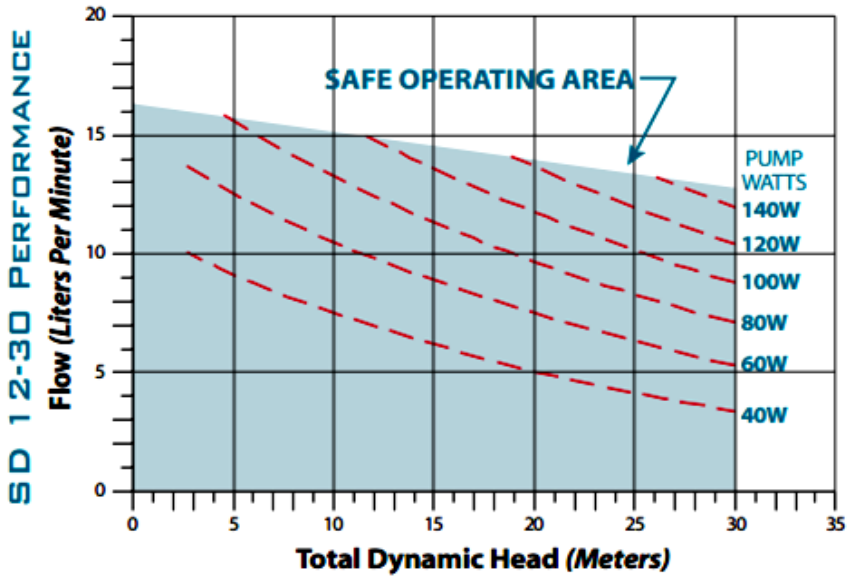

Figure 3-6: SD 12-30 water pump performance chart[26]

In this section, a mathematical model of Kyocera SD 12-30 DC motor-pump load has been established using practical data taken from [46]in their pumping test facility. Figure 3-7Figure 3-7 shows the experimental values obtained with Positive Displacement Pump, which represents the dependence of the current versus the voltage for each head which has been found to be linear.

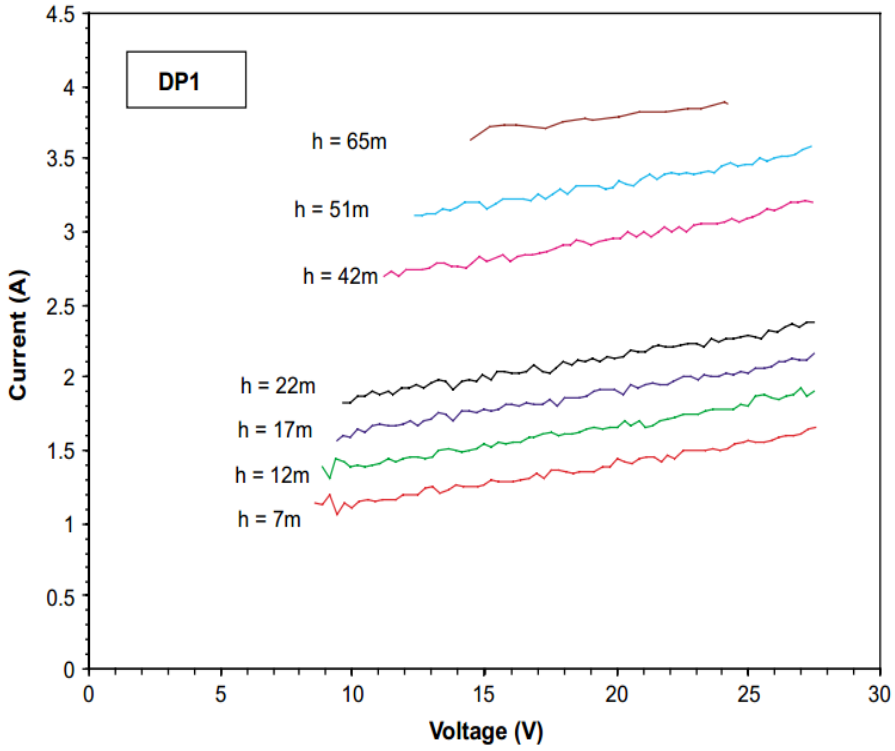

Figure 3-7: I-V characteristics graph of motor-pump load at different heads [46]

A simplified model is developed to obtain the parameters of Figure 3-7in the following ways:

From that experimental I-V curve inFigure 3-7, it's very vivid that the relationship between current and voltage is linear. So, it can be modeled as:

$$I = a * V + b \tag{3-15}$$

The slope a, is same for every different head.FromFigure 3-7, it is clear that b is a linear function of heads. So b can be modeled as:

$$b(h) = b_1 * h + b_o \tag{3-16}$$

By taking 3 different heads (h = 7m, h = 12m, h = 17m) and using MATLAB curve-fitting facilities, the following 3 equations have been developed:

$$I = 0.0296 * V + 0.82 \quad (3\text{-}17)$$

$$I = 0.03 * V + 1.08 \quad (3\text{-}18)$$

$$I = 0.0287 * V + 1.35 \quad (3\text{-}19)$$

From those above three equations, the value of 'a' has been chosen as 0.03 and 'b' has been modeled as:

$$b = 0.053 * h + 0.4473 \quad (3\text{-}20)$$

So, combining the equations generate the following one:

$$I = 0.03 * V + 0.053 * h + 0.4473 \quad (3\text{-}21)$$

Now, for a head of 22 m and using curve fitting tool in MATLAB provides the following final modeling equation of motor-pump load:

$$Rload = 0.0001 * V_o^3 - 0.0096 * V_o^2 + 0.6087 * V_o + 0.0131 \quad (3\text{-}22)$$

Where: V_O is the output voltage of converter. This equation characterizes the DC pump motor, and MATLAB uses it in the simulations.Figure 3-8 illustrates the graphical representation of the modeling equation.

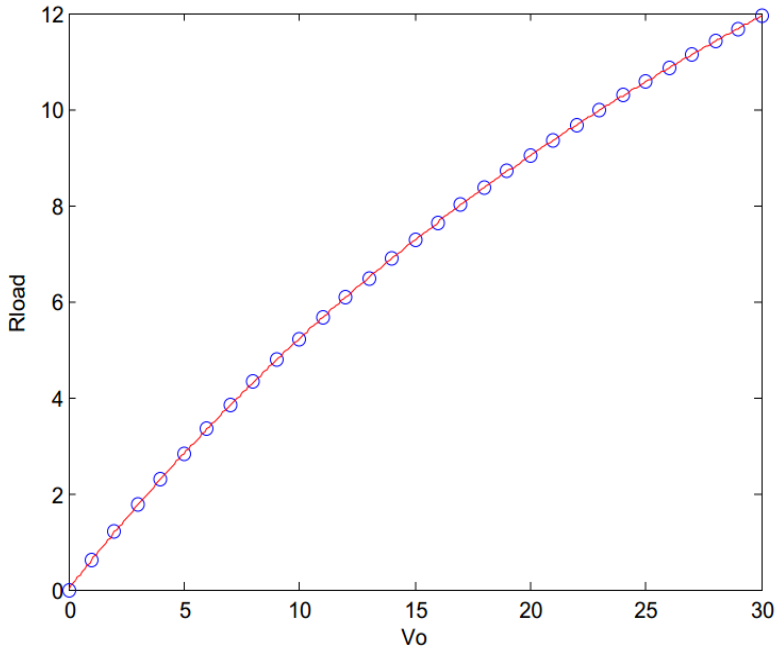

Figure 3-8: MATLAB plot of motor-pump modeling equation

3.5 Validation of the Proposed MPPT Algorithm

In order to validate the developed model, the performance of the model has been tested to all the important irradiance slopes developed in the standard [41].Figure 3-9, Figure 3-10, Figure 3-11,Figure 3-12 portray the performance of the developed algorithm under irradiation ramps with gradients of very steep inFigure 3-9, 0.5 W/m^2/s inFigure 3-10, 5 W/m^2/s in Figure 3-11and 20, 50, 100 W/m^2/s inFigure 3-12. From those figures, it's very clear that the quality of the MPP tracking is very good and it is similar with all ramps. There is a small lag in all the cases, but it is acceptable because the algorithm has to first detect how the irradiance varies and then set the reference voltage accordingly. Another noticeable fact in all the figures is that the current always tracks the irradiance changes accurately whereby the voltage is either lagging or leading the MPP point by a very small amount. It makes sense since current is linearly proportional to irradiation which is described in chapter-2. It is almost impossible to detect the exact MPP voltage because the algorithm has to use an epsilon value which is less than a preset value (the difference between exact VMPP and found VMPP which is

very close to exact MPP but not equal) to get very close to exact VMPP point. Therefore the detected VMPP point lies either before or after the exact VMPP point, however, very close.

3.5.1 Very Steep Gradient:

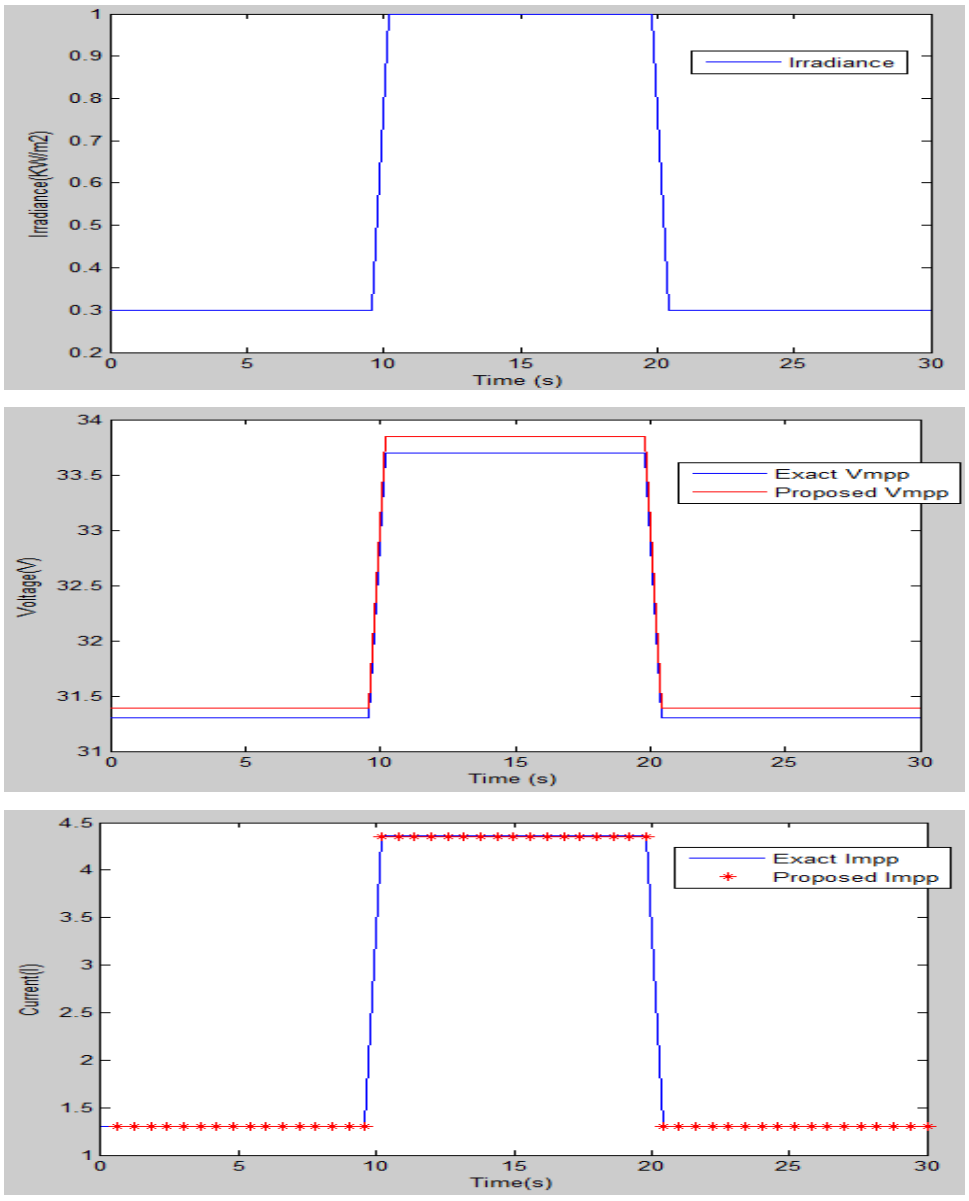

Figure 3-9: Performance of the developed algorithm under step changes from 300 to 1000 W/m^2 irradiance change

3.5.2 Gradient of 0.5 W/m^2/s

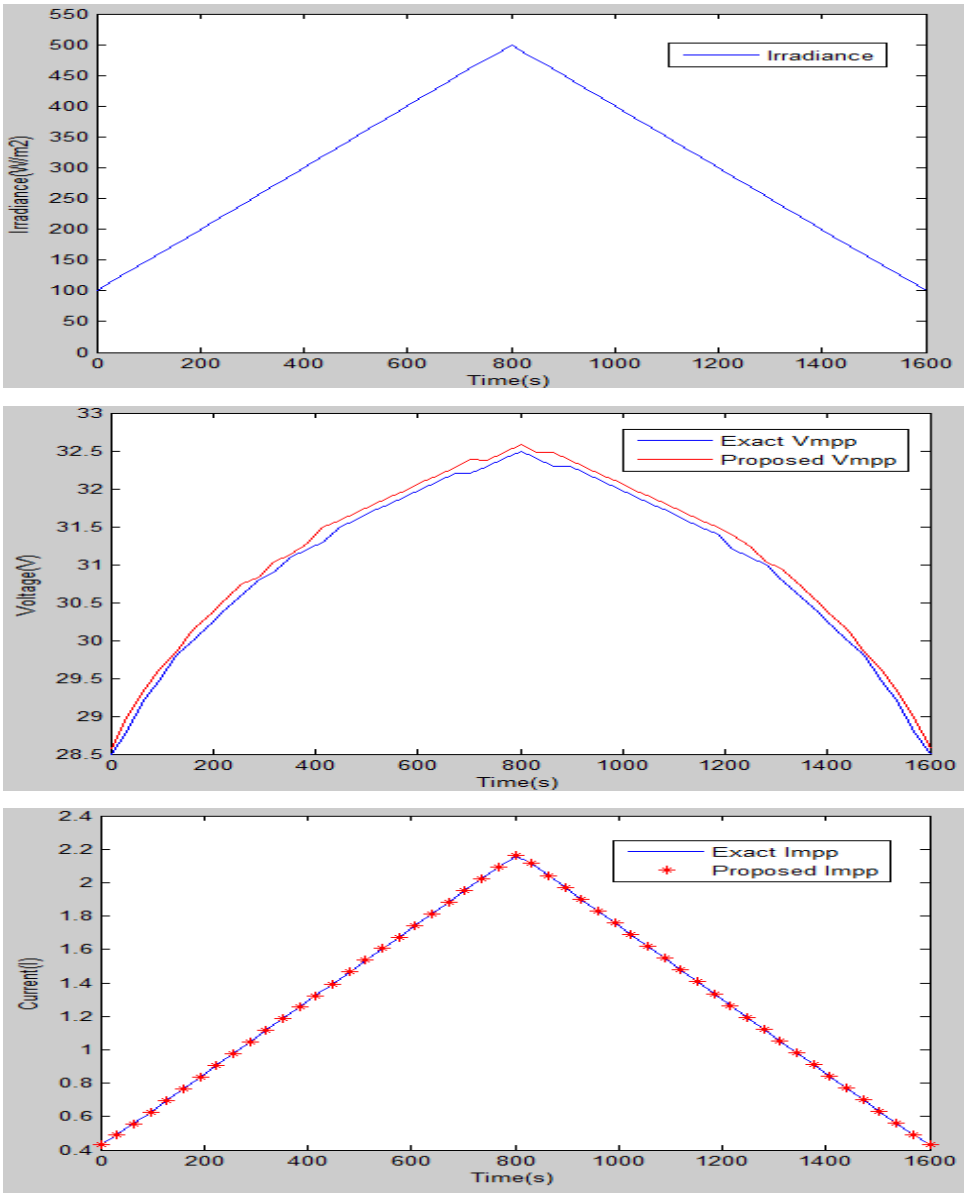

Figure 3-10: Performance of the developed algorithm under the slope of 0.5 W/m^2/s from 100 to 500 W/m^2 irradiance change

3.5.3 Gradient of 5 W/m^2/s

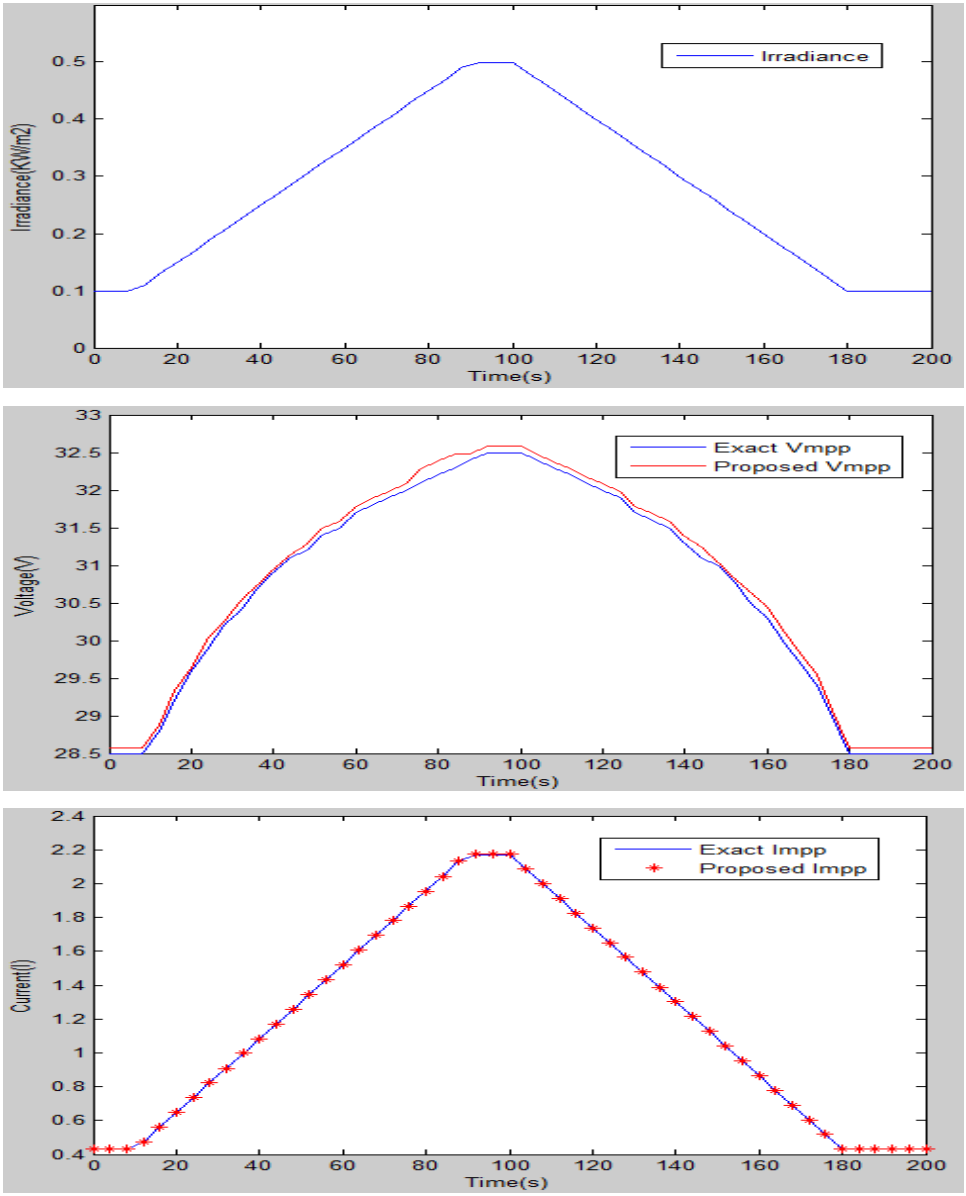

Figure 3-11: Performance of the developed algorithm under the slope of 5 W/m^2/s from 100 to 500 W/m^2 irradiance change

3.5.4 Gradient of 20, 50, 100 W/m^2/s

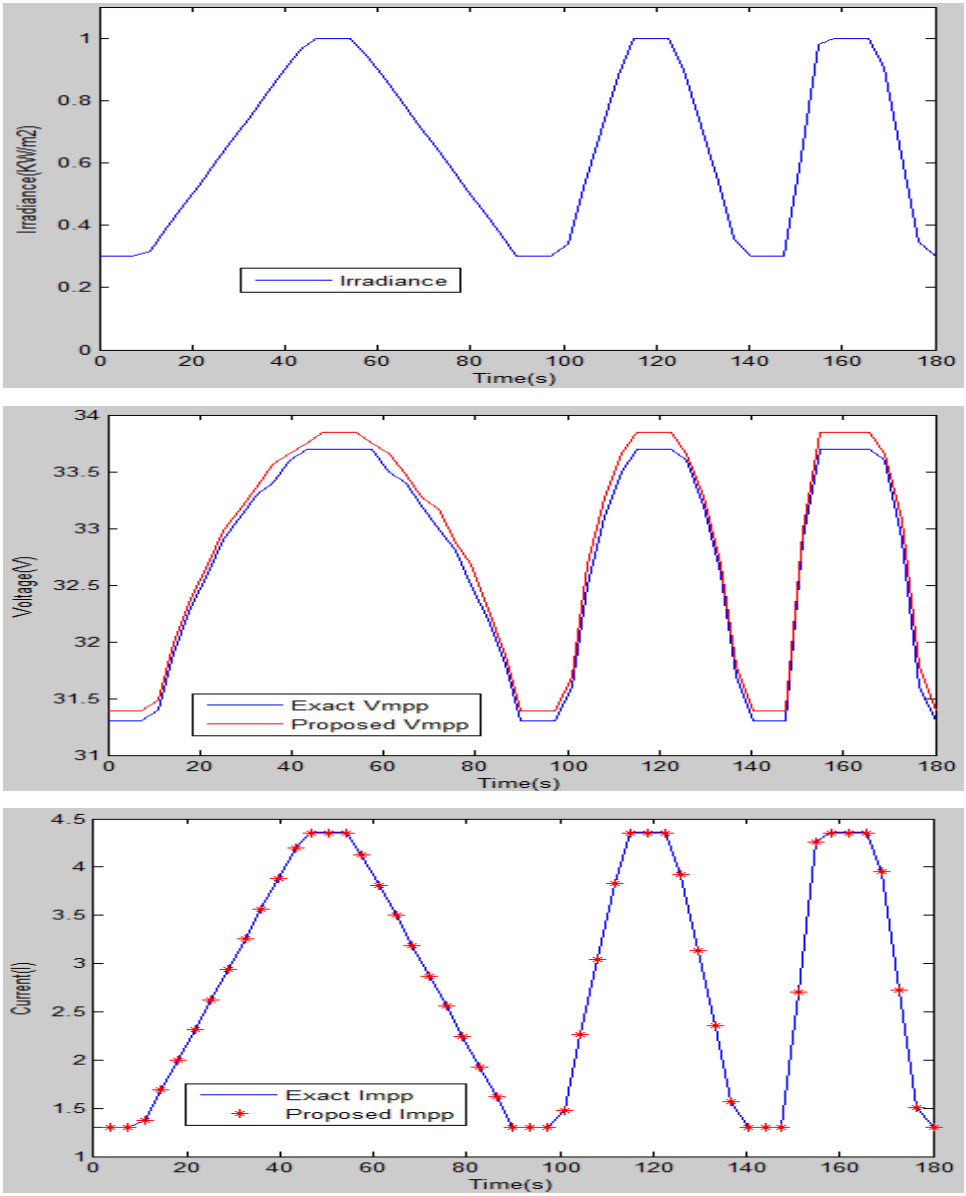

Figure 3-12: Performance of the developed algorithm under the slope of 20, 50, 100 W/m^2/s from 300 to 1000 W/m^2 irradiance change

3.5.5 Validation of the proposed MPPT algorithm for duty cycle and MPP point under varying weather conditions:

In the table below, irradiance has been changed from 0.3 KW/m^2 to 1.2 KW/m^2 along with temperature from 0^{o}C to 40^{o}C, in order to check the response of the proposed model at duty cycle and MPP points. It is very clear from

Table 3-1 that the duty cycles and MPP points of the proposed model are very close to exact duty cycles and MPP points.

Table 3-1: Closeness of Duty cycle and MPP point of the proposed method with exact values under changing irradiance and temperature conditions.

(G,T)in (KW/m^2, ^oC)	D_exact	D_proposed	P_exact	P_proposed
(0.3, 0)	0.3177	0.3201	46.8442	46.8059
(0.3, 10)	0.3228	0.3200	44.8187	44.7739
(0.3, 20)	0.3275	0.3280	42.7801	42.7802
(0.5, 0)	0.3725	0.3720	80.4209	80.4200
(0.5,10)	0.3774	0.3780	77.1584	77.1546
(0.5,20)	0.3824	0.3820	73.8728	73.8702
(0.8,10)	0.4314	0.4320	126.4301	126.4219
(0.8,20)	0.4367	0.4350	121.3375	121.3139
(0.8,30)	0.4415	0.4420	116.2146	116.2139
(1.0,20)	0.4627	0.4620	153.1360	153.1256
(1.0,30)	0.4683	0.4680	146.8280	146.8288
(1.0,40)	0.4734	0.4720	140.4862	140.4611
(1.2,20)	0.4848	0.4850	184.8904	184.8890
(1.2,30)	0.4897	0.4890	177.4167	177.4042
(1.2,40)	0.4948	0.4950	169.9001	169.9017

Chapter 4: Results and Discussion

4.1 MPPT Simulation with Resistive Load (With Proposed MPPT Algorithm)

The selection of the Developed algorithm permits the use of the output sensing direct control method which eliminates the input voltage and current sensors which makes the system simple and low cost.

The simulated system consists of the BP SX 150S PV model, the ideal CUK converter, the MPPT control, and the resistive load (5 Ω). The MATLAB function that models the PV module is the following:

$$I_a = tt(V_a, G, T) \tag{4-1}$$

The function, $tt(V_a, G, T)$, calculates the module current (I_a) for the given operating module voltage (V_a), irradiance (G in KW/m^2), and module temperature (T in ^oC).

The operating point of the PV module is located by the following relationship which has been described in chapter -2:

$$R = \frac{V_a}{I_a} \tag{4-2}$$

$$V_a = I_a * R \tag{4-3}$$

$$V_a - I_a * R = 0 \tag{4-4}$$

$$V_a - tt(V_a, G, T) * R = 0 \tag{4-5}$$

Equation (**4-5**) has one unknown variable which is Va that can be solved using fzero() function in MATLAB once G,T,R values are known. G and T are the state variables of the PV module which are always available for a particular irradiance value and temperature. R can be calculated using following equation as mentioned in chapter – 2.

$$R = \frac{(1-D)^2}{D^2} * R_{load}$$

In the way to investigate the responses with load, practical Irradiance data have also been taken from the country report of SWERA, Bangladesh (Sunny Day)[47]for 12 hour period from 6 am to 6 pm in the month of April. For cloudy day data, Global (total) irradiance on a horizontal surface in Greenbelt, MD (Thekaekara, 1976)[48]has been chosen. This Global Horizontal Irradiance (GHI) is plotted for sunny day data and cloudy day data inFigure 4-1and Figure 4-2respectively in the process of verifying the MPPT algorithm.

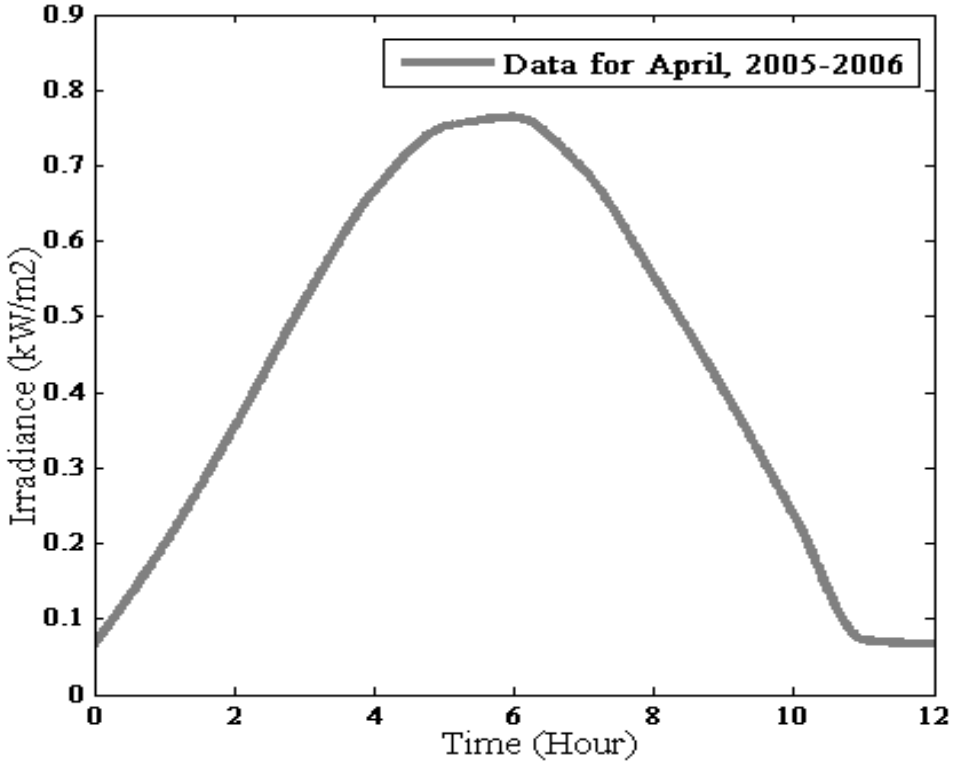

Figure 4-1: Sunny Day Irradiance Data from 6 AM to 6 PM

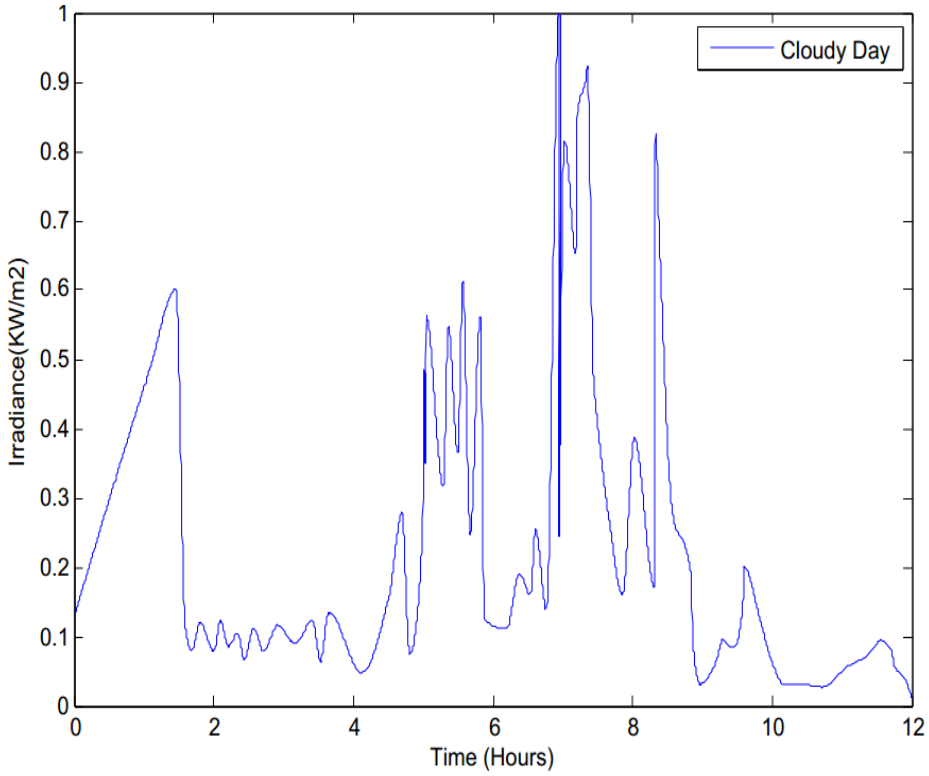

Figure 4-2: Cloudy Day Irradiance Data from 6 AM to 6 PM

4.1.1 Simulations of resistive load without protection

Figure 4-3, Figure 4-4, Figure 4-5 and Figure 4-6 show the validation of the developed algorithm for a Sunny day in four different graphs. InFigure 4-3, module power vs module voltage graph has been plotted when irradiance was changing from 0.6 KW/m^2 to 0.8 KW/m^2. Though the maximum power output from the PV panel is 150 W, it's providing approximately 120 W for the irradiance data chosen. The red dots shown in Figure 4-3are the exact MPP points and the green curve is the output of the developed algorithm. It's very clear from the figure that the developed algorithm has correctly identified the exact MPP points. The same reflection happened inFigure 4-4 where the pv panel current and voltage graph is shown.Figure 4-5shows how the module power can be varied just by varying the duty cycle which ensures that the operating point of the PV panel can be varied by changing the duty ratio. Figure 4-6 shows the output voltage versus output current characteristics which has been found as linear as it is supposed to

be for a resistive load. Figure 4-7 and Figure 4-8illustrate the validation of the developed algorithm even for a cloudy day data set.

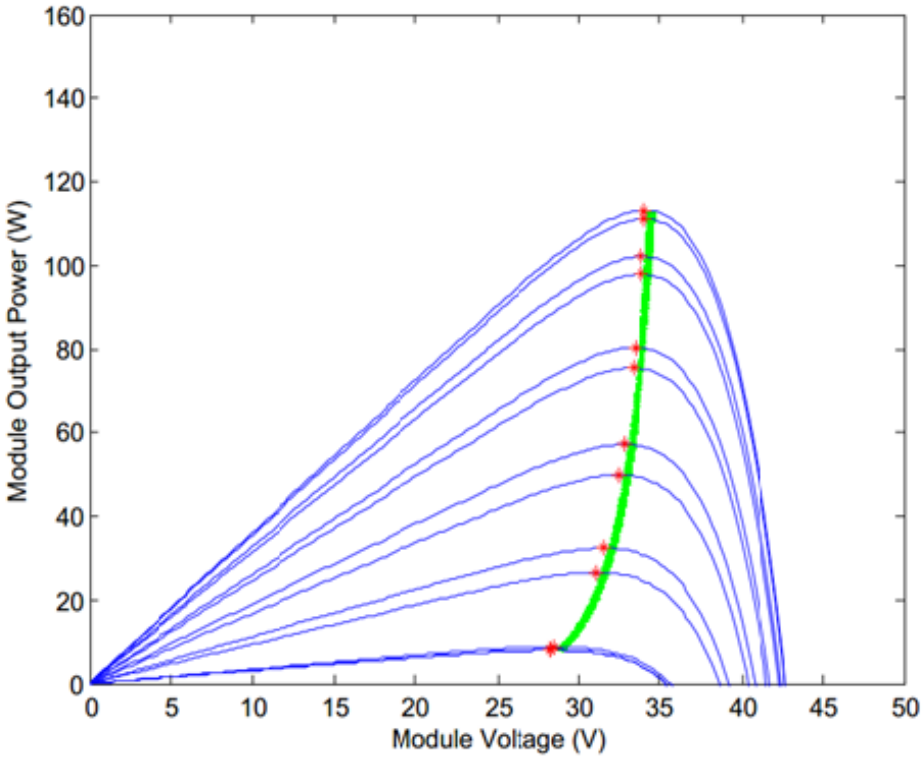

Figure 4-3: PV panel Output Power vs PV output voltage

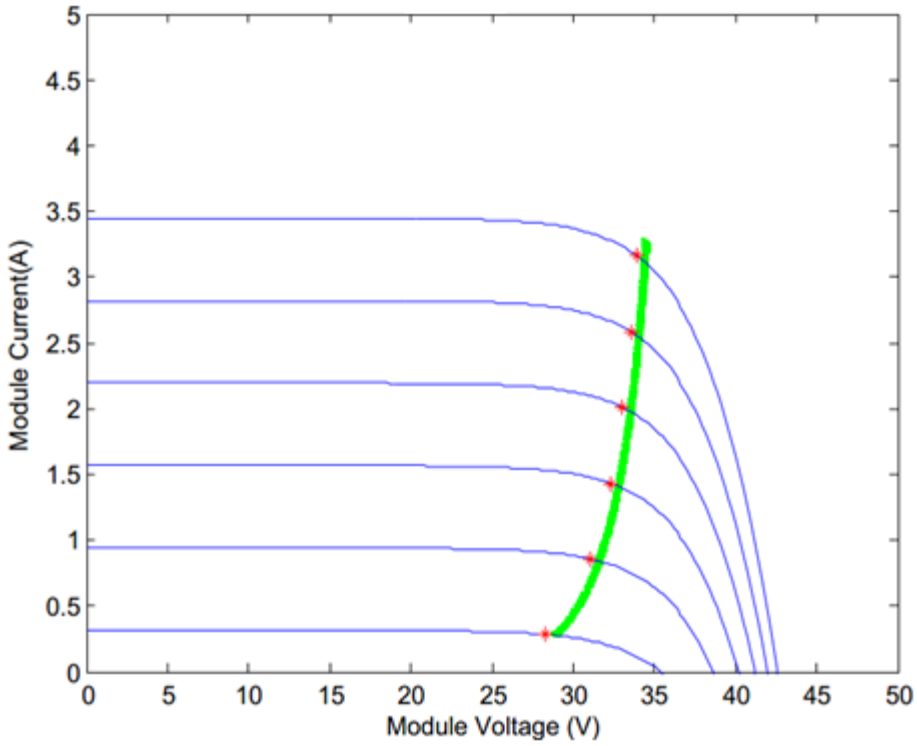

Figure 4-4: PV panel Current vs PV panel voltage

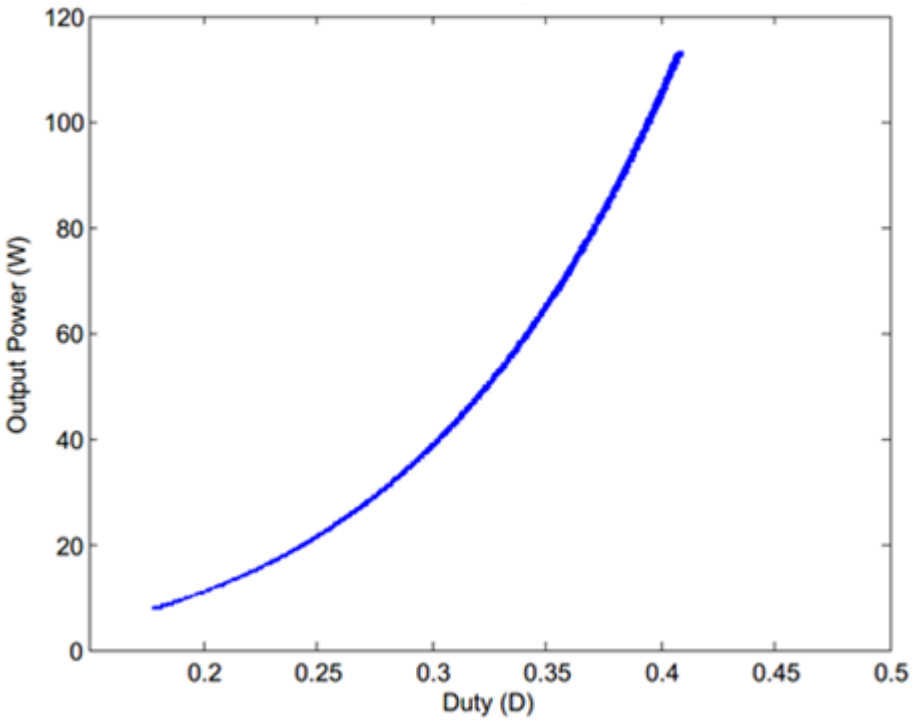

Figure 4-5: Duty vs Output Power

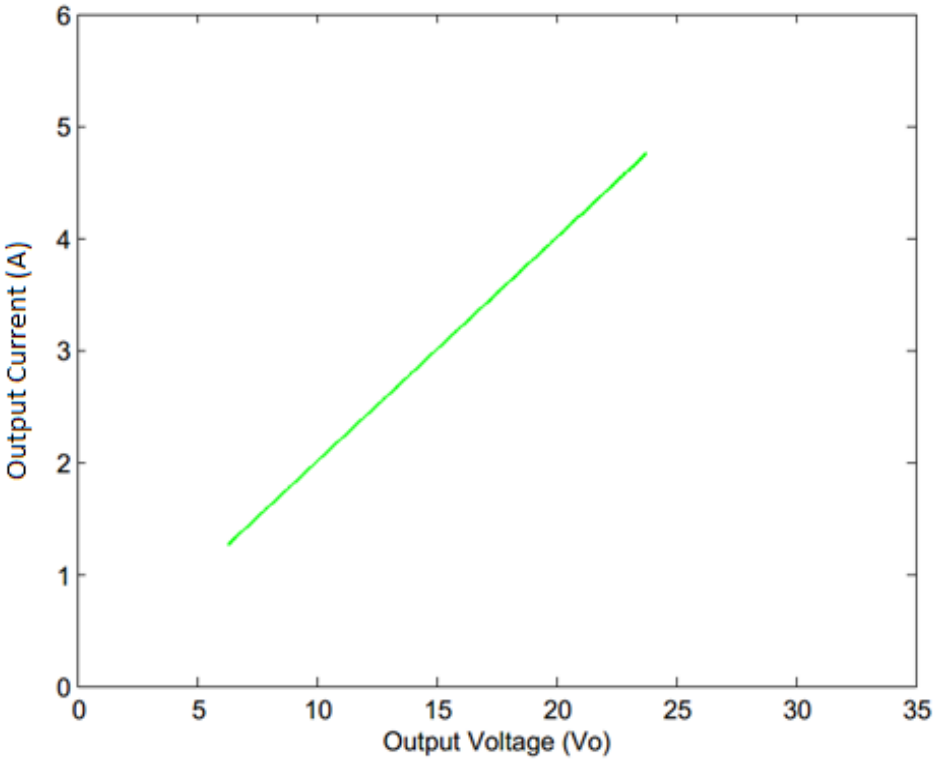

Figure 4-6: Output Current vs Output Voltage

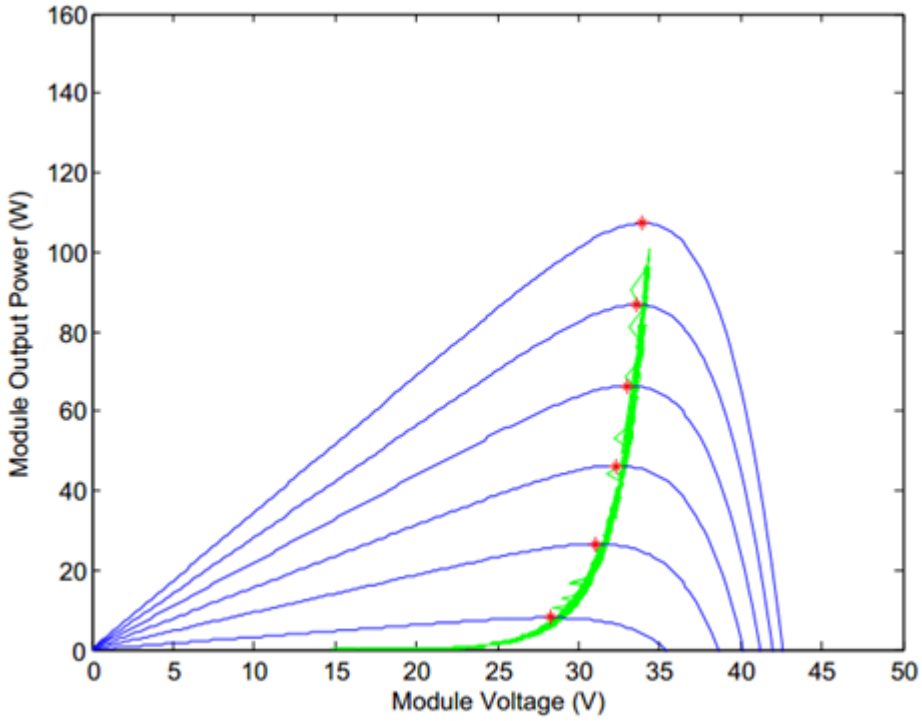

Figure 4-7: Panel voltage vs Power for a Cloudy Day

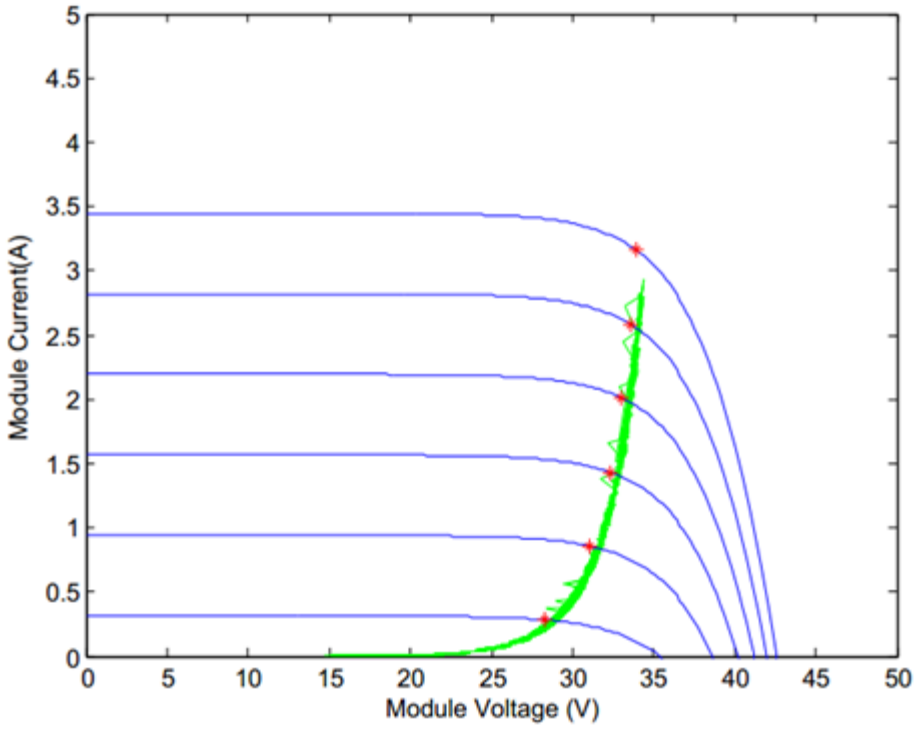

Figure 4-8: Panel voltage vs Current for a Cloudy Day

4.1.2 Simulations of resistive load with protection

As mentioned in previous chapter, the control algorithm contains two loops: the main loop for MPPT and another loop for output protection. During the normal operation, it operates in MPPT mode. When the load cannot absorb all the power produced by PV, its voltage or/and current will exceed the limit. To protect the load from failure, the control algorithm stops operating in MPPT mode and invokes the output protection illustrated from Figure 4-9 to Figure 4-11, not allowing the output to exceed the limit. In the simulation, it sets when the output voltage goes beyond 30V or 4A for the output current. In Figure 4-12, the two different modes as mentioned above work exclusively for 5 Ω load. In Figure 4-12, it shows that the protection part of the developed algorithm is not letting the output current go beyond 4 A as preset. So, before reaching to a particular irradiance value, the algorithm works in MPPT mode and when irradiance goes a little above of that particular value, it gets into Protection mode and remains idle at that point to protect the load. Here it's clear that the load is not utilizing

the whole effect of irradiance which indicates of selecting an appropriate size of load thus it can utilize the full capacity of PV module or array.

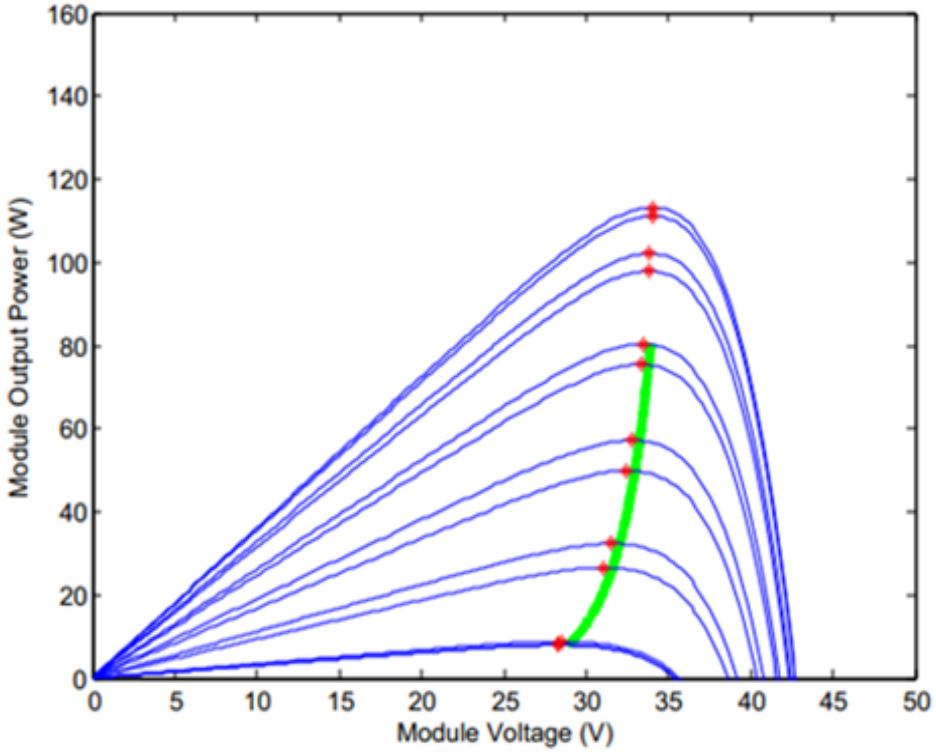

Figure 4-9: PV voltage vs PV power with Protection Scheme

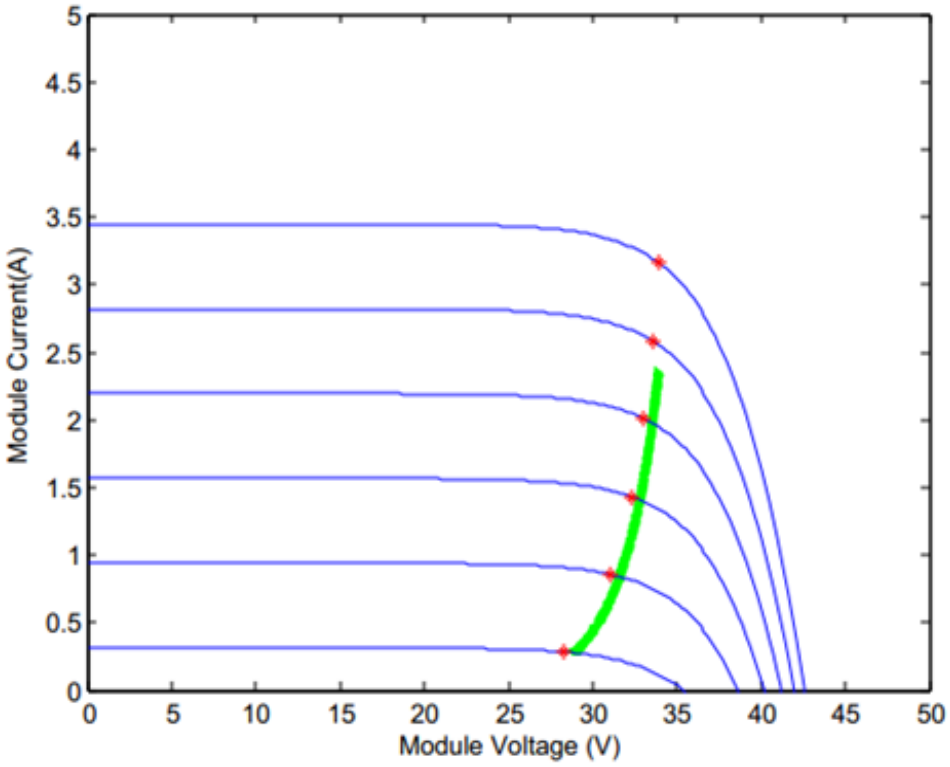

Figure 4-10: PV voltage vs PV Current with Protection Scheme

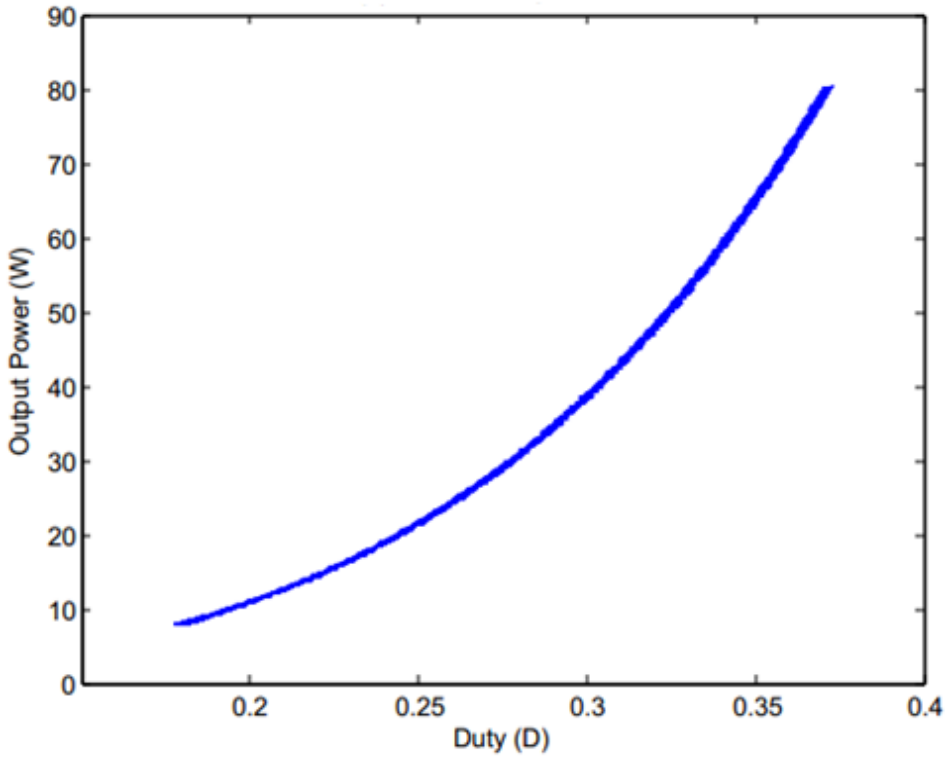

Figure 4-11: Duty vs Output Power with Protection Scheme

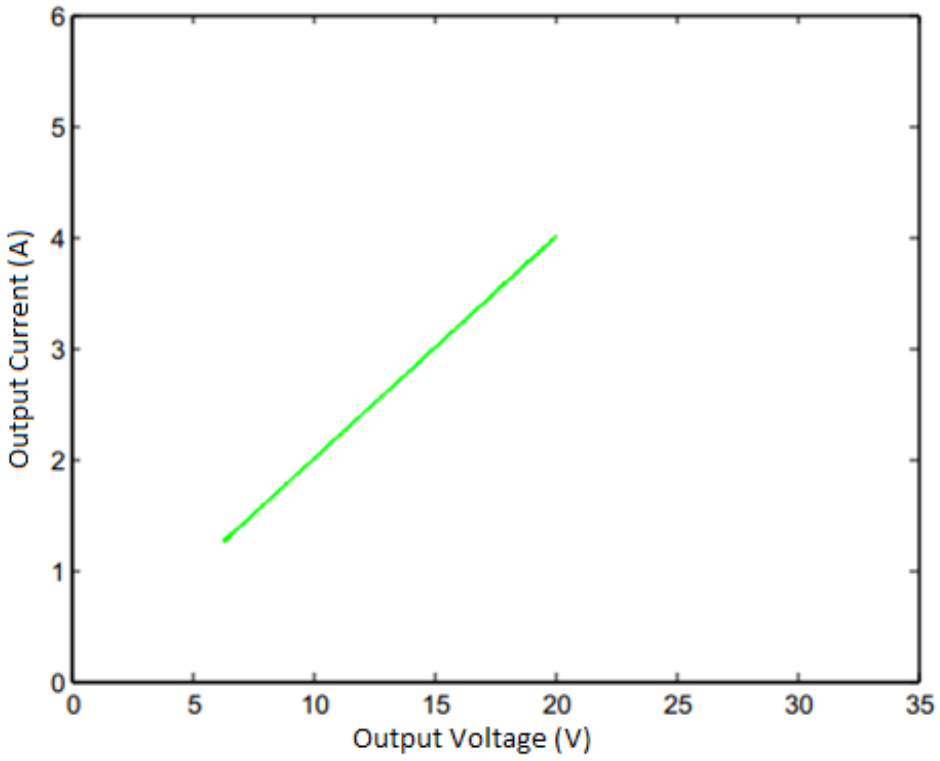

Figure 4-12: Output Voltage vs Output Current with protection scheme

4.1.3 MATLAB Simulation Results for motor-pump load with protection scheme:

The simulations are carried out in a similar way as that has been done for a resistive load. Here, motor-pump modeling equation(**3-22**) has replaced the 5 Ω load for a Sunny Day data set shown earlier in Figure 4-1.Figure 4-13 to Figure 4-16 show the validation of the proposed algorithm with the protection scheme. It is very clear from the graphs that the developed algorithm traces the operating points which are very close to MPP until a particular irradiance value. The protection algorithm doesn't allow the motor-pump load to go beyond 30 V as preset. The motor-pump load modeling equation which has been developed for 22 m of head in the previous chapter has been utilized as a load equation as mentioned above. At that specific head, Figure 4-17shows that when output voltage is 15 V, the corresponding output current is 2 A which has been reflected inFigure 4-16, output voltage vs output current graph (X = 15, Y = 2.052). Therefore, it can be concluded that the simple MATLAB model of DC motor used here is valid.

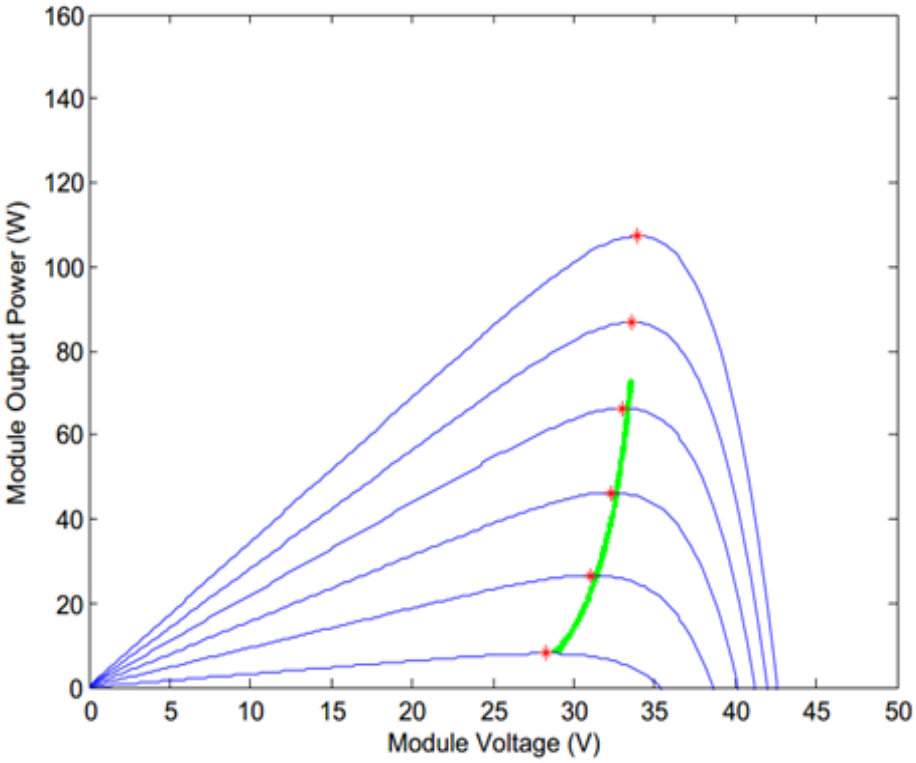

Figure 4-13: PV voltage vs power graph for motor-pump load

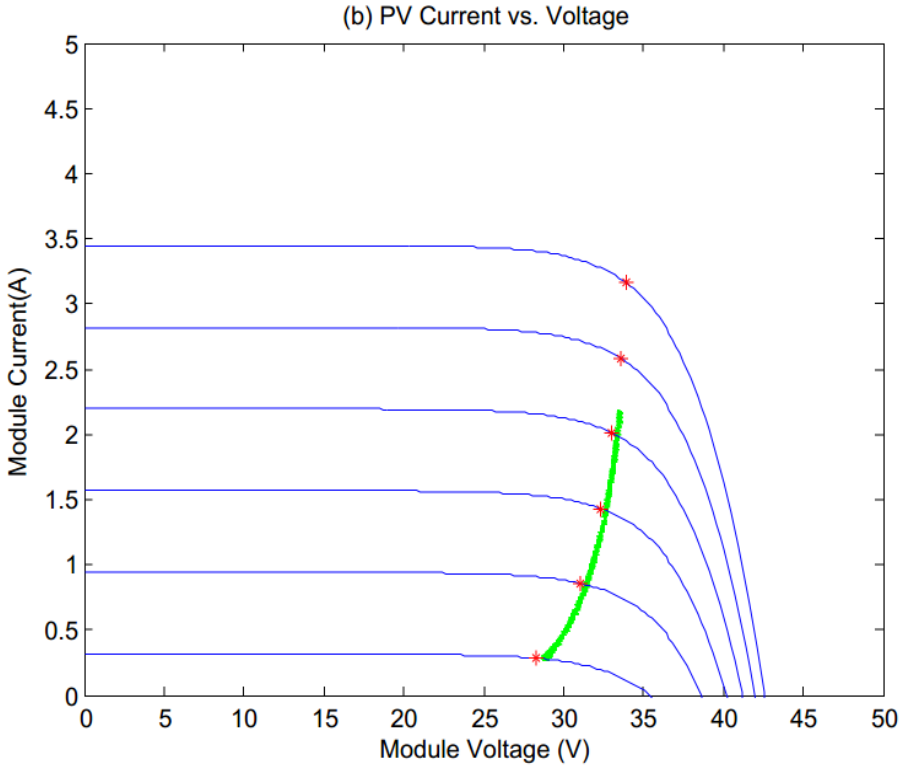

Figure 4-14: PV voltage vs current graph for motor-pump load

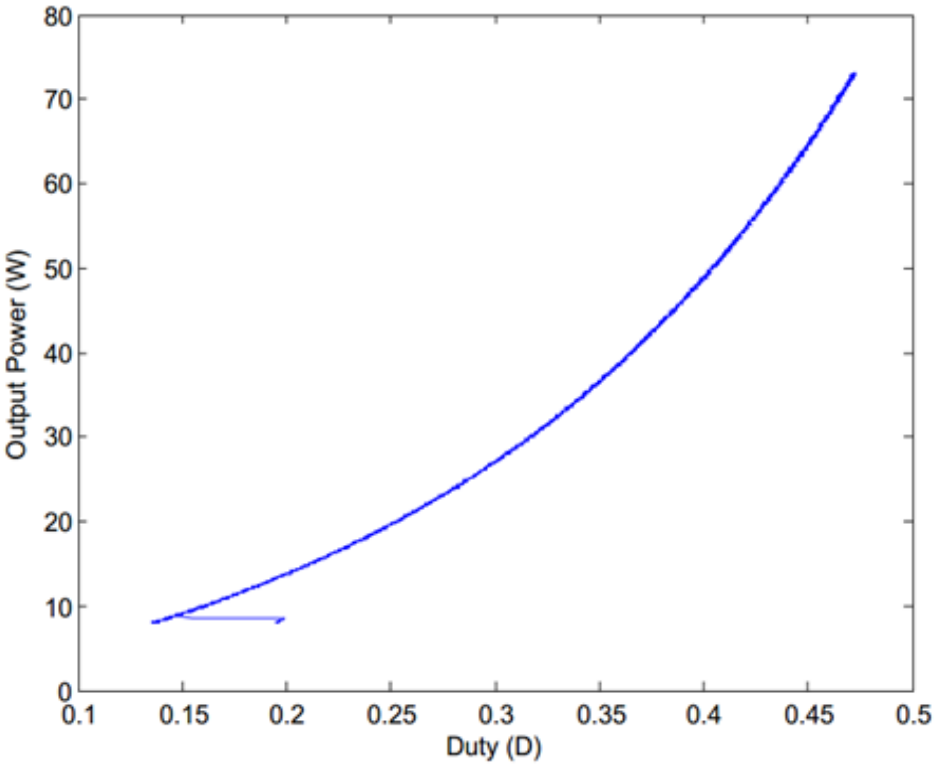

Figure 4-15: Duty cycle vs Output Power for motor-pump load

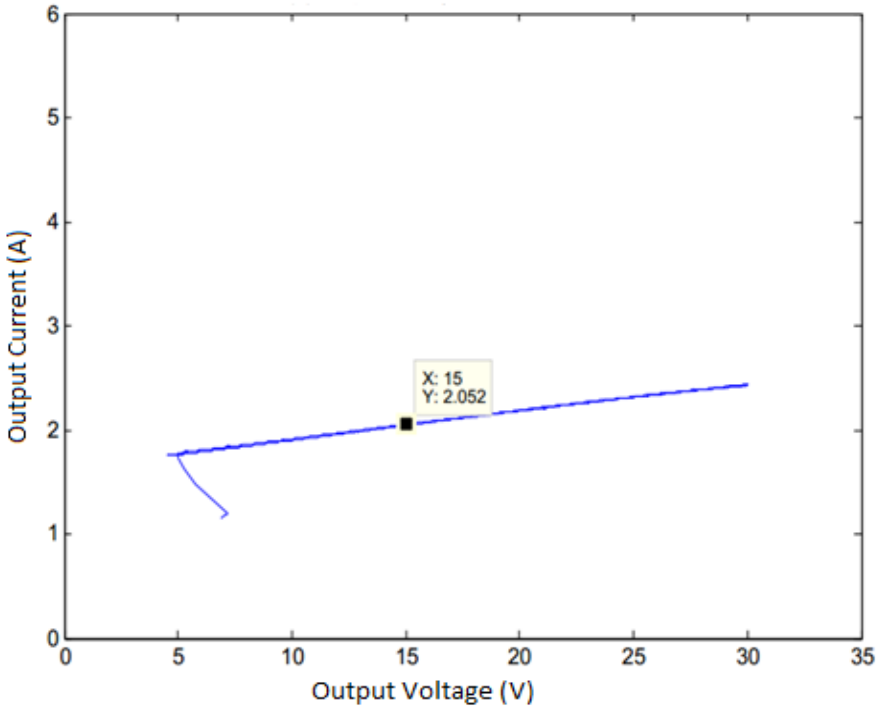

Figure 4-16: Output voltage vs Output power with DC motor-pump load

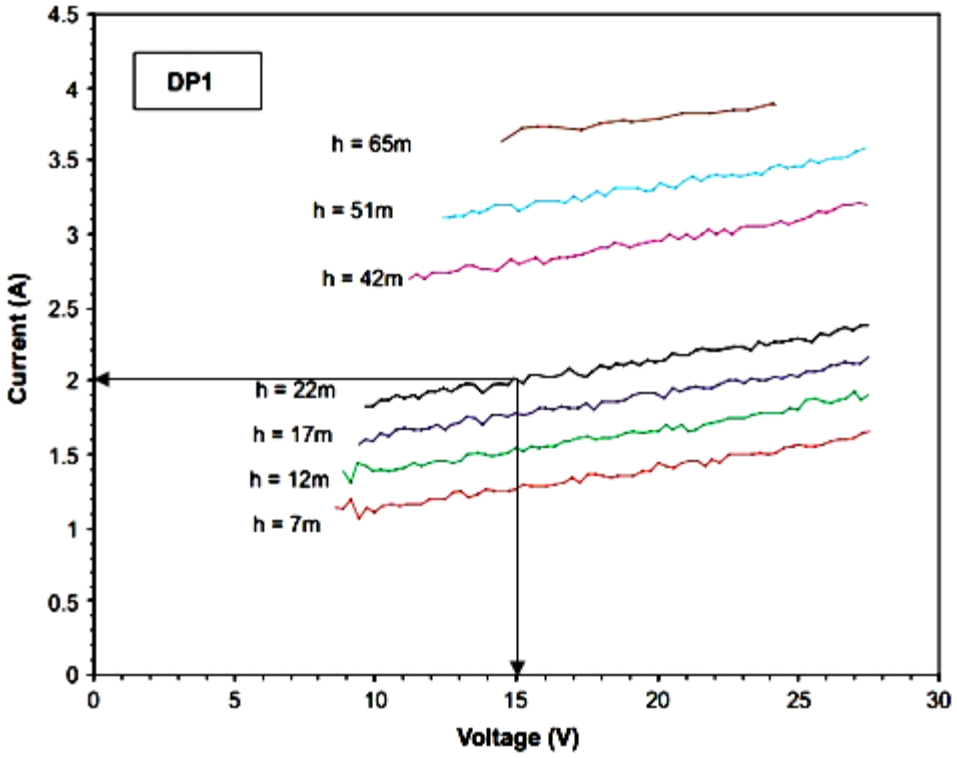

Figure 4-17: Output current and voltage validation at head = 22 m

4.2 Direct Coupled DC Water Pump Load (without MPPT algorithm)

Here, the same motor-pump modeling equation has been applied to the PV module directly without the MPPT charge controller. Consequently, the operating points (the green curve) which have been shown in Figure 4-18 and Figure 4-19are very far away from the exact MPP points shown in red dots causing tremendous amount of power loss resulting poor efficiency.

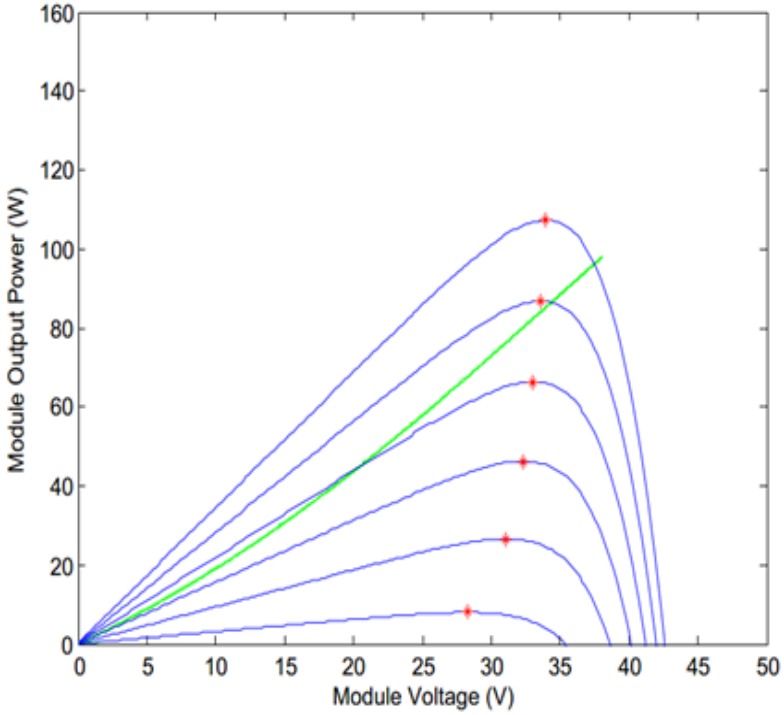

Figure 4-18: Simulation resultof PV panel voltage vs power when coupled directly with motor-pump load

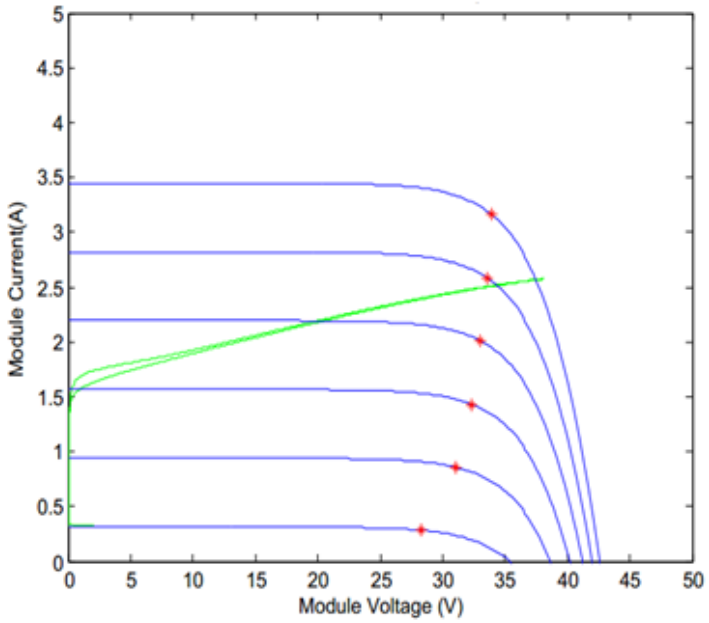

Figure 4-19: Simulation result of PV panel voltage vs current when coupled directly with motor-pump load

4.3 Result comparison of system with and without MPPT

The PV water pumping system simulated in the previous section is compared with the direct-coupled PV water pumping system without MPPT. The irradiance data used here are the measurements from the country report of SWERA, Bangladesh (Sunny Day) [47]for 12 hour period from 6 am to 6 pm in the month of April discussed in previous section. The total electric energy produced during a 12-hour period is calculated and tabulated inTable 4-1.

Table 4-1: Comparison of Energy Production and Efficiency of system with and without MPP

	System with MPP	System without MPP
Total Theoretical Energy	764.1868Wh	764.1868Wh
Total Simulated Energy	763.5758Wh	555.1209Wh
Efficiency	99.92%	72.64%

The MPP tracking efficiency measured by the following formula:

Efficiency = (Total Simulated Energy) ÷ (Total Theoretical Energy) ×100%

The result clearly shows the difference in efficiency of the system with and without MPPT. The MPPT system can extract more than 99% of the energy whereas direct coupled system can take only about 73%. Even considering a converter with 90% efficiency, the system with MPPT can increase the overall efficiency by about 20% which is significant. In contrast, a system without MPPT is providing poor efficiency because of mismatching of PV module operating points and MPP points.

Another comparison simulation has been made between these two systems (with and without MPPT) in terms of flow rate which have been depicted in

Figure 4-20 and Figure 4-21. The results show that the direct-coupled PV water pumping system has a serious drawback because the pump remains idle for more than one hour in the morning while the same system with MPPT is already pumping water.

Similarly, it remains idle more than one hour in advance than the system with MPPT in the afternoon. The flow rate of water is also lower throughout the operating period.

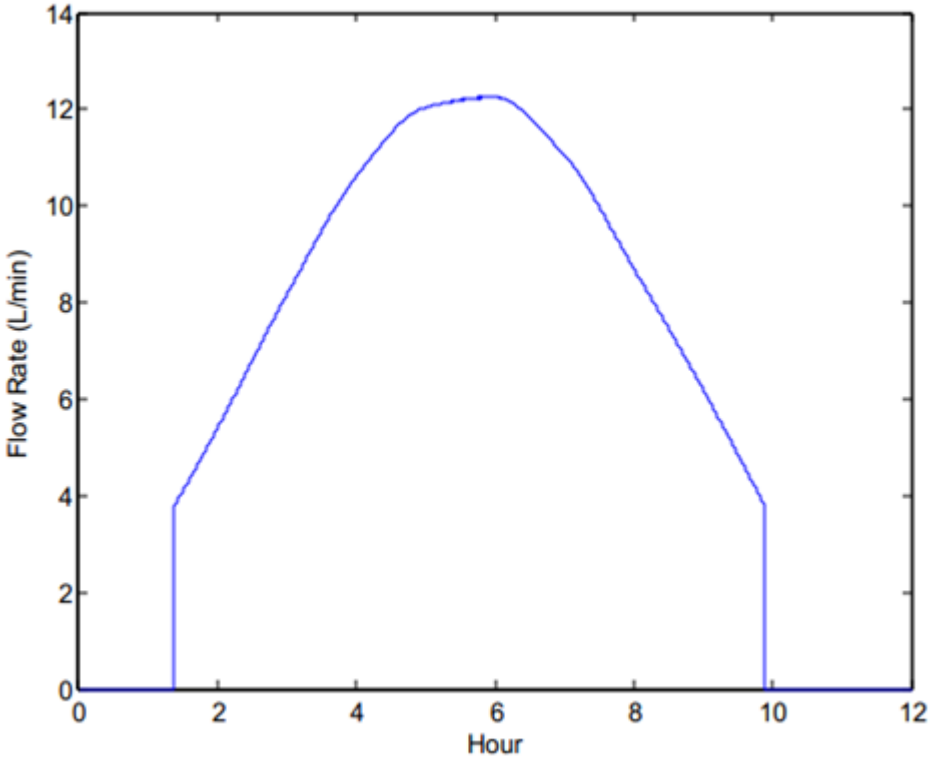

Figure 4-20: Graph of Time vs Flow rate of water with MPPT

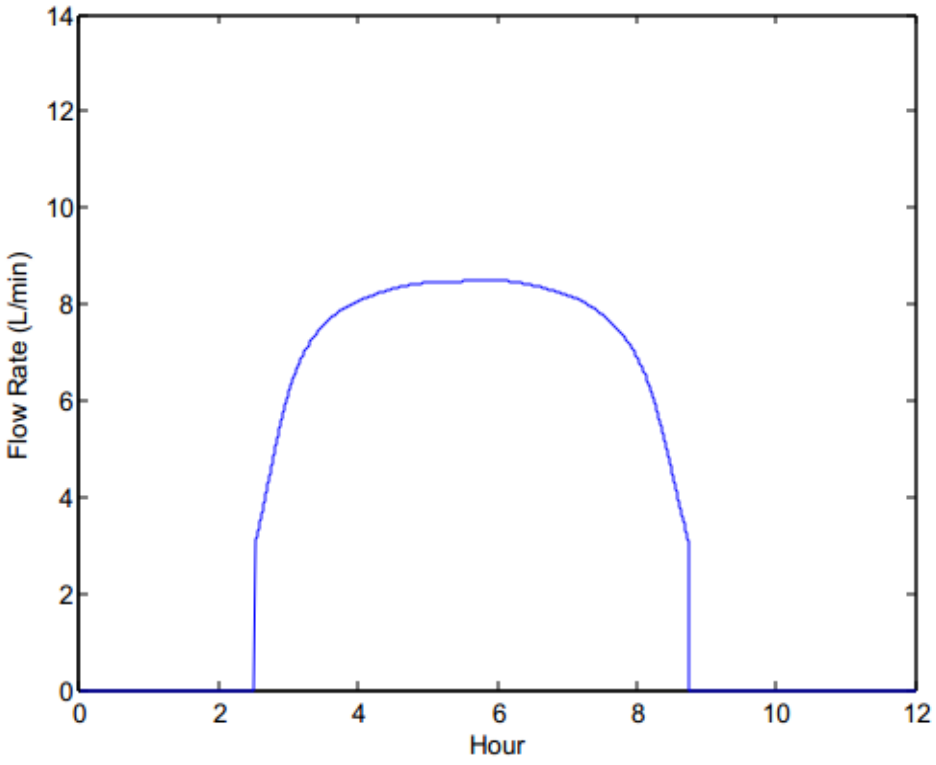

Figure 4-21: Graph of Time vs Flow rate of water without MPPT

4.4 Comparison of no of iterations between P&O and the developed method:

Here, the number of iterations to reach at the MPP point has been compared between the developed method and P&O method for the following conditions:

Irradiance, G = 1 KW/m^2

Temperature, TaC = 25^o C

Operating Point, Va = 5 V (Left side of MPP Point)

Table 4-2: No of Iterations comparison between developed and P&O when operating point lies at left of MPP

	Perturb & Observe Step Size = 0.1	Developed Algorithm (Step Size = 0.1, 2)	Exact Value
MPP Voltage	34.6	34.5346	34.5
MPP Power	149.9709	149.9825	149.9858
Intersection Voltage	NA	32.2346	NA
No of Iterations from operating point to Intersection point	NA	15	NA
No of Iterations from Intersection point to MPP	NA	22	NA
Total of Iterations	296	37	NA

When the operating point is lying at the left of MPP, Table 4-2 shows that total number of iterations with the developed method is much less than that of P&O method. Initially, the developed method has big steps (2V) in order to get the intersection point (32.2346 V) of two straight lines and takes 15 iterations. The intersection point is close to the MPP as mentioned earlier. From intersection point to MPP point, the algorithm takes 22 iterations since it goes with small step (0.1 V). The small steps after finding the intersection point provides not only small oscillations around MPP point but also gives the freedom of taking even bigger steps for finding intersection point which certainly will reduce the total number of iterations even further.

When the operating point is lying at the right side of MPP, another table data has been provided in a same manner for the following conditions:

Irradiance, G = 1 KW/m^2

Temperature, TaC = 25^o C

Operating Point, Va = 40 V (Right side of MPP Point)

Table 4-3: No of Iterations comparison between developed and P&O when operating point lies at right of MPP

	Perturb & Observe Step Size = 0.1	Developed Algorithm (Step Size = 0.1, 2)	Exact Value
MPP Voltage	34.6	34.3498	34.5
MPP Power	149.9709	149.9784	149.9858
Intersection Voltage	NA	37.1498	NA
No of Iterations from operating point to Intersection point	NA	3	NA
No of Iterations from Intersection point to MPP	NA	29	NA
No of Iterations	54	32	NA

4.5 Comparison between Perturb & Observe and Developed Algorithm when rapid changes occur in Irradiance

In this section, comparison of VMPP has been made between developed and P&O algorithm in MATLAB/SIMULINK environment. Then SIMULINK object "to workspace" has been used to transfer the graphs in MATLAB environment in order to compare in the same axis.

The modeling diagram is created in Figure 4-22where both P&O and developed operating point has been set as 5V.

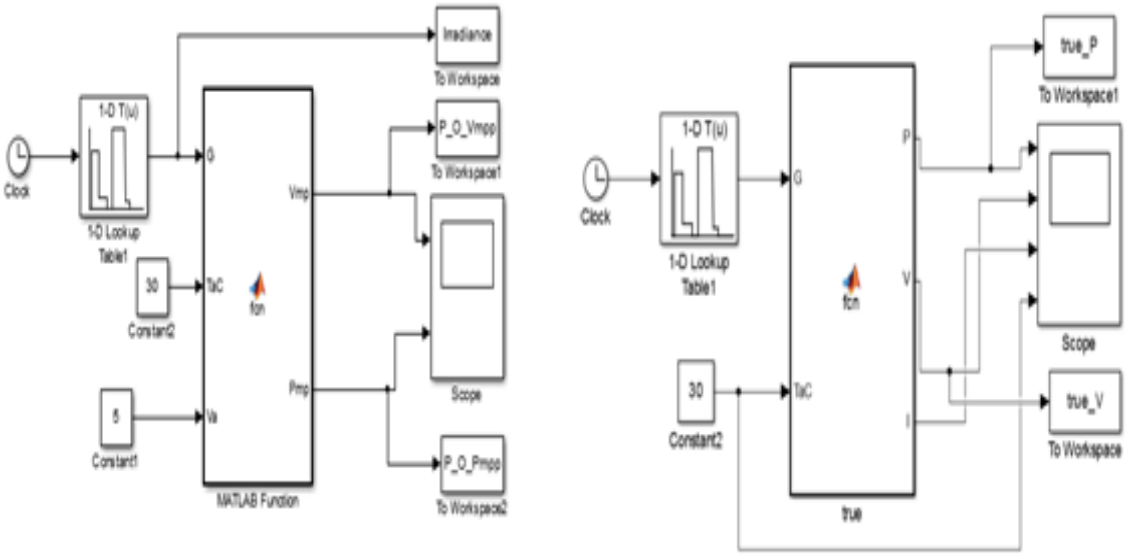

Figure 4-22: Simulink Diagram for comparing V_{mpp}

Here very sharp slope ($W/m^2/s$) of irradiance vs time graphhas been chosen which has been depicted inFigure 4-23 in order to check the response of both algorithms.

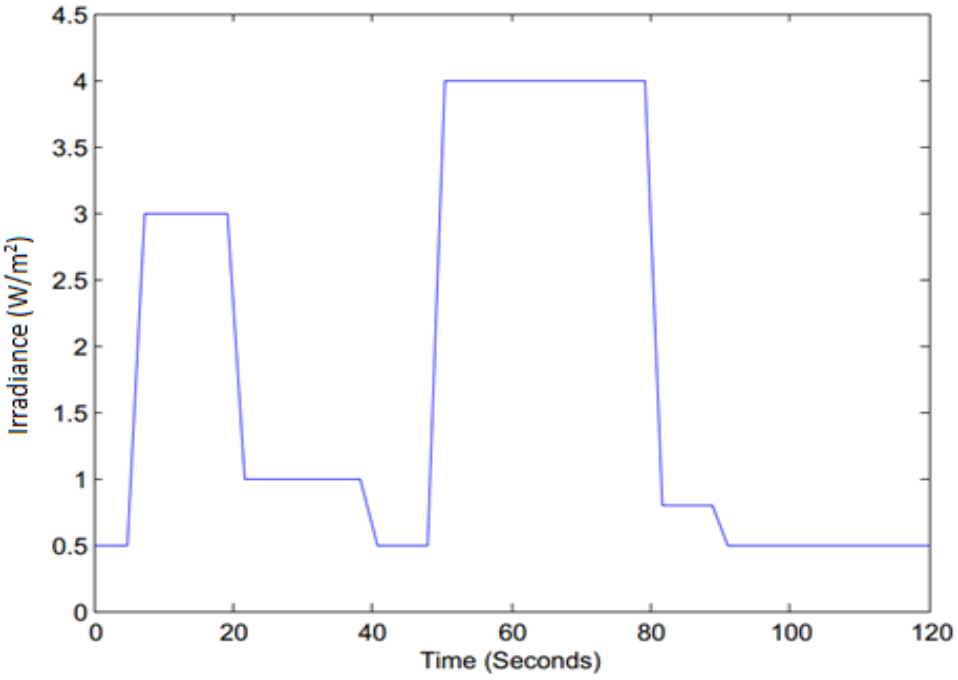

Figure 4-23: Sharp changes of Irradiance with time simulating rapid weather condition

Figure **4-24** and Figure **4-25**show the comparison of VMPP between developed and Perturb and Observe algorithm. Figure **4-24**shows that both of the methods are tracking the exact MPP very closely, however, perturb and observe method has chosen 0.1 V as step size which increases the number of iterations greatly comparing to the developed method as mentioned earlier. In order to reduce the number of iterations, the step size has been slightly increased which results in complete breakdown of P&O method shown with a green curve inFigure **4-25**.

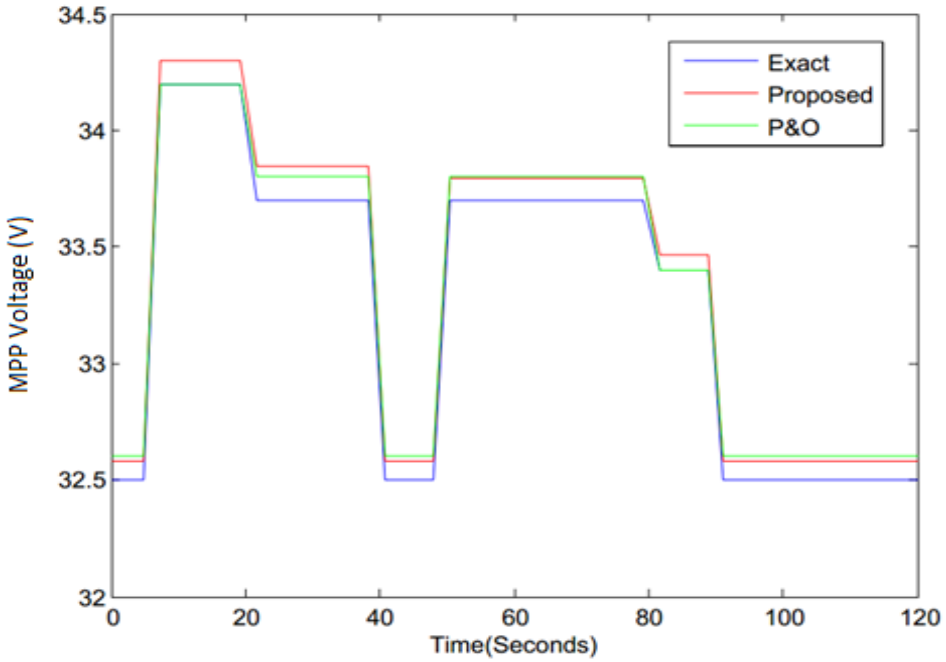

Figure 4-24: Comparison of MPP voltages with small step size when rapid weather changes

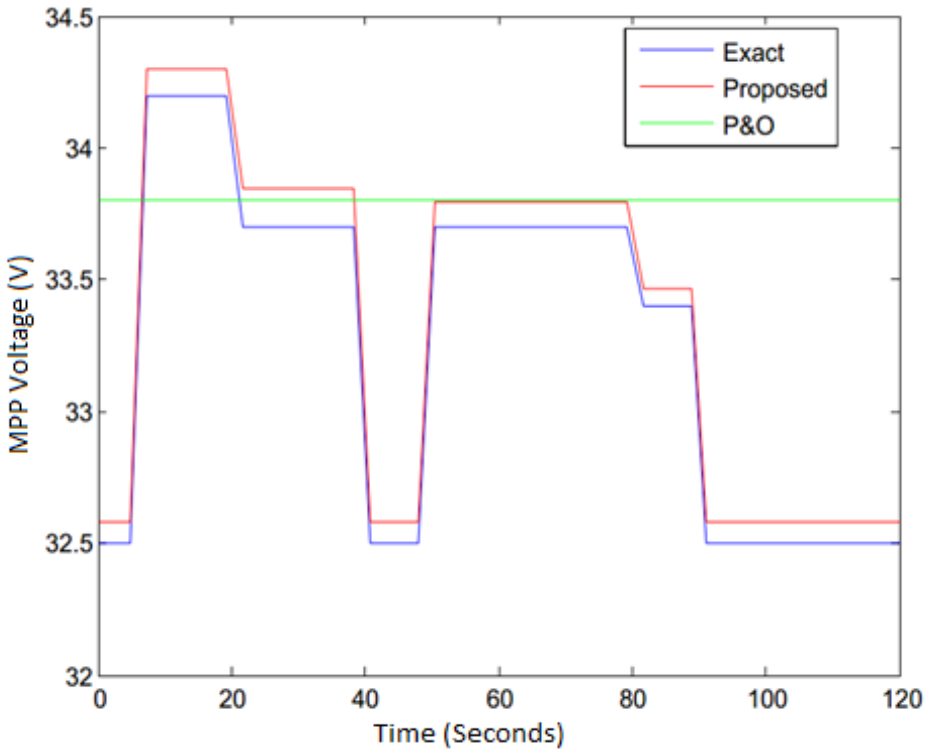

Figure 4-25: Comparison of MPP voltage and breakdown of P&O algorithm for moderate step size when rapid change occurs in irradiance

4.6 Comparison between proposed and perturb & observe algorithm in terms of duty and maximum power point:

Here, the irradiance and temperature have been varied to analyze the performance and compare the two algorithms. It is very apparent from Table 4-4that both algorithms have identified the duty cycle and maximum power point with same step size which is 0.03, however, the proposed method has obtained the duty cycles and maximum power points much closer to exact duty cycle and maximum power points than the perturb and observe method under varying weather conditions.

The parameters percentage error in duty cycle and percentage error in maximum power point are defined in the following way:

Percentage Error in Duty Cycle = $(D_{TRUE} - D_{PROPOSED/PER\_OBS}) / D_{TRUE} * 100$ %

Percentage Error in Maximum Power Point = $(P_{TRUE} - P_{PROPOSED/PER\_OBS}) / P_{TRUE} * 100$ %

It is evidential from Figure 4-26 that the proposed algorithm has very small error in finding the correct duty cycle under varying irradiance conditions. The error is less than ±0.5% whereas perturb and observe algorithm has more than ±1%error in finding the correct duty cycle. The similar scenario has been observed in Figure 4-27 as well where percentage error in finding maximum power point under varying irradiance conditions is less than 0.03% for the proposed algorithm whereas it is more than 0.23% in the case of perturb and observe method.

Table 4-4: Comparison of duty cycle and maximum power between proposed and p & o algorithm at different irradiance and temperature

(G,T) in (KW/m2, oC)	D_exact	D_proposed	D_per_obs	P_exact	P_proposed	P_per_obs
(0.3, 0)	0.3177	0.3201	0.3100	46.8442	46.8059	46.4333
(0.3, 10)	0.3228	0.3200	0.3100	44.8187	44.7739	43.8932
(0.3, 20)	0.3275	0.3280	0.3310	42.7801	42.7802	42.7203
(0.5, 0)	0.3725	0.3720	0.3730	80.4209	80.4200	80.4165
(0.5,10)	0.3774	0.3780	0.3790	77.1584	77.1546	77.1326
(0.5,20)	0.3824	0.3820	0.3790	73.8728	73.8702	73.7657
(0.8,10)	0.4314	0.4320	0.4270	126.4301	126.4219	126.1785
(0.8,20)	0.4367	0.4350	0.4390	121.3375	121.3139	121.2492
(0.8,30)	0.4415	0.4420	0.4390	116.2146	116.2139	116.1323
(1.0,20)	0.4627	0.4620	0.4630	153.1360	153.1256	153.1357
(1.0,30)	0.4683	0.4680	0.4690	146.8280	146.8288	146.8160
(1.0,40)	0.4734	0.4720	0.4750	140.4862	140.4611	140.4538
(1.2,20)	0.4848	0.4850	0.4870	184.8904	184.8890	184.7909
(1.2,30)	0.4897	0.4890	0.4870	177.4167	177.4042	177.2795
(1.2,40)	0.4948	0.4950	0.4990	169.9001	169.9017	169.6730

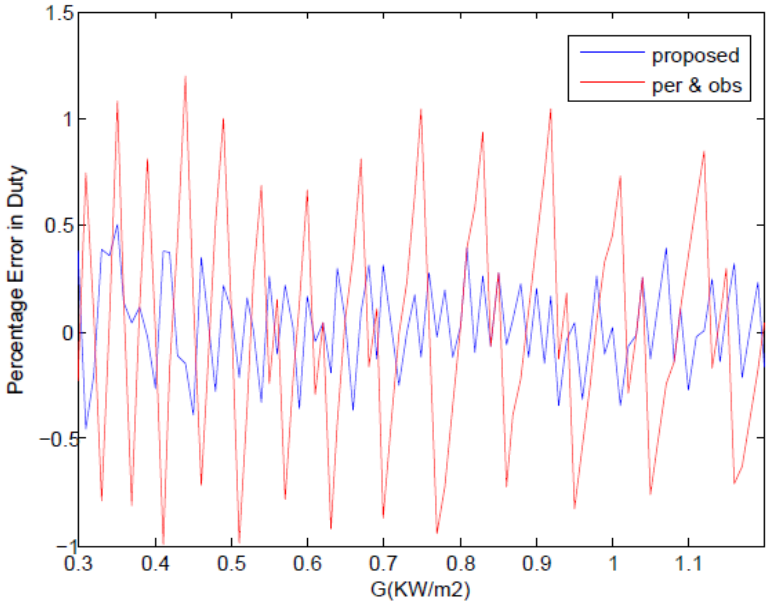

Figure 4-26: Comparison ofPercentage of Error in Duty cycle under 25ºC of proposed and p & o algorithm

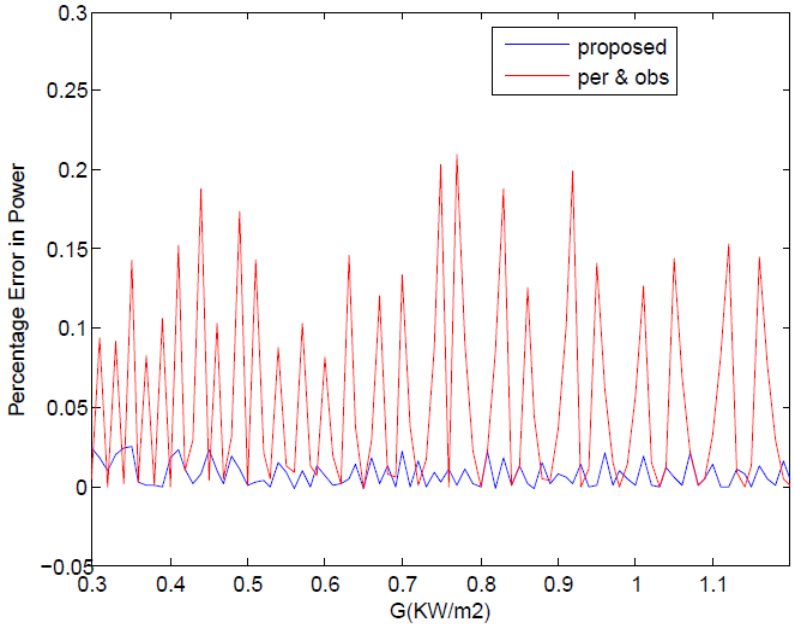

Figure 4-27: Comparison ofPercentage of Error in Maximum Power Point under 25ºC of proposed and p & o algorithm

Chapter 5: A case study: Developing Mathematical Technique for finding Cost Effective solution at Kutubdia Island and Khulna regions

In order to satisfy the Load demand, single generator (either Solar or Wind) operating alone would require to be sized for the minimum of the corresponding energy supply. Because of that, a huge amount of energy surplus would be generated which is wasted. The mismatch between energy supply and energy demand leads to excessive cost of this renewable energy system which can be addressed to a great extent by a Hybrid generation system.

The Graphical linear programming[49] sizing tool has beenmodified and simplified which is then used for the daily averages of the solar and wind energy values for Kutubdia and Khulna.

5.1 Forming of Daily Energy Balance Condition:

The sizes of the two generators Solar and Wind Generator as As, and Aw, will be defined in terms of the conversion efficiency multiplied by the effective area of the generator. Thus, for the PV array, we have:

$$As = n * A \tag{5-1}$$

Where:

n = efficiency

As: solar panel area in m^2

For the Wind Generator:

$$Aw = Cp * \pi * r^2 \tag{5-2}$$

Aw: wind turbine area in m^2

Cp = power coefficient

r = radius of the turbine

The energy resources will be described by the average daily energy incident on a unit area. For the solar energy S, the required value refers to the inclined plane of the modules which is usually calculated from the meteorological data for a horizontal plane. The wind energy W is measured in a plane perpendicular to the wind direction:

$$W = \left(\frac{1}{2}\right) * D * \rho_{AIR} * v^3 \quad (5\text{-}3)$$

Where:

ρ_{AIR}: air density

v: average wind velocity

D: Duration of 1 day, i.e. 24 hours

The assumption is the average daily Load (here it is water demand) over the year is known, we can then write down the following condition which satisfies the demand:

Condition:

For every day,

$$S * As + W * Aw \geq L \quad (5\text{-}4)$$

S: Solar Energy

W: Wind Energy

L: Load

The main objective is to characterize the optimized values of As and Aw that satisfies the above equation at all times of the year using the average values of S, W and L.

For Pump & Motor, the following formula has been used to calculate the daily hydraulic energy, E_h in KWh:

$$E_h = \rho * g * h * V \tag{5-5}$$

ρ:density of water

V = daily amount of water required in m^3

H: Total Pumping Head in m

The daily amount of water has been assumed to be 25 L (0.025 m^3), after plugging other arguments, the daily load demand energy turns out to be 5 KWh.

Hybrid Optimized Cost:

$$\text{Minimize:} Cw * Aw + Cs * As \tag{5-6}$$

Cw: cost of wind turbine / $meter^2$

Cs: cost of solar panel / $meter^2$

Here Cs and Cw have been chosen as 100 unit currency and 150 unit currency respectively.

Subject to:

$$Si * As + Wi * Aw \geq Li \tag{5-7}$$

i: i-th day where i varies from 1 to 365

5.2 Solar and Wind Data for Kutubdia Island

5.2.1 The Hybrid System

The Table 5-1below shows monthly average daily solar and wind energy in Kutubdia Island[50]. Figure 5-1 shows the graphical representation of that.

Table 5-1: Monthly average daily solar energy and wind energy in Kutubdia Island

Month	Solar(KWh/m^2)	Wind(KWh/m^2)
Jan	6.2	2.91
Feb	6.27	2.15
Mar	6.3	2.29
Apr	5.84	2.09
May	4.97	5.98
Jun	3.58	8.99
Jul	3.37	9.88
Aug	3.75	7.77
Sep	4.19	2.33
Oct	5.11	3.35
Nov	5.54	1.99
Dec	6.13	2.12

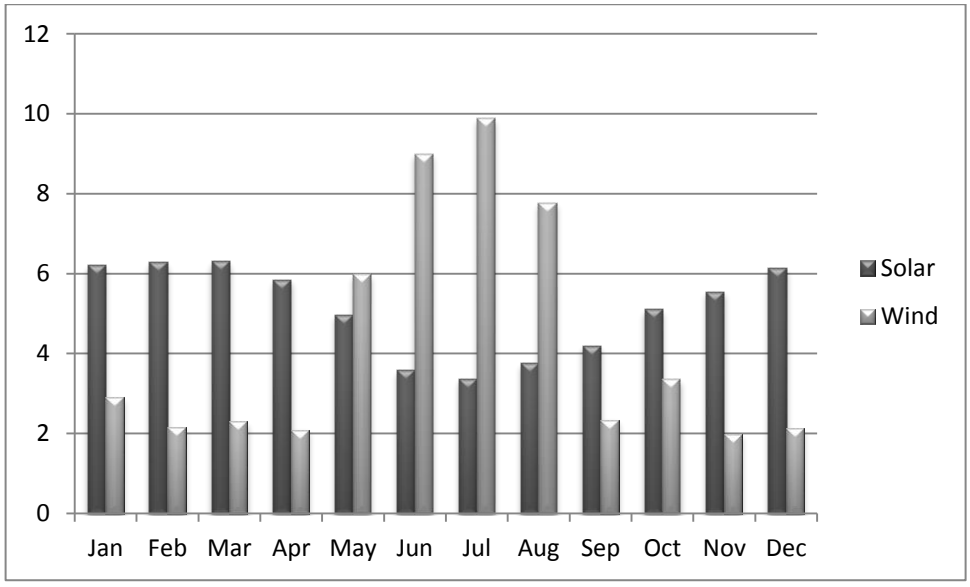

Figure 5-1: Graph of Monthly average daily Solar and Wind Energy in Kutubdia Island

Then MATLAB curve fitting technique "cubic interpolation" has been utilized for generating daily average solar and wind energy for all 365 days. In the Figure 5-2 and Figure 5-3below the discrete blue circles correspond to Solar energy at 12 specific days in 12 months and then using the above mentioned curve fitting technique, the continuous curve marked in "green" has been generated for all 365 days.

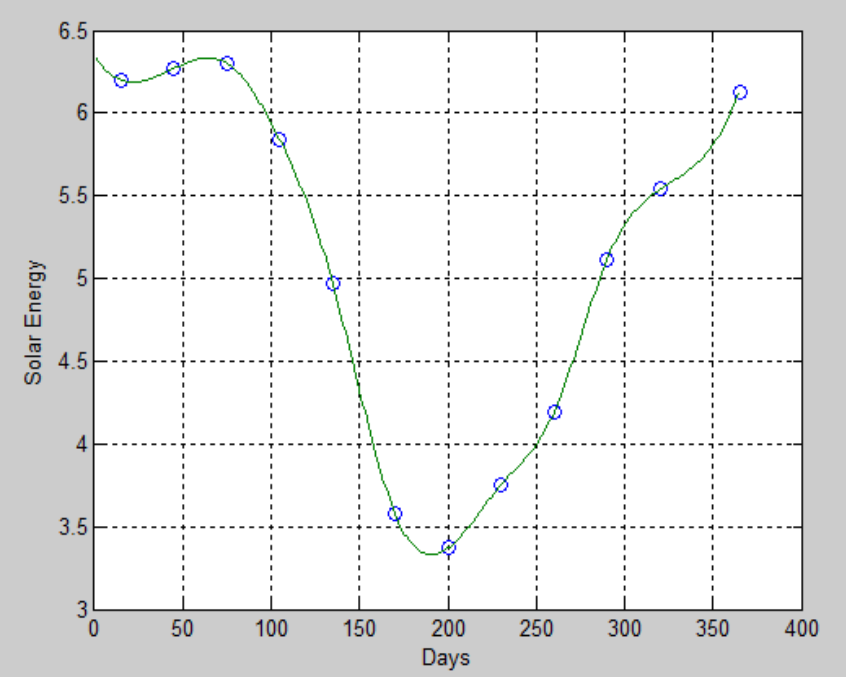

Figure 5-2: Solar Energy for 365 days of Kutubdia Island

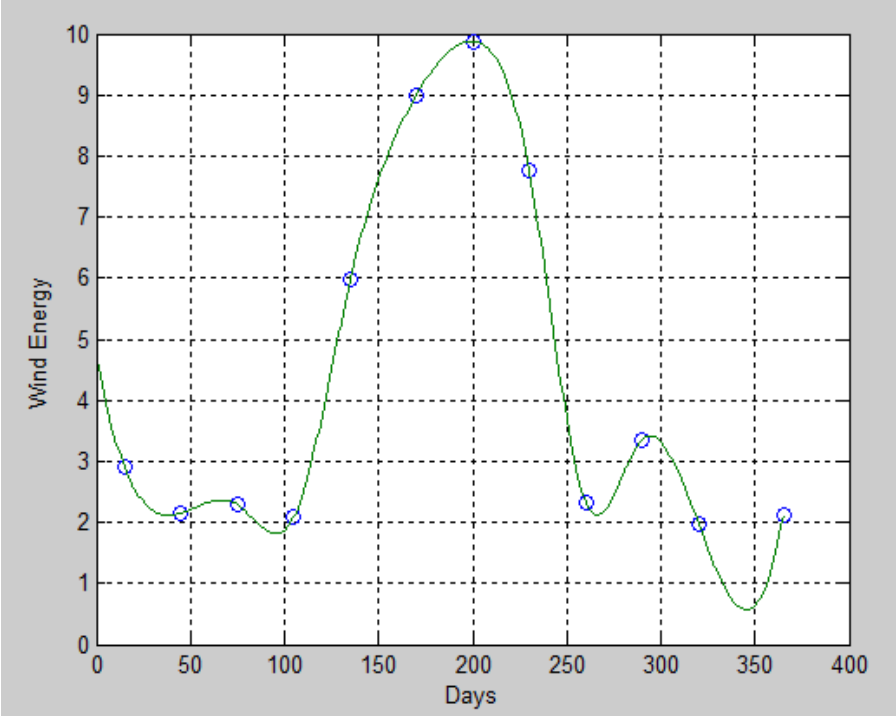

Figure 5-3: Wind Energy for 365 days of Kutubdia Island

Figure 5-4 has been generated using equation (**5-7**)which is the graphical drawing of all the constraints for 365 days. After plotting As versus Aw graph for all 365 days, the feasible region, marked using 'arrow', can be identified very easily. Then the boundary region has been utilized for developing the following piece-wise defined functions:

$$Aw = -10..21 * As + 8.81 \qquad 0 \leq As \leq 0.79$$

$$Aw = -1.86 * As + 2.21 \qquad 0.79 < As \leq 1.14$$

$$Aw = -0.27 * As + 0.3923 \qquad 1.14 < As \leq 1.46$$

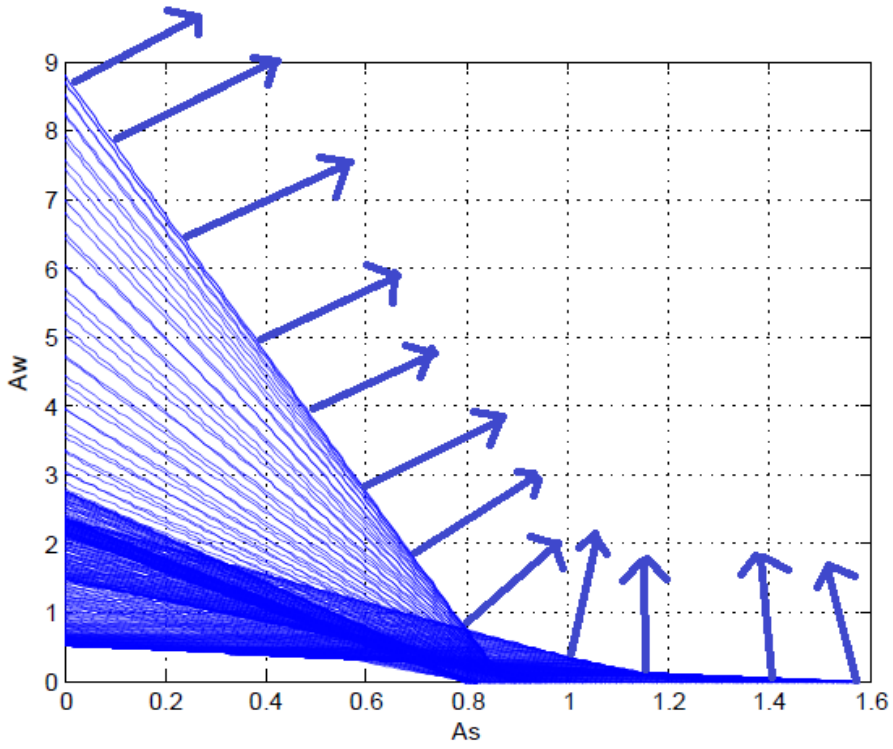

Figure 5-4: Finding the optimum Boundary surface of Kutubdia Island

Then above mentioned piece-wise defined functions have been used along with the minimum cost equation (**5-6**) for generating the minimum cost which has been shown in the Figure 5-5 below. Here for a Load of 5 KWh, the corresponding As, Aw and minimum cost values are in the following:

As = 1.141 m^2

Aw = 0.08423 m^2

Minimum Cost = 126.7unit currency

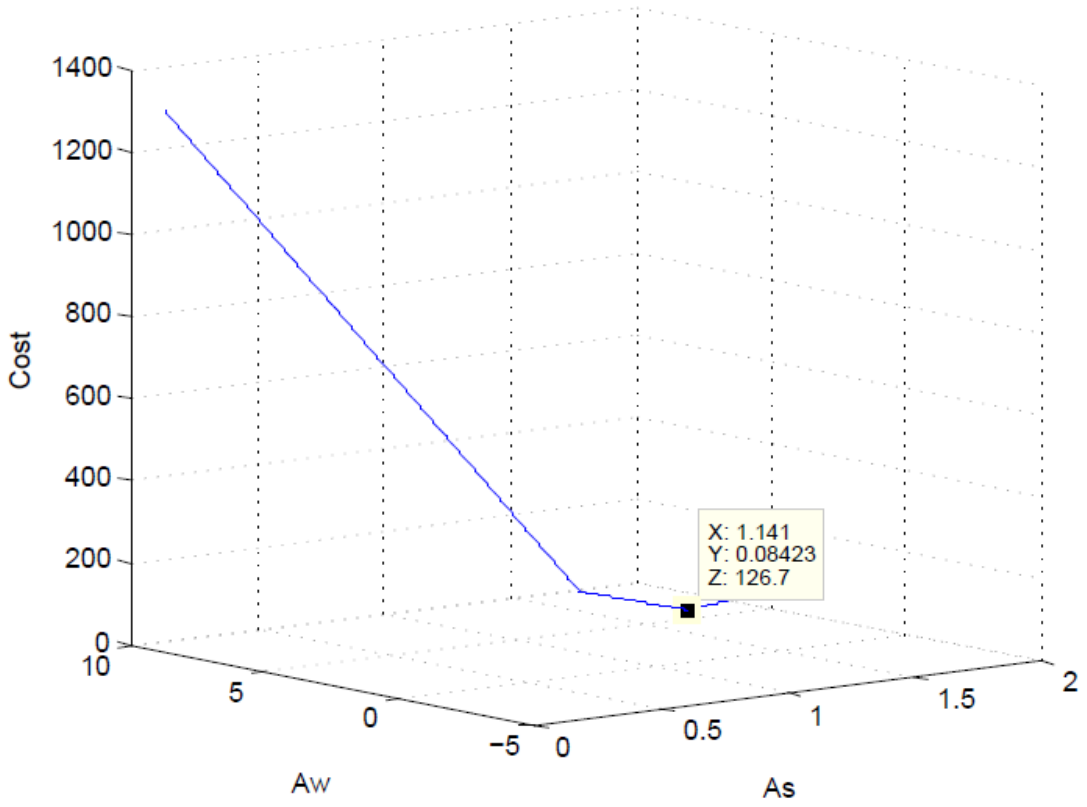

Figure 5-5: Finding minimum cost of the Hybrid system for a particular As and Aw for Kutubdia Island

5.3 Finding minimum cost of Solar-Only and Wind-Only system:

5.3.1 Minimum cost of Solar-Only System:

In order to calculate the minimum cost of Solar-Only and Wind-Only system, the day with the worst case combination of solar radiation energy and wind energy and water demand is used. The following formulas are being used for the calculation of Solar-Only System.

As = Load energy / minimum Solar energy

Equation (**5-6**) has been modified by plugging Aw = 0 for calculating Solar-Only System.

Minimum Cost of Solar-Only System = Cs * As

Using those equations, the main parameters are provided below:

As = 1.5006 m^2

Cost = 150.0647 unit currency

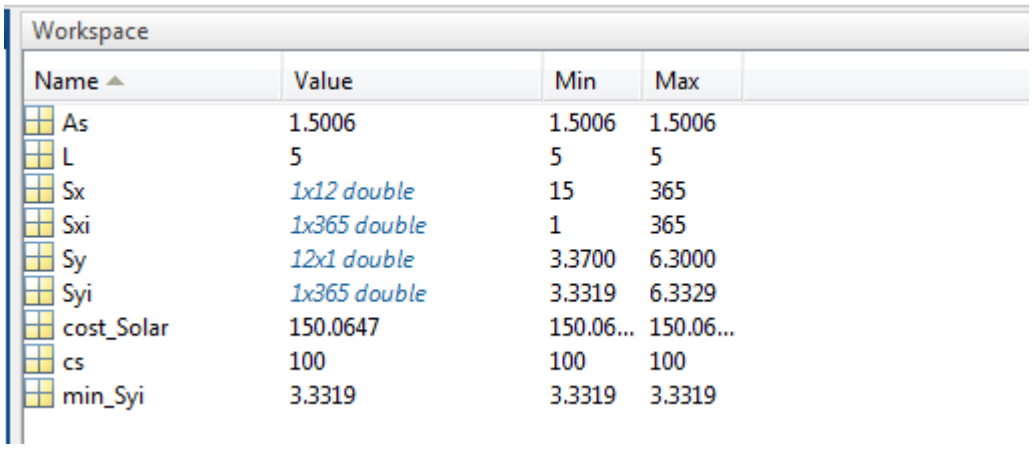

Figure 5-6:MATLAB screenshot for all parameters of Solar-Only System of Kutubdia Island

5.3.2 Minimum cost of Wind-Only System:

The following formulas are being used for the calculation of Wind-Only System.

Aw = Load energy / minimum Wind energy

Minimum Cost of Wind-Only system = Cw * Aw

The main parameters are listed below:

Aw = 8.8031 m^2

Cost = $1.32x10^3$ unit currency

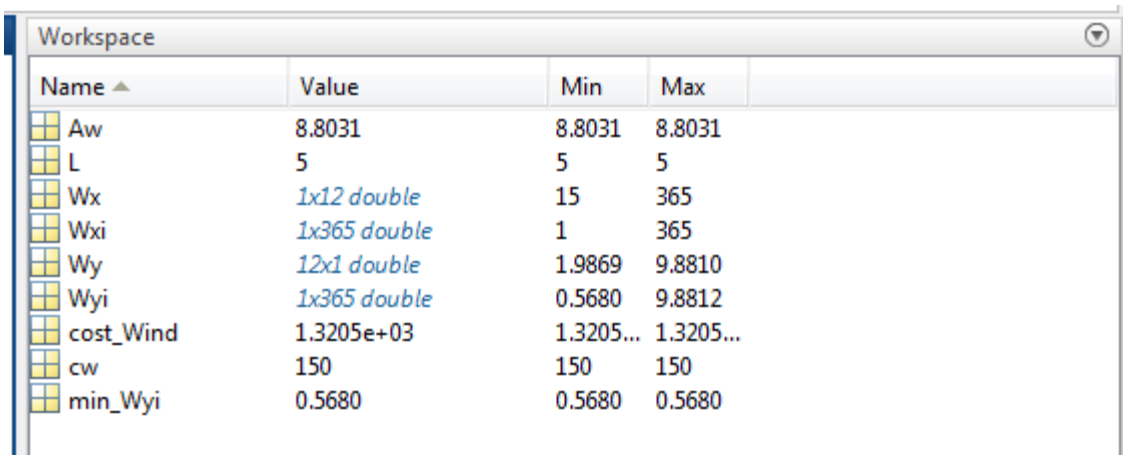

Figure 5-7: MATLAB screenshot for all parameters of Wind-Only System of Kutubdia Island

5.4 Comparison among Hybrid, Solar-Only and Wind-Only System of Kutubdia Island:

Figure 5-8shows the comparison of Hybrid, Solar-Only and Wind-Only system in terms of delivering energy to the demand which has been remain constant as 5 KWh throughout a year. In the graph, the dotted black line correspond to Load line, the blue line refers to energy supplied by hybrid system, the red line refers to energy supplied by solar-only system and the green line for wind-only system. It is very apparent in the graph that matching between load line and hybrid system is the best amongst others which leads to least system cost.

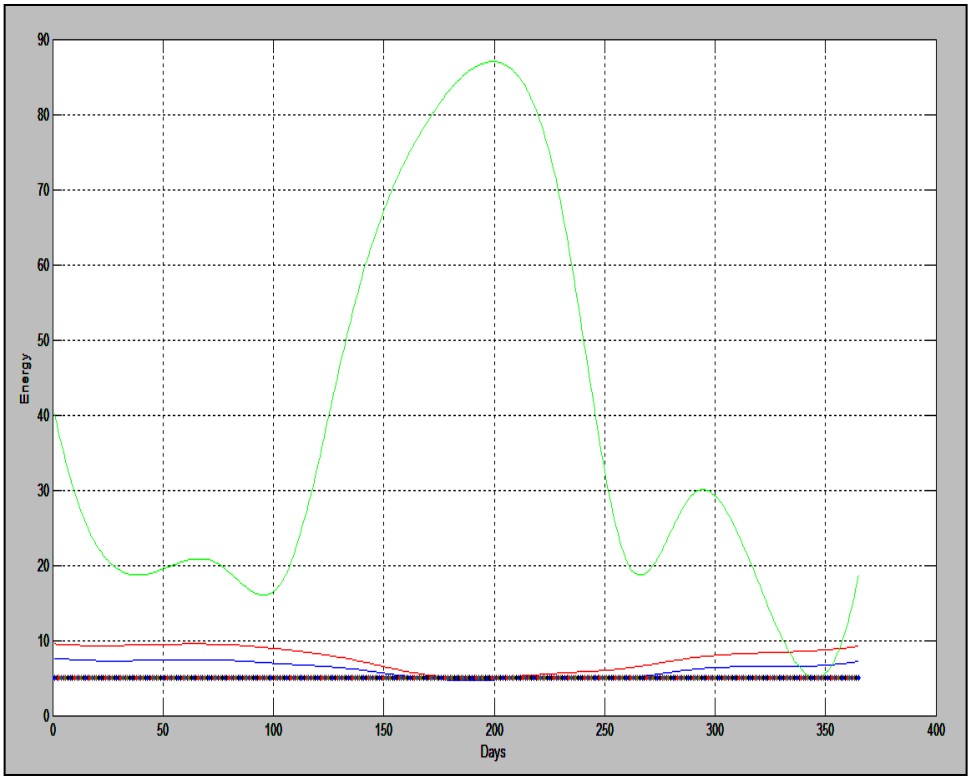

Figure 5-8: Comparison Graphs of Hybrid, Solar-Only and Wind-Only System

Table 5.2 also reflects those points where cost and waste of energy of hybrid system is lowest amongst others.

Table 5-2: Cost and Waste of Energy comparison at optimum parameters of Hybrid, Solar-Only and Wind-Only system of Kutubdia Island

	As in m^2	Aw in m^2	Cost	Waste of Energy
Hybrid System	1.141	0.08423	126.7	425.3556
Solar-Only System	1.5006	NA	150.0647	951.7382
Wind-Only System	NA	8.8031	$1.32x10^3$	1.1919e+04

5.5 Solar and Wind Data for Khulna:

5.5.1 Hybrid System:

Table 5-3: Monthly average daily solar energy and wind energy in Khulna region[50]:

	KHULNA	
Months	Solar(KWh/m^2	Wind(KWh/m^2)
Jan	4.58	8.53
Feb	5.53	8.59
Mar	5.92	21.58
Apr	6.11	25.38
May	6.2	34.57
Jun	4.95	25.70
Jul	4.14	15.12
Aug	4.67	12.78
Sep	4.72	13.68
Oct	4.81	17.09
Nov	4.38	7.70
Dec	4.15	6.69

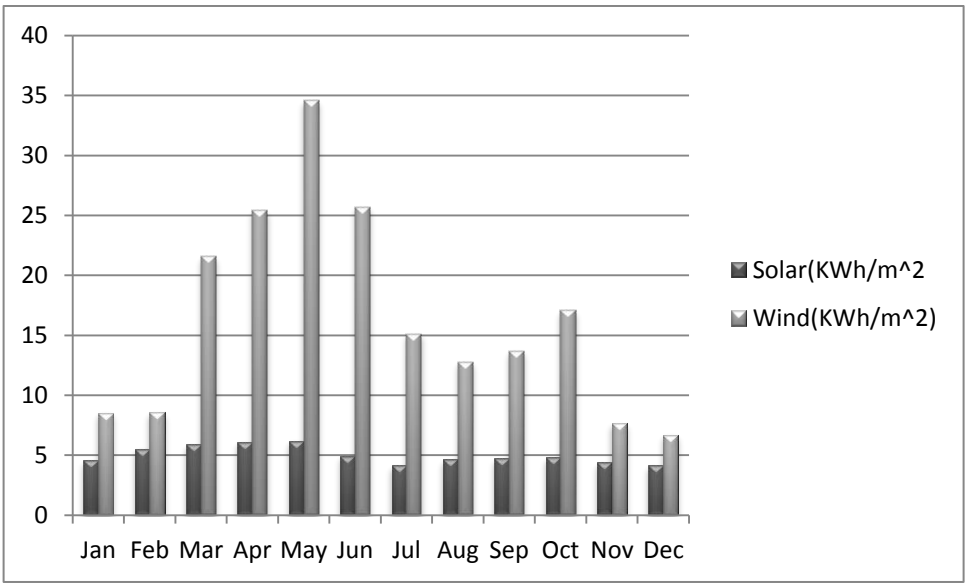

Figure 5-9: Graph of Monthly average daily Solar and Wind Energy in Khulna

Piece-wise defined function of Figure **5-10**:

$$Aw = -4.3218 * As + 5.41 \qquad 0 \leq As \leq 1.25$$

$$Aw = -0.0521 * As + 0.0729 \qquad 1.25 < As \leq 1.4$$

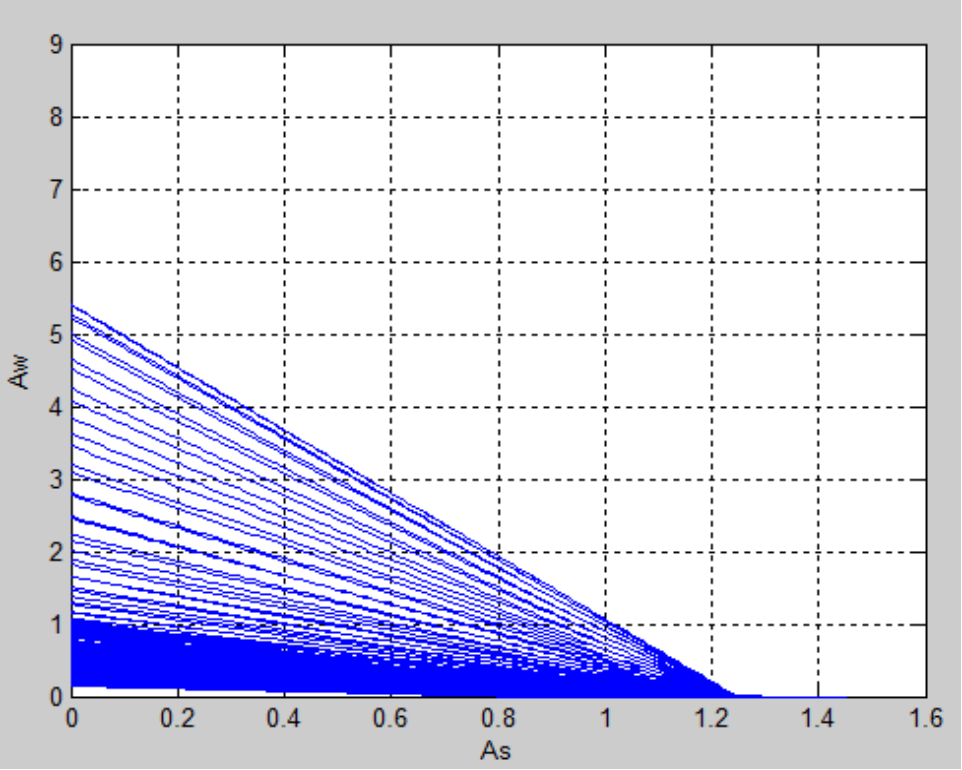

Figure 5-10: Finding the optimum Boundary surface of Khulna

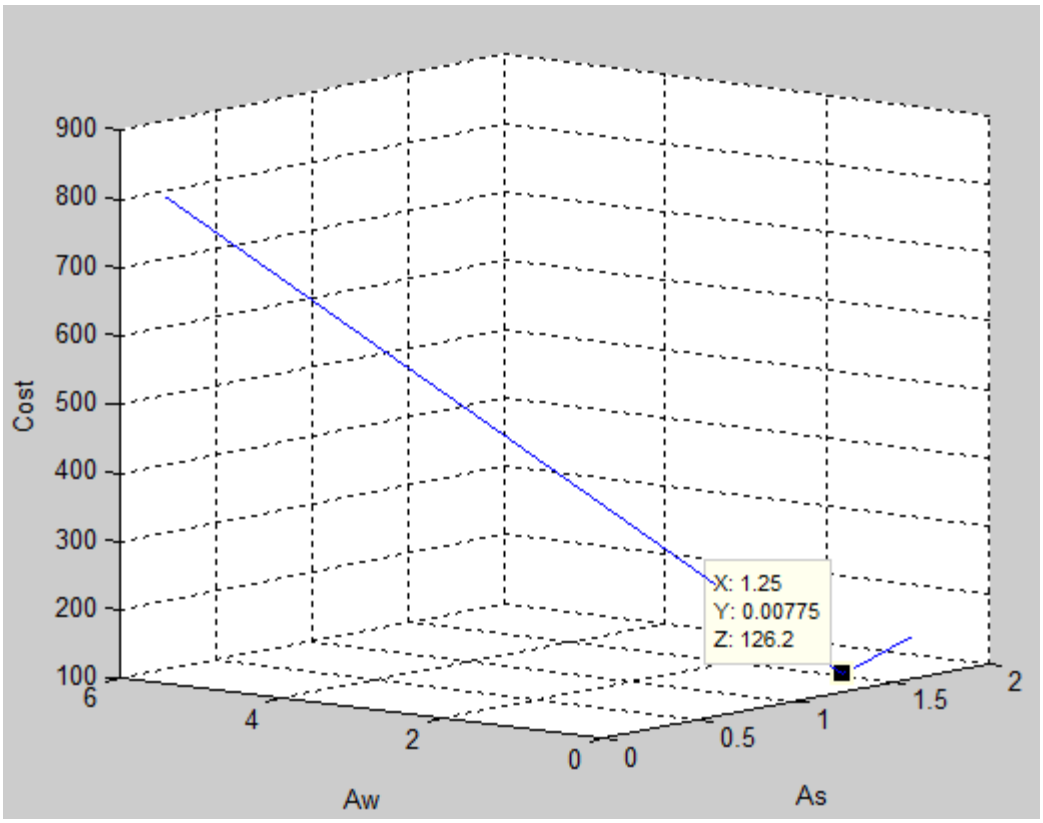

Figure 5-11: Finding minimum cost of the Hybrid system for a particular As and Aw of Khulna

5.5.2 Solar-Only System:

Workspace

Name	Value	Min	Max
As	1.2962	1.2962	1.2962
L	5	5	5
Sx	*1x12 double*	15	365
Sxi	*1x365 double*	1	365
Sy	*12x1 double*	4.1400	6.2000
Syi	*1x365 double*	3.8575	6.2623
cost_Solar	129.6182	129.61...	129.61...
cs	100	100	100
min_Syi	3.8575	3.8575	3.8575

Figure 5-12:MATLAB screenshot for all parameters of Solar-Only System of Khulna

5.5.3 Wind-Only System:

Workspace

Name	Value	Min	Max
Aw	5.4096	5.4096	5.4096
L	5	5	5
Wx	*1x12 double*	15	365
Wxi	*1x365 double*	1	365
Wy	*12x1 double*	6.6861	34.5685
Wyi	*1x365 double*	0.9243	34.7596
cost_Wind	811.4446	811.44...	811.44...
cw	150	150	150
min_Wyi	0.9243	0.9243	0.9243

Figure 5-13:MATLAB screenshot for all parameters of Wind-Only System of Khulna

5.6 Comparison among Hybrid, Solar-Only and Wind-Only System of Khulna:

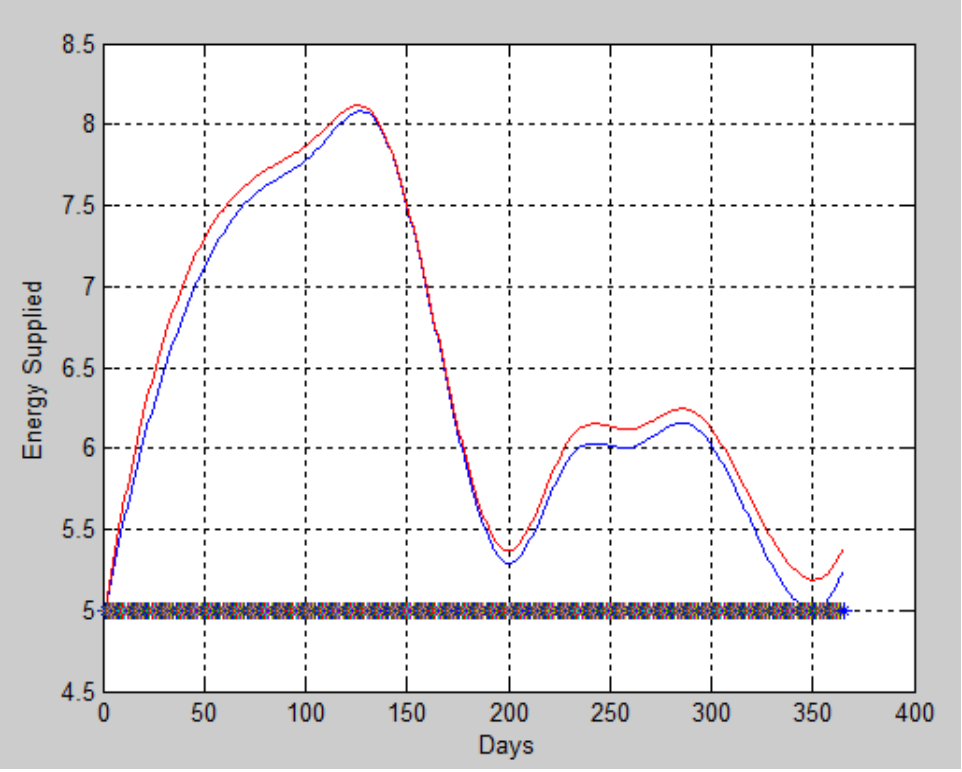

Figure 5-14: Comparison between Hybrid and Solar-Only system of Khulna

It is very clear from Figure 5-15 why the wind-only system has the highest wastage of energy and highest amount of cost mentioned in Table 5-4. As we see, matching between energy generation and load demand is very far away from each one which causes the system as the worst system in term of optimum cost effective design.

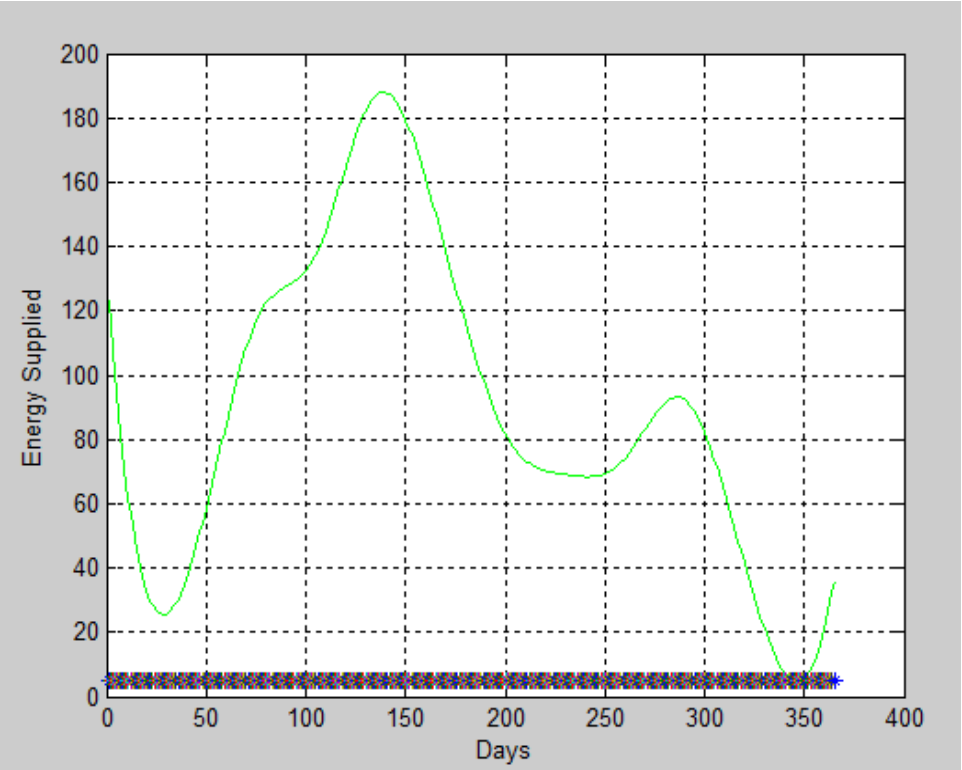

Figure 5-15: Energy Supplied to Load of Wind-Only System of Khulna

Table 5-4:Cost and Wasteof Energy comparison at optimum parameters of Hybrid, Solar-Only and Wind-Only system of Khulna

	As in m^2	Aw in m^2	Cost	Wasted Energy
Hybrid System	1.25	0.00775	126.20	506.0330
Solar-Only System	1.2962	NA	129.62	544.0193
Wind-Only System	NA	5.4096	811.45	3.0577e+04

So, a mathematical technique has been developed for finding the optimum combination of solar and wind for the hybrid system from the meteorological data for Kutubdia Island and Khulna depending on the solution of energy-generation and load demand condition. The solution has been illustrated in a graphical form using the optimum sizes of PV and Wind components.

The main reason why the hybrid system is cheaper than solar-only and wind-only system is the fact that the energy generated by the hybrid system is closer to the load comparing to solar-only and wind-only system alone which has been illustrated in Figure 5-8 and Figure 5-14.

Chapter 6: Conclusion& Future Work

6.1 Conclusion

In this thesis, a simple however efficient photovoltaic water pumping system with a new maximum power point tracking principle, its theoretical basis and mathematical development and working algorithm are presented. The study developed a coding based presentation to depict the developed technique and to test it fortracking speed, tracking accuracy, capability to rapid transition and maximum power point efficiency with a conventional hill climbing P&O algorithm. Results shows that the system reaches to MPP voltage in much less iteration and hence very fast to converge to MPP point. In order to develop a simple low-cost system, this thesis adopts the direct control method which requires only two sensors for getting desired output. Moreover, it can precisely track a true MPP dynamic graph, whereas conventional hill climbing or normal P&O had just failed for the most rapid variation. The duty cycle and maximum power point under various weather conditions have been analyzed and compared between proposed and perturb and observe method. It has been found evidential that the percentage of errors in finding duty cycles and maximum power points of the proposed algorithm are much less than its counterpart perturb and observe method. Later, the developed system has been tested according to international standard and confirms the validation as reported in the literature. Additionally, in comparing with other MPPT algorithms, the developed method holds the implementation freedom from PV array parameters and therefore, can be easily adopted for any brand of PV module on the market. Simulations also make comparisons with the system without MPPT in terms of total energy produced and total volume of water pumped a day. The results validate that developed MPPT can significantly increase the efficiency of energy production from PV and the performance of the PV water pumping system compared to the system without MPPT. A case study also has been investigated where a mathematical model has been developed using linear programming concept in order to determine a cost effective solution for Kutubdia and Khulna regions of Bangladesh. It has been found from the analysis that for both cases, the hybrid system turns out to be the most optimized solution comparing to solar and wind alone system. The principal reason is best load-

matchingbetween hybrid system generation and load demand than that of solar-only and wind-only system generation and load demand.

6.2 Future Scope

- Practical implementation of the system remains for future research which would include microcontroller, A/D converter, and water level sensors etc for detecting the height of water level. It will also involve performance analysis of the practical system by comparing with the simulated one.
- The future scope also could include of utilizing the surplus energy being produced by the hybrid system and supplying those energy to a micro-grid system or in the main-grid for enhancing more reliability in power system. It will also analyze the effect when large scale renewable generators get connected with grid.
- It might also incorporate designing an optimized cost effective solutionby adding more renewable sources like bio-mass with solar and wind and also designing the optimized storage system such as battery or generator which can be utilized for extreme cases to bring more reliability into the system.
- The future scope is also open forassociating Artificial Neural Network (ANN) for making the best prediction of solar and wind energy in order to make the system-design more robust.

REFERENCES

1. Muhsen, D.H., T. Khatib, and F. Nagi, *A review of photovoltaic water pumping system designing methods, control strategies and field performance.* Renewable and Sustainable Energy Reviews, 2017. **68**: p. 70-86.
2. Kazem, H.A., et al., *Design, measurement and evaluation of photovoltaic pumping system for rural areas in Oman.* Environment, Development and Sustainability, 2017. **19**(3): p. 1041-1053.
3. Muhsen, D.H., et al., *Techno-economic study and optimal sizing of a stand-alone photovoltaic water pumping system.* International Transactions on Electrical Energy Systems, 2017. **27**(9).
4. Chandel, S., M.N. Naik, and R. Chandel, *Review of solar photovoltaic water pumping system technology for irrigation and community drinking water supplies.* Renewable and Sustainable Energy Reviews, 2015. **49**: p. 1084-1099.
5. Li, G., et al., *Research and current status of the solar photovoltaic water pumping system–A review.* Renewable and Sustainable Energy Reviews, 2017. **79**: p. 440-458.
6. Kumar, A., G. Acharya, and H.K. Singh, *Effective use of Roof Surface Area for Electricity Generation using Solar Energy: A Case Study of Jodhpur.* 2014.
7. Siddig, M.H., *Design of a Rural Hybrid pumping System*. 2015, UOFK.
8. Foster, R. and A. Cota, *Solar water pumping advances and comparative economics.* Energy Procedia, 2014. **57**: p. 1431-1436.
9. Stone, P., M. Islam, and Y.-J. Shin. *Power quality impact of wind turbine generators on the electrical grid*. in *Energytech, 2012 IEEE*. 2012. IEEE.
10. Mohammadpour, H., et al., *SSR Damping in Fixed-Speed Wind Farms using Series FACTS Controllers.*
11. Islam, M., et al., *Time-frequency based instantaneous power components for transient disturbances according to IEEE standard 1459.* 2014.
12. Islam, M.M., *Advanced Digital Signal Processing Based Redefined Power Quality Indices, and Their Applications to Wind Power.* 2014.
13. Lynn, P.A., *Electricity from sunlight: an introduction to photovoltaics*. 2011: John Wiley & Sons.
14. Markvart, T., *Solar electricity*. Vol. 6. 2000: John Wiley & Sons.
15. Azevedo, G., et al. *Evaluation of maximum power point tracking methods for grid connected photovoltaic systems*. in *Power Electronics Specialists Conference, 2008. PESC 2008. IEEE*. 2008. IEEE.
16. Solar, B. and B. SX150, *150W Multi-crystalline Photovoltaic Module*. 2001, Datasheet.
17. Walker, G., *Evaluating MPPT converter topologies using a MATLAB PV model.* Journal of Electrical & Electronics Engineering, Australia, 2001. **21**(1): p. 49-56.
18. Taufik, A.O., M. Anwari, and M. Taufik. *Modeling and simulation of photovoltaic water pumping system*. in *Modelling & Simulation, 2009. AMS'09. Third Asia International Conference on*. 2009. IEEE.
19. Algazar, M.M., H.A. EL-halim, and M.E.E.K. Salem, *Maximum power point tracking using fuzzy logic control.* International Journal of Electrical Power & Energy Systems, 2012. **39**(1): p. 21-28.

20. Gilbert, M., *Masters, Renewable and efficient electric power systems.* Wiley-Interscience, John Wiley & Sons, Inc, New Jersey, 2004. **75**: p. 76.
21. Messenger, R.A. and J. Ventre, *Photovoltaic systems engineering*. 2010: CRC press.
22. Oi, A., *Design and simulation of photovoltaic water pumping system.* California Polytechnic State University, 2005.
23. Hassan, A.A., et al., *Modeling and simulation of a single phase grid connected photovoltaic system.* WSEAS Transactions on Systems and Control, 2010. **5**(1): p. 16-25.
24. Rashid, M.H., *Power electronics handbook: devices, circuits and applications*. 2010: Academic press.
25. Mohamed, A., A. Berzoy, and O. Mohammed. *Optimized-fuzzy MPPT controller using GA for stand-alone photovoltaic water pumping system*. in *Industrial Electronics Society, IECON 2014-40th Annual Conference of the IEEE*. 2014. IEEE.
26. Mohamed, A.A., A. Berzoy, and O. Mohammed. *Optimized-fuzzy MPPT controller using GA for stand-alone photovoltaic water pumping system*. in *Industrial Electronics Society, IECON 2014-40th Annual Conference of the IEEE*. 2014. IEEE.
27. Aashoor, F., *Maximum power point tracking techniques for photovoltaic water pumping system*. 2015, University of Bath.
28. Hussein, K., et al., *Maximum photovoltaic power tracking: an algorithm for rapidly changing atmospheric conditions.* IEE Proceedings-Generation, Transmission and Distribution, 1995. **142**(1): p. 59-64.
29. Hohm, D. and M.E. Ropp, *Comparative study of maximum power point tracking algorithms.* Progress in photovoltaics: Research and Applications, 2003. **11**(1): p. 47-62.
30. Oi, A., M. Anwari, and M. Taufik. *Modeling and simulation of photovoltaic water pumping system*. in *Modelling & Simulation, 2009. AMS'09. Third Asia International Conference on*. 2009. IEEE.
31. Mohan, N. and T.M. Undeland, *Power electronics: converters, applications, and design*. 2007: John Wiley & Sons.
32. Hart, D.W., *Power electronics*. 2011: Tata McGraw-Hill Education.
33. Robinson, F., *Power electronics converters, applications and design: Ned Mohan, Tore M. Undeland and William P. Robbins , John Wiley, Chichester, 1995, 802 pp., ISBN: 0-471-30576-6,£ 22.50*. 1997, Elsevier.
34. Ovaska, S., *Maximum power point tracking algorithms for photovoltaic applications.* Diss. Aalto University, 2010.
35. Esram, T. and P.L. Chapman, *Comparison of photovoltaic array maximum power point tracking techniques.* IEEE TRANSACTIONS ON ENERGY CONVERSION EC, 2007. **22**(2): p. 439.
36. Femia, N., et al. *Optimizing sampling rate of P&O MPPT technique*. in *Power Electronics Specialists Conference, 2004. PESC 04. 2004 IEEE 35th Annual*. 2004. IEEE.

37. Sera, D., et al. *Improved MPPT algorithms for rapidly changing environmental conditions*. in *Power Electronics and Motion Control Conference, 2006. EPE-PEMC 2006. 12th International*. 2006. IEEE.
38. Femia, N., et al., *Optimization of perturb and observe maximum power point tracking method.* Power Electronics, IEEE Transactions on, 2005. **20**(4): p. 963-973.
39. Zhang, C., et al. *A modified MPPT method with variable perturbation step for photovoltaic system*. in *Power Electronics and Motion Control Conference, 2009. IPEMC'09. IEEE 6th International*. 2009. IEEE.
40. Xiao, W. and W.G. Dunford. *A modified adaptive hill climbing MPPT method for photovoltaic power systems*. in *Power Electronics Specialists Conference, 2004. PESC 04. 2004 IEEE 35th Annual*. 2004. Ieee.
41. Andrejašič, T., M. Jankovec, and M. Topič, *Comparison of direct maximum power point tracking algorithms using EN 50530 dynamic test procedure.* IET renewable power generation, 2011. **5**(4): p. 281-286.
42. Piegari, L. and R. Rizzo, *Adaptive perturb and observe algorithm for photovoltaic maximum power point tracking.* IET Renewable Power Generation, 2010. **4**(4): p. 317-328.
43. Noguchi, T., S. Togashi, and R. Nakamoto, *Short-current pulse-based maximum-power-point tracking method for multiple photovoltaic-and-converter module system.* Industrial Electronics, IEEE Transactions on, 2002. **49**(1): p. 217-223.
44. Yuvarajan, S. and S. Xu. *Photo-voltaic power converter with a simple maximum-power-point-tracker*. in *Circuits and Systems, 2003. ISCAS'03. Proceedings of the 2003 International Symposium on*. 2003. IEEE.
45. <*sdseries.pdf*>. Available from: http://www.windsun.com/Solar_Pump_PDF/sdseries.pdf.
46. Arab, A.H., M. Benghanem, and F. Chenlo, *Motor-pump system modelization.* Renewable Energy, 2006. **31**(7): p. 905-913.
47. <*Solar_Irradiance_Data.pdf*>. Available from: dspace.bracu.ac.bd/bitstream/handle/10361/.../Id%2009221159.pdf?...13.
48. <*Cloudy_Day_Data.pdf*>.
49. Khatib, T., et al., *Optimal sizing of building integrated hybrid PV/diesel generator system for zero load rejection for Malaysia.* Energy and Buildings, 2011. **43**(12): p. 3430-3435.
50. Islam, M., *Assessment of renewable energy resources of Bangladesh.* Electronic book, 2002.